POLITECNICO DI MILANO

Facoltà di Ingegneria Industriale e dell'Informazione
Dipartimento di Energia

Corso di Laurea Magistrale in Ingegneria Energetica

DESIGN, MODELLING, AND CONTROL OF A WASTE HEAT RECOVERY UNIT FOR HEAVY-DUTY TRUCKS

Relatore: Prof. Francesco CASELLA

Relatore estero: Prof. Piero COLONNA

Supervisore: PhD. Carlo DE SERVI

Tesi di Laurea di:

Stefano TRABUCCHI Matr. 800815

Anno Accademico 2013-2014

Tra vent'anni sarete più delusi per le cose
che non avete fatto che per quelle che avrete fatto.
Quindi mollate le cime.
Allontanatevi dal porto sicuro.
Prendete con le vostre vele i venti.
Esplorate. Sognate. Scoprite.

Twenty years from now
you will be more disappointed by the things
that you didn't do than by the ones you did.
So throw off the bowlines.
Sail away from the safe harbor.
Catch the trade winds in your sails.
Explore. Dream. Discover.

Mark Twain

Acknowledgment

Il primo ringraziamento non può che essere rivolto alla mia famiglia ed in particolare ai miei genitori, i quali mi hanno sempre spinto a dare il massimo e con non pochi sacrifici mi hanno permesso di tagliare questo importante traguardo.

Un caloroso ringraziamento va al prof. Casella, sempre disponibile con un sorriso a chiarire tutti i miei dubbi, anche i più banali, e al prof. Colonna e a tutto il suo gruppo di ricerca, che mi hanno accolto presso la TU Delft per svolgere parte del presente lavoro e mi hanno aiutato giorno per giorno, specialmente il mio "daily supervisor" Carlo.

Un grazie speciale va ai compagni e amici di viaggio Alessandro, Riccardo, Enrico, Andrea, Januario, Lucrezia e Marco. Senza la vostra compagnia e le vostre "perle d'ignoranza" passare 5 anni al Poli sarebbe stato decisamente più noioso. Una menzione particolare la merita Federico, che negli ultimi 3 mesi mi ha affiancato per l'ultima parte del lavoro.

Un pensiero un po' nostalgico va ai colleghi della Room 6.01 di Delft e a tutta la truppa italo-olandese, sempre pronti a fare una lunga pausa caffè di giorno e una lunga pausa "Che buona la birra belga!!" di sera.

Non posso poi non pensare ai miei amici di sempre Giulia, Michela, Silvia, Daniel, Valentina e Veronica, con cui ho condiviso gli interminabili viaggi in treno e auto verso casa e le innumerevoli occasioni di divertimento milanesi. In particolare ringrazio Francesca, mia coinquilina negli ultimi due anni, per avermi sopportato come sua "suocera" preferita.

Infine voglio ricordare tutte le altre numerose persone incontrate lungo il percorso. Anche se alcuni di essi sono "spariti dai radar", hanno contribuito non poco al raggiungimento di questo risultato.

Riassunto esteso

Scopo del lavoro

Il presente lavoro di tesi si pone come obiettivo principale la progettazione di un sistema di recupero di energia dal calore di scarto di un motore a combustione interna di grossa taglia, e il successivo studio di un sistema di controllo dell'impianto.

Le incertezze legate al futuro prezzo del petrolio, unite soprattutto alla previsione di un abbassamento dei limiti di emissione di inquinanti sia locali (NO_x) sia globali (CO_2) e alla possibile introduzione a livello europeo di una Carbon Tax anche in ambito automotive, hanno spinto i costruttori di autoveicoli adibiti al trasporto merci a cercare nuove e innovative soluzioni al fine di aumentare l'efficienza dei sistemi di trazione. Considerando il fatto che nel prossimo futuro non si prevedono importanti miglioramenti nel campo dei motori Diesel in termini di rendimento di primo principio, e quindi di consumo di combustibile ed emissioni, una delle soluzioni più promettenti è la realizzazione di un sistema di recupero che sfrutti come fonte di energia il calore di scarto del motore stesso: con un valore attuale di rendimento per il motore Diesel intorno al 42%, rimane infatti ancora disponibile nei fumi e nel sistema di raffreddamento oltre la metà dell'energia introdotta con il combustibile.

La tecnologia più adatta a tal fine è quella basata sui cicli Rankine organici, dato che ha degli elementi in comune con i cicli di refrigerazione, soprattutto in termini componentistici, fattore che permette l'abbattimento dei costi di sviluppo iniziali.

In termini economici, l'investimento diventa remunerativo quando la potenza generata con il ciclo a recupero è pari ad almeno il 5% della potenza meccanica erogata dal motore primo in condizioni di funzionamento nominali. Lo sviluppo di un modello dinamico completo del sistema risulta quindi di primaria importanza se si vuole massimizzare il recupero energetico anche in condizioni lontane da quella nominale e verificare l'efficacia del sistema di controllo lungo un generico percorso di guida.

Il presente lavoro si inserisce in un progetto di ricerca presso la Technische Universiteit Delft (NL), su un arco temporale di 4 anni e in collaborazione con alcune aziende del settore automotive, fra cui l'olandese DAF Trucks NV e l'americana

Dana. Essendo il progetto ancora in fase iniziale all'inizio del presente lavoro, si è reso innanzitutto necessario un progetto preliminare del ciclo termodinamico, in termini di analisi della fonte di calore, layout e dimensionamento dei componenti e scelta del fluido di lavoro. I risultati ottenuti, sebbene preliminari, permettono una prima valutazione dei benefici del sistema a recupero, di verificare la validità della soluzione impiantistica adottata, e mettono in luce le principali criticità specifiche per il sistema sviluppato.

Struttura del lavoro e scelte progettuali

Il presente lavoro di tesi si articola come segue.

Review bibliografica Inizialmente è stata svolta una breve review bibliografica riguardante il recupero termico da motori Diesel e i metodi di progetto e ottimizzazione dei cicli ORC;

Potenzialità delle sorgenti termiche Per prima cosa è stato introdotto un modello a parametri concentrati di un motore Diesel di grossa taglia per il trasporto pesante. Successivamente, sulla base di una serie di dati sperimentali messi a disposizione dalla DAF Truck NV, i principali parametri empirici del modello sono stati calibrati, attraverso un processo di tuning ai minimi quadrati, per ottenere stime verosimili delle portate e delle temperature delle sorgenti termiche del ciclo ORC.

Il modello richiede come input il numero di giri dell'albero motore, la portata di combustibile, l'apertura percentuale della valvola di ricircolo EGR e l'apertura percentuale delle pale statoriche della turbina centripeta del turbocompressore. Il primo è legato attraverso la trasmissione alla velocità di rotazione delle ruote, ovvero alla velocità longitudinale del veicolo. Gli altri tre sono output della centralina di bordo, ovvero del sistema di controllo del motore. La portata di combustibile è linearmente proporzionale alla coppia richiesta al motore, a sua volta derivante da un bilancio di forze longitudinali, mentre la valvola di ricircolo e l'apertura del turbocompressore sono comandate attraverso delle mappe presenti nella centralina di bordo. Non essendo queste ultime disponibli, sono state appositamente create attraverso un processo di ottimizzazione del funzionamento del motore, il cui obiettivo è la minimizzazione del consumo di carburante.

Progetto preliminare del ciclo ORC L'ottimizzazione del progetto del ciclo di recupero, sia in termini di dimensione fisica dei componenti, loro configurazione e scelta del fluido, è funzione delle caratteristiche delle sorgenti di calore. Considerata l'elevata efficienza dei moderni motori diesel di grossa taglia, il recupero di

calore dai soli fumi di scarico a valle del turbocompressore non è risultato sufficiente a garantire un output di potenza meccanica accettabile. Per questo motivo il recupero di calore avviene in due evaporatori in parallelo, sfruttando le seguenti sorgenti termiche:

1. circuito di ricircolo dei gas combusti (EGR). Ai fini di ridurre le emissioni di NO_x parte dei gas combusti viene ricircolato dal collettore di scarico a quello di aspirazione. Per non deteriorare le prestazioni del motore a causa della bassa densità dei gas caldi ricircolati, uno scambiatore di calore intermedio raffredda fortemente tale corrente prima di immetterla nel collettore di aspirazione. L'attuale scambiatore ad acqua può essere quindi sostituito da un evaporatore a fluido organico, la cui potenza termica è 21 kW nel punto di design;

2. gas di scarico a valle del turbocompressore. La presenza del sistema SCR, i cui catalizzatori necessitano di una temperatura minima per funzionare correttamente, limita il raffreddamento dei gas ad un valore di 200 °C. Per questo motivo è opportuno inserire un rigeneratore a monte dell'evaporatore, che preriscalda il fluido di lavoro che fluisce in questo ramo raffreddando la corrente di fluido a valle della turbina. Questa soluzione è vantaggiosa anche perchè riduce gli impatti negativi sul motore primo: un evaporatore più piccolo si traduce in minori perdite di carico dei gas combusti, ovvero in una minore contropressione allo scarico del turbocompressore. Una configurazione alternativa consiste nel porre l'evaporatore a valle del sistema SCR, ma ciò comporta un minore recupero di calore a causa dell'assorbimento termico del letto catalitico. La potenza termica del secondo evaporatore nel punto nominale è 16.5 kW

I vincoli di volume derivanti dalla particolare applicazione hanno suggerito l'adozione di scambiatori a piastre, le cui dimensioni possono essere più compatte rispetto ai più comuni shell & tube.

Per quanto riguarda la scelta del fluido di lavoro, i vincoli su GWP e ODP e soprattutto sulla bassa tossicità ed infiammabilità, derivanti dall'utilizzo a bordo di un veicolo, limitano la scelta alla famiglia dei silossani. Fra questi, il fluido che garantisce il miglior accoppiamento termodinamico con le due sorgenti termiche è l'esametildisilossano (MM), che presenta inoltre buone proprietà lubrificanti e una pressione di condensazione vicina a quella atmosferica nel range di temperature considerate.

Con un approccio innovativo, i principali parametri del ciclo di recupero, quali la pressione di evaporazione e il surriscaldamento del fluido, sono stati ottimizzati insieme ai principali parametri geometrici della turbina, al fine di garantire la fattibilità di quest'ultima. L'obiettivo dell'ottimizzazione è quello di massimizzare

la potenza meccanica netta estratta dal ciclo di recupero, fissate le condizioni termodinamiche delle sorgenti calde, il rendimento fluidodinamico della pompa, la temperatura di condensazione, la temperatura di scarico dei gas combusti e alcuni vincoli geometrici della turbina. Per quanto riguarda il tipo di espansore, la scelta è ricaduta su una turbina assiale bistadio, che nel punto di design produce 4.8 kW con un rendimento isentropico $\eta_{is} = 0.715$. La pompa adottata è di tipo volumetrico a diaframma, particolarmente adatta visto l'elevato carico del circuito e la bassa portata circolante.

Vista l'elevata variabilità delle condizioni operative del ciclo, legate al carico del motore primario, è stato sviluppato un codice di calcolo in grado di stimare le prestazioni off-design della turbina, la cui geometria è un risultato del processo di ottimizzzazione. In particolare, il codice fornisce i valori di portata elaborata e rendimento isentropico al variare delle condizioni termodinamiche all'ingresso, della pressione di scarico e della velocità di rotazione. Quest'ultima non rappresenta un grado di libertà del sistema, ma è legata alla velocità di rotazione del motore: per ridurre peso, costi e complessità dell'intero sistema, infatti, l'accoppiamento meccanico fra motore primo e turbina attraverso un riduttore di giri è stato preferito rispetto ad un accoppiamento turbina-alternatore con un sistema di accumulo a batterie.

Infine, considerando il fatto che la pompa di circolazione del radiatore è anch'essa vincolata meccanicamente all'albero motore, la cui velocità di rotazione varia poco in termini relativi, il circuito di raffreddamento esterno del motore non è stato modellato. La sorgente fredda del ciclo a recupero è quindi rappresentata da una portata costante di acqua a 70 °C.

Implementazione dei modelli in linguaggio Modelica Il linguaggio di modellazione Modelica offre la possibilità di costruire con relativa facilità modelli dinamici di sistemi complessi multidominio. Per questo motivo è stato utilizzato per modellare prima i singoli componenti del sistema (scambiatori, turbomacchine, valvole etc..) e successivamente, per aggregazione di questi ultimi, i modelli del motore Diesel, dell'unità di recupero termico e del sistema di controllo.

Alcuni hanno richiesto una modellazione *ex-novo*, in particolare il modello a parametri concentrati del motore e delle turbomacchine. Per quanto riguarda gli scambiatori di calore, sono stati utilizzati dei modelli a volumi finiti già esistenti in altre librerie (*Thermopower*, *ORC*).

In questa fase si è reso necessario l'inserimento nel ciclo ORC di un serbatoio per il fluido di lavoro a valle del condensatore, con l'ipotesi di equilibrio bifase al suo interno. A livello di progettazione statica del sistema esso non ha alcuna influenza, mentre a livello dinamico permette di avere un disaccoppiamento fra le sezioni di alta e bassa pressione del sistema, oltre che di accumulare il fluido di lavoro quando il sistema di recupero è spento. In fase di inizializzazione della

simulazione garantisce inoltre una corretta distribuzione della massa all'interno del circuito.

Obiettivi del controllo e analisi delle prestazioni off-design del sistema Una volta terminato lo sviluppo del modello, il passaggio successivo del lavoro è stato la valutazione degli obiettivi che il sistema di controllo deve soddisfare. Essi sono:

1. mantenere la temperatura di scarico dei gas combusti sopra i 200 °C, in modo da garantire un corretto funzionamento del sistema SCR;
2. evitare che il fluido di organico superi la propria temperatura di decomposizione, qui fissata con un buon margine di sicurezza a 300 °C;
3. garantire un grado di surriscaldamento minimo del fluido all'ingresso della turbina, per evitare l'iniezione di gocce di liquido;
4. mantenere costante la pressione di condensazione;
5. evitare il fenomeno della cavitazione all'ingresso della pompa a diaframma;
6. garantire il raffreddamento dei gas combusti del circuito EGR;
7. mantenere la pressione di evaporazione inferiore alla pressione critica, al fine di evitare problemi meccanici negli scambiatori di calore a piastre;
8. massimizzare l'output di potenza meccanica del ciclo ORC.

Considerando il fatto che le variabili di controllo sono solamente due, ovvero il numero di giri della pompa e l'apertura della valvola che distribuisce il fluido di lavoro sui due rami di evaporazione, le variabili controllate vanno scelte in modo che il loro controllo permetta il soddisfacimento simultaneo del maggior numero di obiettivi. Essendo fondamentale il corretto funzionamento del sistema SCR, la prima variabile di controllo scelta è proprio la temperatura di scarico dei gas combusti a valle dell'evaporatore. La seconda variabile di controllo è invece il surriscaldamento del fluido all'ingresso della turbina: il suo controllo infatti può evitare sia che il fluido raggiunga temperature prossime a quella di decomposizione sia l'iniezione di liquido in turbina, e al contempo garantire la massimizzazione della potenza recuperata.

La presenza del serbatoio e di un piccolo scambiatore di calore aggiuntivo fra esso e la pompa permette di soddisfare i punti 4, 5 e 6, mentre il vincolo sulla pressione di evaporazione (punto 7) può essere garantito da una valvola di by-pass sulla turbina.

Una volta definite le variabili controllate, i loro set-point ottimi sono stati trovati attraverso un'analisi approfondita delle condizioni operative off-design del ciclo, in funzione del carico del motore primario. Le condizioni ottime garantiscono a regime la massimizzazione della potenza meccanica estratta e il rispetto di tutti i vincoli imposti.

Analisi dinamica e progetto preliminare di un sistema di controllo La parte finale del lavoro di tesi consiste nello studio di un sistema di controllo per il ciclo ORC che garantisca l'inseguimento dei set-point ottimi delle variabili controllate e una buona reiezione dei disturbi.

Poichè la teoria di controllo classica si basa sull'ipotesi di linearità del sistema, inizialmente il processo controllato, ovvero il ciclo di recupero, è stato linearizzato attorno a diversi punti di equilibrio. Al fine di ridurre le non linearità è stato operato un cambio di variabile: le variabili di controllo reali sono state sostituite da due variabili virtuali, ovvero le portate di fluido organico nei due rami di evaporazione, normalizzate rispetto ai loro valori di equilibrio. Ai fini del controllo tale scelta non modifica i risultati, poichè le due portate sono determinate da un'opportuna combinazione del numero di giri della pompa e della posizione della valvola a 3 vie.

Vista l'elevata interazione fra input e output del sistema, valutata grazie al calcolo della matrice RGA, l'architettura del controllo scelta è di tipo centralizzato: la portata di fluido di lavoro del ramo EGR comanda il surriscaldamento, mentre quella del ramo gas combusti comanda la temperatura di scarico dei fumi stessi. Un disaccoppiatore statico riduce l'influenza reciproca dei due anelli di controllo, i quali sono comandati da due regolatori di tipo PI.

Ai fini dello studio del sistema di controllo è stato ricavato un modello ridotto del sistema linearizzato, in grado di catturare le componenti principali della dinamica del processo. Esso ha permesso di spiegare in maniera più approfondita i risultati di un primo processo di taratura dei regolatori, la cui frequenza di taglio è stata inizialmente scelta pari a $\omega_c = 0.01\,\mathrm{rad\,s^{-1}}$.

Materiali utilizzati

Per quanto concerne i materiali utilizzati, la DAF Truck NV ha reso disponibile un set di misure statiche dei principali parametri di funzionamento del motore, oltre che un set di dati dinamici su un ciclo guida reale. Queste informazioni sono state utilizzate per la taratura e per la validazione del modello del motore a combustione interna, in modo da garantire un dimensionamento del ciclo di recupero in linea con le reali prestazioni dei motori Diesel di ultima generazione.

I software impiegati sono:

- *Matlab*: taratura delle mappe di controllo del motore, attraverso il modello Simulink dello stesso; utilizzo ed estensione del programma "in-house" *ORCHID_vpe* per l'ottimizzazione del ciclo ORC; sviluppo del codice *Off1D* per il calcolo delle prestazioni off-design della turbina; funzioni del Control Toolbox per il bilanciamento e la riduzione del modello linearizzato.
- *Aspen - Exchanger Design & Rating*: dimensionamento degli scambiatori di calore.
- *Dymola*: ambiente di modellazione tool-independent *Modelica*, implementazione dei modelli dinamici dei componenti, dei cicli termodinamici e dei sistemi di controllo.

Risultati e conclusioni

Il primo obiettivo del presente lavoro di tesi era il progetto di un sistema di recupero termico dal calore di scarto di un motore a combustione interna di grossa taglia. La configurazione di ciclo adottata, insieme alla scelta del silossano MM come fluido di lavoro, permette di centrare l'obiettivo del 5% di potenza aggiuntiva ricavata dal sistema di recupero termico: infatti, per una potenza globale nominale di 101.5 kW e corrispondente ad una velocità di crociera di 85 km h^{-1}, il sistema ORC fornisce 4.7 kW sottoforma di potenza meccanica all'albero della turbina, a fronte di 96.8 kW di potenza del motore Diesel. Considerato che il recupero energetico di altre fonti di calore comporta soluzioni impiantistiche troppo complesse, e che la posizione ottimale dell'evaporatore dei gas combusti è a monte del sistema SCR, tale risultato può essere migliorato solo dall'abbassamento della temperatura minima di funzionamento del letto catalitico, così da permettere un maggiore recupero termico, e da una più bassa temperatura di condensazione.

Per quanto riguarda il progetto di un sistema di controllo, l'elevata inerzia termica degli scambiatori e la scarsa efficacia dal punto di vista dinamico del disaccoppiatore statico adottato limitano fortemente le prestazioni dinamiche del sistema nel suo complesso. Una semplice architettura di controllo centralizzata con due regolatori PI e un disaccopiatore statico non è quindi sufficiente a garantire il soddisfacimento degli obiettivi preposti a fronte di un carico realistico del motore primo.

Possibili sviluppi futuri possono riguardare l'implementazione di un sistema di controllo di tipo classico con disaccoppiamento dinamico e compensazioni feedforward, nonche' la realizzazione di un sistema di controllo model-predictive, che potrebbe gestire in maniera più efficace i vincoli di funzionamento del sistema e l'accoppiamento tra le diverse variabili di controllo. Si potrebbe anche valutare la modifica del progetto del sistema volta alla riduzione dell'inerzia termica degli scambiatori, in modo da rendere possibile l'aumento della banda del controllo.

Andrebbero infine approfonditi la gestione del transitorio di avviamento del ciclo ORC, nonche' la gestione delle situazioni di sovraccarico degli evaporatori tramite bypass di turbina.

Contents

List of Figures

List of Tables

English abstract

Recent regulations about efficiency and CO_2 emissions of energy production systems, together with unpredictable fluctuations in fuel prices, have created a renewed interest in middle and low temperature waste heat recovery technologies. There are many possible applications which cover a wide range of power, from few kW to some MW, depending on the primary thermal source of the system. The most suitable technology for this purpose is the Organic Rankine Cycle (ORC) technology, whose potentialities have been already demonstrated: the degree of freedom concerning the working fluid selection let this technology satisfy both environmental and feasibility issues, and recover heat from extremely low temperature sources, if compared with conventional plants.

The aim of the work is the study of the dynamic behaviour of a combined cycle composed by an heavy duty Internal Combustion Engine (ICE) as topping cycle and an Organic Rankine Cycle as bottoming cycle, in order to develop an appropriate control strategy. In fact, the ORC operating point is often far from design condition, due to the extremely variable engine load: the need for a dynamic simulation tool comes from the necessity of designing a fast response control system, to check the reliability of the design of the WHR unit and to identify bottlenecks during transient operation.

The first part of the work consists of the design of the whole ICE-ORC system, in all its components: internal combustion engine, heat exchangers (evaporator, condenser..), tank, pump and turbine. About the latter component, an off-design 0D code has been developed, in order to predict the off-design performance of small turbo generators. The whole model has been implemented with the modelling language Modelica, and simulated with commercial code Dymola.

In the second part the control objectives and strategies are defined. The aim is to evaluate the main dynamic characteristics of the whole combined cycle. Moreover, the complete Modelica model has been used to find the optimal set point of the controlled variables: it is worth to remind that without this tool the control optimization process is not trivial because of the complex ORC configuration and interaction between topping and bottoming cycle. In conclusion, a simple control configuration with two PI controllers has been implemented and tested with two different load configuration.

Keywords: Organic Rankine Cycle, dynamic modelling, Modelica, optimal control.

Italian abstract

Le recenti normative in tema di efficienza energetica e di riduzione delle emissioni di CO_2, unite alle incertezze riguardanti l'andamento dei prezzi dei combustibili fossili, hanno portato al centro dell'attenzione il tema del recupero di energia da fonti di calore a media e bassa temperatura. Le applicazioni possibili sono numerose e coprono un range di potenza variabile da pochi kW a qualche MW, in funzione della tipologia di fonte di calore primaria. La tecnologia più adatta risulta essere quella ORC, le cui potenzialità sono già state ampiamente dimostrate: la possibilità di utilizzare diversi fluidi di lavoro permette infatti di soddisfare contemporaneamente sia requisiti di tipo ambientale sia di tipo tecnologico, e di recuperare calore anche a temperature estremamente basse rispetto agli impianti convenzionali. Il tema affrontato in questo lavoro è stato lo studio del recupero termico da un motore a combustione interna di grossa taglia, principalmente in termini di dinamica del sistema accoppiato ICE-ORC, volto allo sviluppo di un adeguato sistema di controllo. Vista l'elevata variabilità del carico richiesto al motore primo, il sistema ORC sottoposto opera spesso in condizioni di off-design. Ciò rende la modellazione dinamica un aspetto di primaria importanza per verificare l'affidabilità del ciclo di recupero e per identificare eventuali colli di bottiglia durante i transitori.

La prima parte del lavoro consiste in un design preliminare dell'intero sistema ICE-ORC, in tutte le sue componenti principali: motore a combustione interna, scambiatori di calore (evaporatore, condensatore..), serbatoio, pompa e turbina. Per quanto riguarda quest'ultima, è stato sviluppato un codice 0D in grado di stimare le prestazioni off-design di turbogeneratori di piccola taglia. Il modello dell'intero impianto è stato implementato utilizzando il linguaggio di modellazione tool-independent Modelica, e simulato in ambiente Dymola. Nella seconda parte invece vengono definiti obiettivi e strategia di controllo, attraverso lo studio delle principali dinamiche del sistema accoppiato. Il modello completo, inoltre, è stato utilizzato per trovare i valori ottimi dei set point delle variabili controllate: tale processo non è banale senza l'utilizzo di un modello di dettaglio completo, a causa della complessa configurazione dell'ORC e dell'interazione fra i due cicli termodinamici. Infine, è stata implementata una semplice configurazione di controllo con due controllori PI, testati su due condizioni di carico differenti.

Parole chiave: Organic Rankine Cycle, modellazione dinamica, Modelica, controllo ottimo.

Introduction

Internal Combustion Engines (ICE) are the major source of motive power in the world, due to higher power density and lower costs if compared with other technologies, and this prospective for the future is still valid, even after the recent economical crisis. However, high uncertainty on fuel prices and future carbon dioxide emission limits are creating a renewed interest in methods to increase engines thermal efficiency beyond the limit of in-cylinder techniques.

Due to technological reasons, indeed, around 60% of the fuel energy is still lost as waste heat through the coolant circuit or the exhaust gases. Taking into account also that increasingly stringent emissions regulations are causing engine manufacturers to limit combustion temperatures and pressures, improving ICE technology is not enough, and other innovative solutions should be developed to achieve a higher overall efficiency. Many researchers recognize that Waste Heat Recovery (WHR) from engines has the potential to decrease fuel consumption without increasing emissions, while the most suitable technology is the Organic Rankine Cycle (ORC). ORC systems are able to satisfy all the requirements that an on-board application needs: simplicity, small dimensions and lightness of the equipment, eco-friendly and non toxicity of the working fluid [1]. Another primary advantage of the ORC is the use of widely available and affordable components, thanks to the similarities with refrigeration systems.

From the economical point of view, the break even point of the combined system can be expressed as the ratio between the ORC net power output and the engine power, and its estimated value is 5%: this requirement has to be fulfilled at the design point, and possibly also in off-design operating condition, within the imposed bounds.

Before starting with the dynamic modelling, it is necessary to carry out the architecture of the WHR unit. The available thermal sources of the WHR unit are the exhaust gases, the Exhaust Gases Recirculation (EGR) cooler, the turbocharger intercooler and the engine coolant. The former two are the most interesting: the higher outlet temperatures make them more thermodynamically attractive when viewed from the exergy perspective. This results in a higher theoretical efficiency gain when coupled to a primary engine. About the gas recirculation, the preferred

practice is to recycle the exhaust gas from upstream of the turbine to downstream of the compressor (or downstream of the inter-cooler if applicable), i.e. a high pressure loop EGR [9] is generally realised. This implies that the temperature here available is much higher than that at the turbine outlet. Despite the higher complexity, both the exhaust and recirculated gases are used by the ORC because the Diesel engine high efficiency makes the usage of only one of them less attractive.

Another important choice to be made is the working fluid selection, because the efficiency of the ORC varies considerably with the thermodynamic properties of the working fluid. A lot of different fluids are available, but few of them fulfill all the requirements of the application. For instance, hydrocarbons like decane and xylenes show a higher overall thermal efficiency and a good thermal stability. However, they show a high inflammability, toxicity and GWP, so that they can not be used for mobile automotive application. Considering the temperature of exhaust gases (between 250 °C and 350 °C), the most promising fluid seems to be the MM. Thus, it has been considered for the design of the WHR unit.

The selection of the expander architecture, among radial and axial turbine or scroll expander, is another critical choice. An axial architecture has been considered as a starting point. For dynamic simulation purposes, its performances in terms of reduced mass flow and isentropic efficiency play a key role, because the combined ICE-ORC system often operates in off-design condition. A first version of an off-design code has been developed, which gives mass flow rate and isentropic turbine efficiency as a function of inlet total condition and outlet pressure.

Another degree of freedom of the design is the coupling between the ORC turbo expander and truck power-train. The net power generated by the Rankine cycle can be directly supplied to the engine shaft by means of a belt or gearbox, or be used in combination with a generator to produce electricity. In this work the first option has been explored, because it is deemed more advantageous from the economical point of view.

Once the system has been designed in all its components, the complete dynamic model has been implemented in Modelica language. This has required the coding of new components, while others have been taken from other libraries.

Since the system is highly non linear and the off-design conditions are not trivial to calculate, the dynamic model has been used to catch the optimal values of the controlled variables which respect at the same time the system constraints. In particular, these concern the thermal stability of the working fluid and the correct operation of all the ORC components. The chosen controlled variables are the degree of superheating and the exhaust gases temperature at the evaporator outlet: the former is a key issue when controlling an ORC system, as fluid decomposition compromise cycle efficiency and component safety [28]; the latter guarantees the correct operation of the SCR system on the exhaust gases line.

Finally, a control architecture is proposed and tested. First, the non-linear system has been linearised, so that the control theory for LTI systems can be applied. Then, a static decoupler and two PI control loops have been tuned and tested with two different truck's velocity profile.

Thesis structure

This work is structured in the following chapters:

- **Chapter 1 - State of the art**: presentation of the previous work concerning WHR from diesel engine and a review of the design methodologies for ORC systems;
- **Chapter 2 - Internal combustion engine**: exhaustive description of the engine model and calibration;
- **Chapter 3 - ORC preliminary design**: description of the cycle configuration adopted, of the selection of the working fluid, and of the design of all system's components;
- **Chapter 4 - ICORC library**: brief description of the key features of Modelica language and of the Modelica libraries and packages used or developed for the present work;
- **Chapter 5 - Optimal off-design operation**: off-design conditions analysis, and description of optimal set-point of the controller in the operating range of the system;
- **Chapter 6 - Control system design**: design and validation process of the control system;
- **Conclusion and future developments**: final conclusions based on the achieved results and recommendations for the future research;
- **Appendix A - Engine complete model**: complete report of the diesel engine model used in this work.

Chapter 1

State of the art of WHR systems for heavy duty trucks

Growing concerns regards air pollution and the first oil crisis in early 70's pushed researchers to find viable solutions to improve IC engines' performance.

Nowadays Diesel cycle efficiency has arguably reached his maximum. One solution to significantly reduce the CO_2 emission is to try to recover as much as possible the heat rejected into the environment by the engine. A review of the open literature concerning Waste Heat Recovery (WHR) system on board of trucks shows that IC engine exhaust has sufficient exergy to justify implementation of a secondary cycle. There are several technology that can be used to convert medium temperature thermal energy into useful energy: thermodynamic system like the Rankine cycle, the open Brayton cycle, the Stirling cycle, the Kalina cycle or thermoelectric system, that directly convert thermal energy into electrical energy. Among them, ORC provides an attractive combination of efficiency and affordability for engine exhaust WHR.

The next section is a chronological summary of the complete and exhaustive review of ORC for waste heat recovery from internal combustion engine exhaust that can be found in [4] and [5].

1.1 Previous works

The very first attempt was made in 1976 by Patel and Doyle, who designed an ORC whose turbine was coupled through a gear box with a long haul truck engine. The working fluid was Flurinol-50 and they used a three-stage axial turbine. First results were encouraging: the ORC equipped truck demonstrated a 13% increase in maximum power output along with a 15% improvement in fuel economy.

On of the first problem reserchers have faced is the choice of the working fluid. During the 80's Marciniak and Bailey compared different working fluid with water (toluene and RC-1), and they verified that with low temperature hot sources

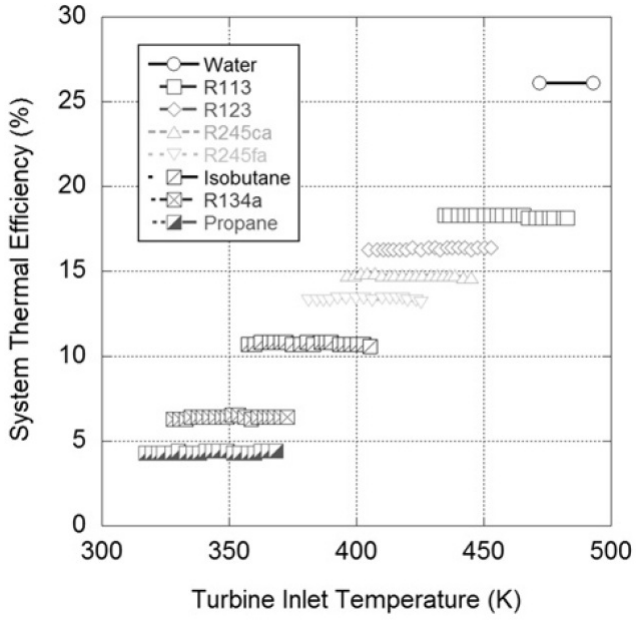

Figure 1.1: Cycle efficiency as function of working fluids

organic fluids perform better than water. The reasons of this behavior has been explained later. In 1984 Angelino et al. analyzed the performances of 14 different ORC systems, showing a small increase as the working fluid's molecular weight increases.

In 1997 Hung discovered that working fluids with larger vaporization enthalpy heat result in inefficient operation since the condenser rejects much of the fluid energy. This is typical for fluids having the hydrogen bonds such as water, ammonia and ethanol: the slope of their saturated vapour line is negative, and they are called "wet". On the other hand, organic fluids in general show a positive slope of the saturated vapour line, and they are called "dry". This fact eliminates the concerns of damage on turbine blades caused by the presence of liquid droplets at the end of the expansion. Hung argued that this property of dry or isentropic fluids would reduce the area of net work in the T-s diagram, but this aspect weakly affects cycle efficiency. In addition, for given evaporator and condenser temperatures, higher critical temperature working fluids exhibit superior first-law efficiency. This result was confirmed ten years later by Mago et al., whose results are presented in Fig. 1.1.

About working fluid choice, we can conclude that it is strictly dependent on the available temperatures of the hot source: for instance, in 1995 Larjola discovered that an ORC with toluene as working fluid achieves the highest efficiency for a thermal source at 425 °C, while in 2007 Quoilin stated that with source temperatures between 100 °C and 200 °C R-123 is the best options. However, the cycle

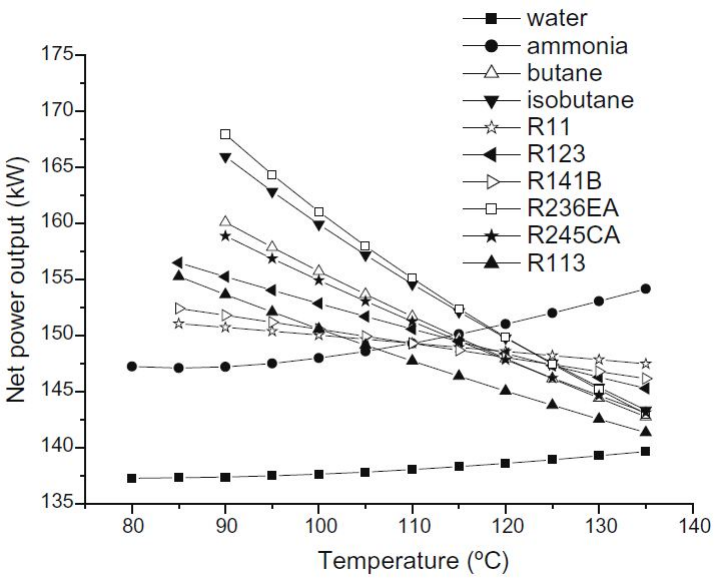

Figure 1.2: Variation of net power output with various turbine inlet temperature under the respective optimal pressure

designer must choose a fluid that also fulfills environmental and sustainability issues.

During the design process, two of the main operational parameters to be optimized are the Turbine Inlet Temperature (TIT) and the evaporation pressure. About the TIT, or the degree of superheating of the fluid in sub critical cycles, in 2005 El Chammas and Clodic demonstrated that dry or isentropic fluids achieve similar or lower efficiencies with increasing superheat at the turbine inlet, while the cycle efficiency increases for wet fluids such as water. The same result was achieved by Yiping Dai et al. [6], whose results are shown in Fig. 1.2.

This phenomenon is due to the fact that the high molecular weight causes a small enthalpy drop over the expansion in the turbine, so that the condenser has to reject a large amount of the heat entering the cycle. This fact would even be worse with a higher superheating, decreasing cycle efficiency. Thermodynamic analysis suggests to minimize the degree of superheating, even to set it equal to 0 °C, but in order to prevent liquid droplets from entering the turbine rotor a minimum temperature difference must be provided [1].

The same study stated that Rankine cycle efficiency increases for higher operating pressures. However, they mentioned that manufacturers must weight these benefits against mechanical and dynamic aspects and costs of the heat exchangers: the higher the maximum cycle pressure, the higher the thickness of tubes/plates, causing higher costs and system thermal inertia. Moreover, in the case of PHEs, a

maximum pressure difference between the two flows is prescribed in order to avoid the "peaking" phenomena, which occurs when plates bend causing a non-uniform distribution of the mass flow between the channels.

To avoid the problem of releasing too much heat in the condenser a possible solution is the regenerative cycle. This configuration leads to a higher cycle efficiency but to a lower heat recovery efficiency, which means a similar overall first principle efficiency. This result was confirmed in 2010 by Vaja and Gambaratta: comparing a regenerative and a simple ORC recovering heat from a 12 cylinder supercharged natural gas engine with benzene as working fluid, the first configuration achieved a 12.5% efficiency, while the second 11.4%. However, the choice between the two configurations is up to the cycle designer.

Together with the working fluid selection, the other crucial aspect of the WHR unit design on board of a truck is the choice of the expander. In general, its isentropic efficiency must be at least 50%-60% in order to achieve sufficient overall conversion efficiency, as reported in [1]. The available options are several: radial or axial turbines and rotary, piston, scroll or screw expanders.

In 2006 Leibowitz et al. suggested the use of a twin-screw type machine, but recent improvements in mini steam turbine keep open this possibility. In the same article authors noted that the high rotational speed of turbines, required at small power capacity, implies high ratio gearboxes and expensive lubrication system. The problem can be partially solved if the working fluid is itself a good lubricant, so that an external lubrication circuit is not necessary.

Wang et al.[4] suggested that the expander choice must be based upon the coupling with the primary engine: turbine-type expanders are preferable when the energy generated is converted in electrical energy because of the relative higher overall efficiency achievable; reciprocating expanders seems to be more appropriate for mechanical coupling direct to the crank shaft, especially for on-board application, where the thermal source conditions are variable, by reason of its flexibility in operation. The former option is suitable if the on-board electrical network consumption is higher than 4 kW [2], otherwise it leads to higher extra weight and costs because of generator and batteries and could be convenient only for a hybrid system.

At a higher level, the cycle designer must choose the thermal sources for which perform heat recovery: the exhaust gases, the EGR cooler, the turbocharger intercooler and the engine coolant. In their review Wang et al.[4] reported some plant configurations, shown in Fig. 1.3.

From the exergy point of view exhaust gases and EGR circuit are the most attractive thermal sources, thanks to their high temperatures. The investigation of Teng et al. indicates that heat recovery from Turbocharger Air Cooler is feasible

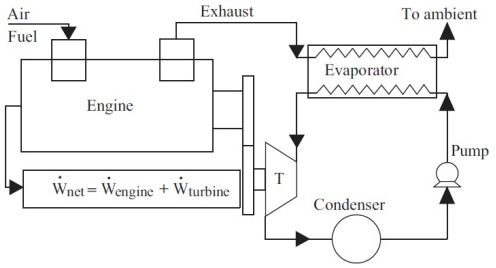

(a) Simple recovery cycle from exhaust gases

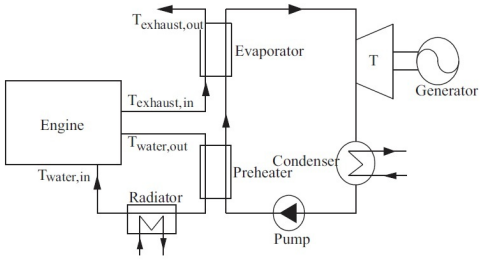

(b) Recovery cycle with pre-heater

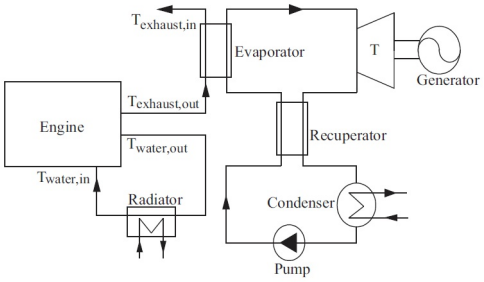

(c) Recovery cycle with pre-heater and recuperator

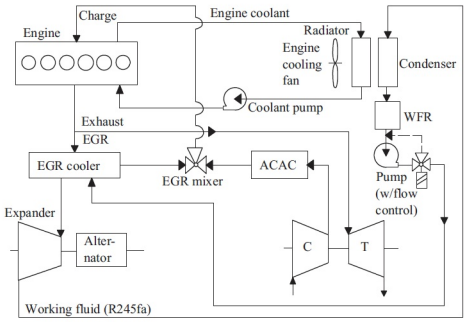

(d) Recovery cycle from EGR gases

Figure 1.3: Recovery cycle configurations

too, but the complexity of the system increases dramatically. About the possibility of pre-heating the working fluid with another source such as the engine's cooling circuit, the previous consideration about the regenerative cycle is still valid. More recently Colonna et al.[1] investigated a recovery cycle exploiting the thermal energy of the exhaust gases and EGR circuit. The powerplant circuit is represented in Fig 1.4. The results are better than those reported in [2] (9.6 kW against 3.5-6.5 kW), but the control system of the two heat exchangers in parallel seems to be more challenging.

In 2010 Espinosa et al. discussed about the optimal ORC configuration for WHR on commercial trucks [2]. They mentioned that exhaust gases are the most feasible source of waste heat, since simultaneous WHR from both EGR and the exhaust line adds complexity and increases costs. Moreover, a substitution of EGR technology is foreseeable, especially in Europe, due to decreasing emission limits that can be achieved only with after-treatment technologies.

In the same article the authors highlighted the principal constraints for an ORC on-board application. First of all they presented a statistic of the engine operating points for a long haul truck travelling on a predominantly flat highway, shown in Fig. 1.5; evaluating the most appropriate engine design point is a key

issue for the ORC sizing procedure.

Moreover, they also investigated the possible options for low-grade heat rejection. This is a key issue because the implementation of a WHR system increases by more than 25% the thermal load at the truck radiator. In fact, a portion of the exhaust gases energy content is absorbed by the evaporator instead of being rejected through the muffler, and due to the low conversion efficiency of the ORC system it has to be mostly rejected through the truck radiator.

The first option is an air-cooled condenser. This is the most promising heat rejection system due to its higher efficiency but at the same time it presents two problems: the additional amount of working fluid required, which can be problematic for certain fluid (high ODP, GWP or inflammability), and the placement of the air-cooled condenser. To avoid aerodynamic impacts, it can be placed in front of the existing cooling system, thanks to the fact that the cooling system of the engine is usually oversized to face the worst scenario. Nevertheless, when the engine load increases it could happen that the cooling system is not able to reject heat from both the engine and the ORC system, so that the recovery cycle must be disengaged.

The second option is the indirect cooling: it allows a small working fluid loop but decreases efficiency by integrating a second temperature difference in the additional heat exchanger.

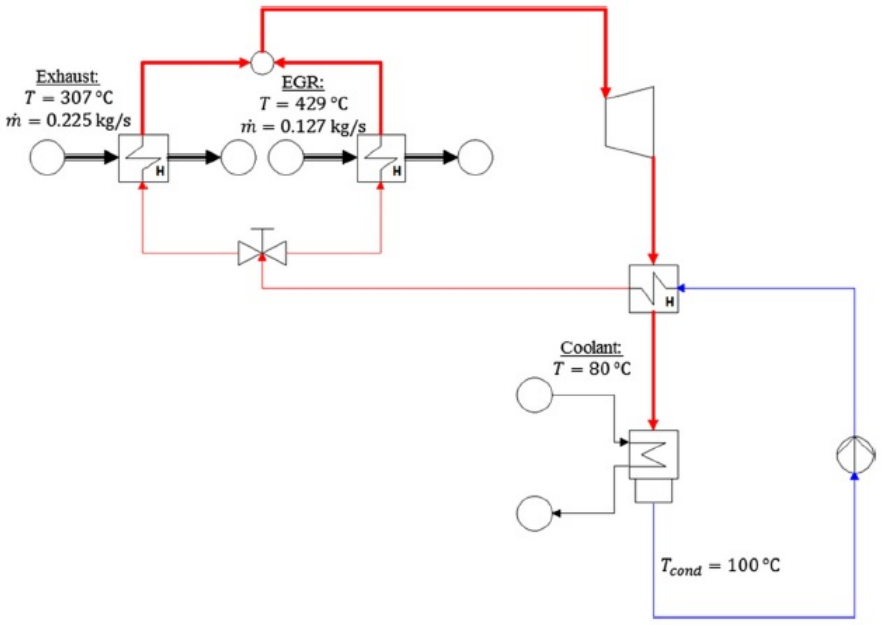

Figure 1.4: Recovery cycle with two heat sources connected in parallel to the ORC turbogenerator

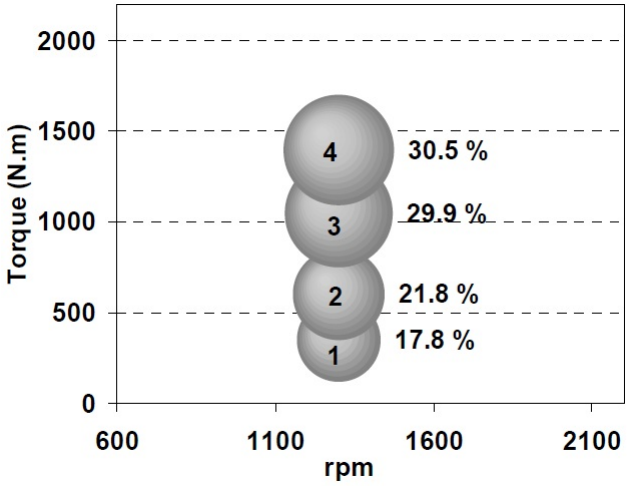

Figure 1.5: Engine operating points and time-weighted factors for a highway route

Another important aspect is the pressure drop of the exhaust gases in the evaporator, which increases the back-pressure of the engine turbocharger. Despite the fact that it should be designed to limit these pressure drops, a by-pass valve is required to avoid large back-pressures when the ORC system is not running.

One year later, in 2011, the same authors investigated the transient behaviour of an ORC unit, a first step on control assessment. They built a 1D model of all the heat exchanger and a 0D model for turbine and pump, used to simulate the start-up of the ORC unit. The evaporator by-pass, the expander by-pass and the pump speed are considered as the main drivers to control the WHR system of a truck. The expander speed can be controlled just in case of the presence of an electric generator, while when considering a mechanical connection to the engine, the turbine speed is imposed by the rotational speed of the engine. Their conclusions stated that the evaporator by-pass time response is slow, compared to the pump speed control and the expander by-pass control. Among the second and third options, the expander by-pass has a stronger influence on the evaporation pressure, while the pump speed imposes the superheating.

In the last two years Peralez et al. published two interesting articles focused on the control optimization of the coupled ICE-ORC system, considered essential to attain satisfactory performances over a broad range of operating conditions.

In the first one [28] the authors underlined the importance of a model-based approach to improve the baseline control strategy. In particular, an interesting simplified model is used to describe the heat exchangers dynamic: a moving-boundary (MB) approach with only three state variables is used to predict the

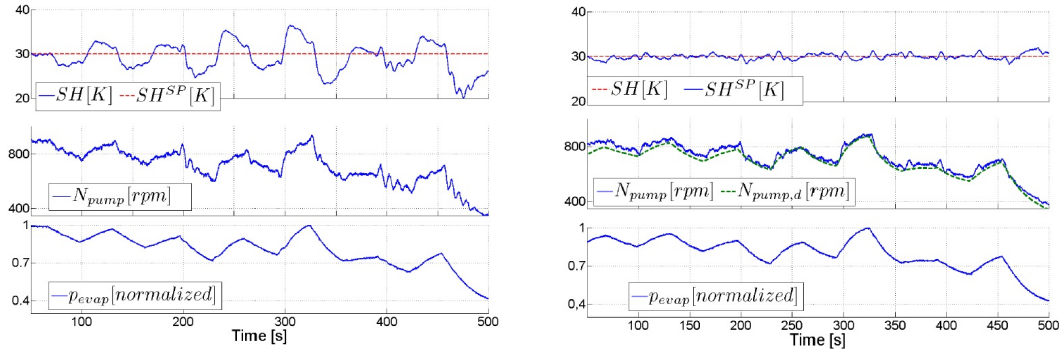

(a) PID alone

(b) PID with dynamic inverse model

Figure 1.6: PID alone vs. Dynamic inverse

average wall temperatures of the heat exchangers in the subcooled, two phases and superheated regions, while the fluid is considered to be in thermal equilibrium with the wall. With this approach they were able to catch the slow evaporator dynamics, the most important information for control design purpose.

The main objective of the control system is to maximize the mechanical power at the turbine shaft. For this purpose, the principal controlled variable is the superheating at the evaporator outlet, which must be kept as low as possible to ensure good ORC efficiency, but at the same time above a certain level to prevent the formation of droplets at the turbine inlet. The use of an inverse model has significant advantages in control performance compared with a gain-scheduled PID, as shown in Fig. 1.6.

In the second one [29] the Dynamic Programming Algorithm is used to optimize the control strategy of the ORC system doing a given vehicle mission. The main outcome of this research is that the solution of the optimal control problem could be useful in order to account for the transient behaviour of the system during the initial design stage.

1.2 Review

As stated in [4], the design process of the ORC unit mainly depends on the characteristics and rated power of the primary engine. However, we can highlight some useful consideration:

- the choice of the ORC architecture and especially of the thermal sources exploited is the first step of the design process. A compromise exists between high efficient configuration and easy and reliable control implementation;
- the working fluid choice is strictly dependent on the temperature range of the exploited thermal sources, but some constraints must be satisfied, such as:
    1. low or even zero ODP and GWP value;
    2. non toxicity;
    3. non inflammability;
    4. positive or "isentropic" slope of saturated vapour line.
- the turbine efficiency should be higher than 60% to achieve acceptable overall conversion results, regardless of the expander configuration and recovered energy usage;
- the condenser position has a strong influence on global performances: the air-cooled condenser is more efficient but tends to require higher heat transfer area due to low heat transfer coefficient. Moreover, ORC should be disengaged at engine full load if the cooling fan is not able to reject heat from both systems;
- the degree of superheating has to be minimized;
- the available control variables are the pump speed and the expander by-pass valve opening, that have a faster dynamic, and the evaporator by-pass valve opening, which shows a slower dynamic.

Chapter 2

Internal combustion engine

The first step of the work consists of modelling the internal combustion engine, because it represents the primary thermal source for the ORC. The turbine outlet and EGR circuit temperatures and mass flows are the most important engine parameters that affect the whole design process. For this reason the model should reproduce the performance of modern engines, especially considering the latest efficiency improvements and low emissions achieved in heavy duty ICE. Moreover, a trustworthy model is required not only during the design process but also during the simulation of the combined cycle, in order to test the effectiveness of the control system.

2.1 Original model

The engine model used in this work is based on the lumped parameter model reported in [7]. It is a 6 cylinders heavy duty engine with a displaced volume of 12.74 liters, which represents a typical truck engine for industrial applications. The model includes also the Variable Geometry Turbocharger (VGT) and the Exhaust Gas Recirculation (EGR) circuit, a recent technology introduced to fulfill the emission limits: the EGR valve that connects the intake manifold and the exhaust manifold allows a portion of combustion products to be recirculated, so that the formation of NO_x decreases. A complete description of the EGR system can be found in [9], while a scheme of the engine is reported in Fig. 2.1.

The model describes the dynamic response of the manifold pressures, turbocharger, EGR and actuators, and the number of state variables has been limited to eight in order to obtain short simulation times. The kinetic of combustion process is considered infinitely fast and the chemical reactions completely shifted towards products, so that it has no dynamics and all the fuel injected is fully oxidized. With regard to Fig. 2.1, the model in state-space form is:

$$\begin{cases} \dot{x} = f\left(x, u\right) \\ x = \left(p_{im}, p_{em}, y_{O_2 im}, y_{O_2 em}, \omega_t, \tilde{u}_{egr1}, \tilde{u}_{egr2}, \tilde{u}_{vgt}\right) \\ u = \left(u_\delta, n_e, u_{egr}, u_{vgt}\right) \end{cases} \tag{2.1}$$

The authors investigated also a more complex model with twelve state variables, but considering the slight difference between the results of the two model when compared with experimental data, they concluded that the inclusion of manifold temperature states, a pressure drop over the intercooler and a control volume before the intercooler do not improve the model accuracy. Note that model parameters have been estimated using weighted least-squares optimization procedure against both stationary and dynamic measurements, and the model shows a mean relative error of 5.8% or lower for all measured variables.

Despite the fact that the model objectives are system analysis, simulation and development of model-based control systems for ICEs, it is suitable also for WHR purposes, thanks to its completeness, accuracy and short simulation times.

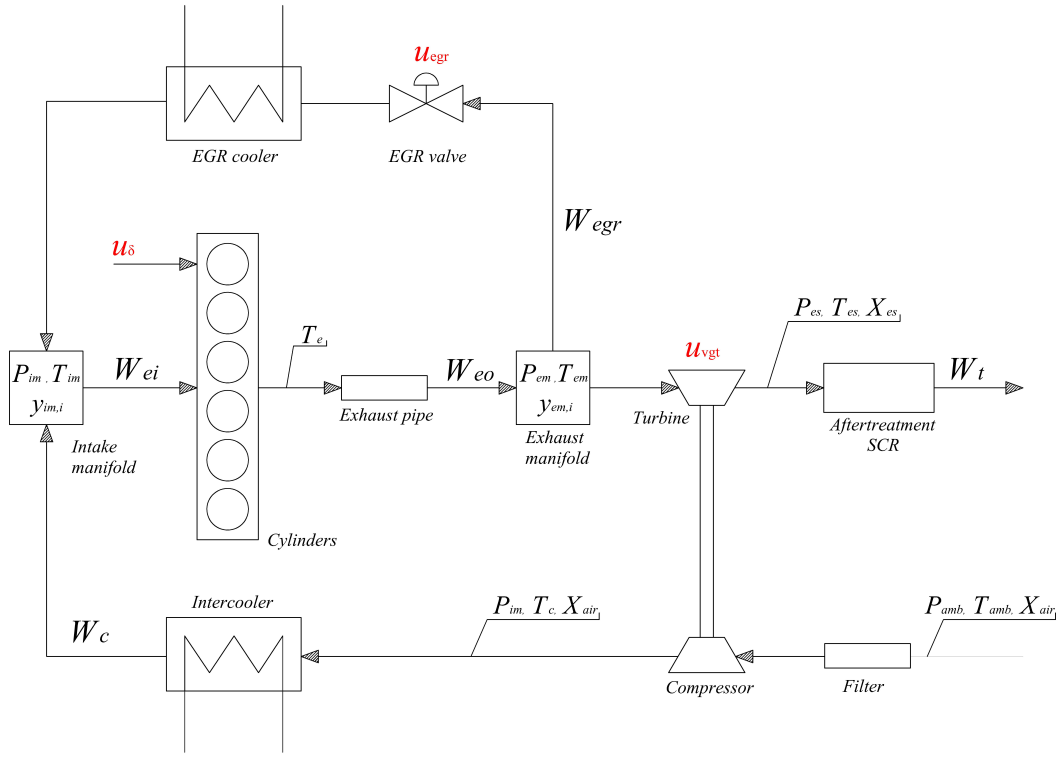

Figure 2.1: Reference scheme of the adopted engine model

2.2 Model extension and tuning

In order to study the dynamic of the add-on ORC unit, the previous model had to be extended in order to calculate turbine outlet conditions, in terms of mass flow, temperature and composition. Later, thanks to the experimental data made available by DAF Trucks N.V., the model components have been tuned using a weighted least-squares error minimization approach. DAF Trucks N.V. provided both steady-state experimental data about 9 operational points at various engine load and transient data. These data refer to the Paccar MX-13 Euro 6, one of the latest engine produced by the company.

2.2.1 Model extension

First of all, the dynamics of CO_2, N_2, H_2O and Ar concentration at inlet and exhaust manifold have been introduced, so that the enthalpy values of exhaust gases can be correctly evaluated. The air/fuel stochiometric ratio is given in order to evaluate the dynamics of oxygen concentration. Considering a stochiometric combustion of 1 kg of gasoline, the following equations system can be derived:

$$\begin{cases} W_{f,in} = W_{C,f,in} + W_{H,f,in} = 1\,kg \\ \dot{N}_{Ar,in} = \dot{N}_{Ar,out} \\ \dot{N}_{N_2,in} = \dot{N}_{N_2,in} \\ \dot{N}_{CO_2,in} + \dot{N}_{C,f,in} = \dot{N}_{CO_2,out} \\ \dot{N}_{H_2O,in} + 0.5\,\dot{N}_{H,f,in} = \dot{N}_{H_2O,out} \\ \dot{N}_{O_2,in} - \dot{N}_{C,f,in} - 0.25\,\dot{N}_{H,f,in} = 0 \end{cases} \tag{2.2}$$

The gasoline can be considered basically made of carbon and hydrogen atoms, thus the chemical reactions considered are:

$$\begin{cases} C + O_2 \rightarrow CO_2 \\ 2\,H + 0.5\,O_2 \rightarrow H_2O \end{cases}$$

The last equation of 2.2 has only one unknown, the carbon or the hydrogen fraction of the gasoline. The solution is a carbon mass fraction equal to 0.866, which is the expected value for commercial gasoline. Using the fluid data in Tab. 2.1 we can find the values of the oxygen-to fuel, water-to-fuel and carbon dioxide-to-fuel ratios that can be used to write mass balances for each component at inlet and outlet manifold, as reported in Appendix A. The final ratios are shown in Tab. 2.2.

Tables 2.1: Air and gasoline molar and mass composition, molecular weight of the main chemical species in the exhaust

Element	MW g/mol	x_{air} mol/mol	y_{air} mol/mol	x_{gas} mol/mol	y_{gas} mol/mol
Ar	39.944	0.0093	0.0128	0.0000	0.0000
N_2	28.013	0.7809	0.7553	0.0000	0.0000
O_2	32.000	0.2095	0.2315	0.0000	0.0000
CO_2	44.000	0.0003	0.0005	0.0000	0.0000
H_2O	18.016	0.0000	0.0000	0.0000	0.0000
C	12.000	0.0000	0.0000	0.3520	0.8661
H	1.008	0.0000	0.0000	0.6480	0.1339

Tables 2.2: Stochiometric combustion ratios

Ratio	Value kg/kg
$O_2/F\|_{st}$	-3.37227
$H_2O/F\|_{st}$	1.19676
$CO_2/F\|_{st}$	3.17555

Turbocharger outlet temperature is generally calculated on the basis of a guess value of the isentropic efficiency. However, the definition of isentropic efficiency considers that there are no heat losses during the expansion. In other words no temperature drops are taken into account between the temperatures T_{em} and T_{es} (see Fig. 2.1) that are due to heat losses. This assumption leads to errors if experimental data are used to tune η_t. Thus, the outlet temperature is given by a polytropic expansion, whose index n has been tuned accordingly to experimental data of the turbocharger. Under the hypothesis of perfect gas, reasonable in this context, we can write:

$$p\,V^n = p^{1-n}\,T^n = \text{cost} \quad \Rightarrow \quad T_{es} = T_{em}\left(\frac{p_{em}}{p_{es}}\right)^{\frac{1}{n}-1} \tag{2.3}$$

Using inlet and outlet turbocharger temperatures and pressures, the index of the polytropic expansion has been evaluated: the result is $n = 1.26$, as expected between 1 and 1.4, and corresponds to a quasi-adiabatic process. The maximum relative error is 5%.

The last extension of the original model is the introduction of the variable T_{im}. In fact, as stated before, the dynamic of the inlet manifold temperature is not taken into account in [7]. Since the EGR evaporator is outside the engine model, the energy balance at the inlet manifold is introduced, so that the mixing of compressor and EGR flows can be computed as:

$$\begin{cases} y_{in,c} = y_{ref,air} \\ y_{in,egr} = y_{em} \\ y_{ei} = y_{im} \\ p = p_{im} \\ E = V_{im}\,(\rho_{im}\,h_{im} - p_{im}) \\ \dfrac{dE}{dt} = W_{egr}\,h_{egr}(p, T_{in,egr}, y_{in,egr}) + W_c\,h_c(p, T_{in,comp}, y_{in,comp}) - W_{ei}\,h_{ei}(p, T_{im}) \\ T_{in,comp} = \text{cost} \end{cases} \tag{2.4}$$

$$\Rightarrow T_{im} = f(p, h_{ei}, y_{ei})$$

Note that in the previous equations system the only unknowns are the inlet manifold temperature and energy as function of pressure, enthalpy and concentrations. $T_{in,c}$ is the temperature at the intercooler outlet, which according to experimental data is almost constant and represents a tuning parameter.

2.2.2 Model tuning

All the measurements available are shown in Fig. 2.2.

The first part of the tuning process involves ambient condition and geometrical parameters of the engine, that can be found in [38]. Heat capacities are kept constant in the original model, so they have been evaluated as the mean value of the heat capacities inferred by experimental data regarding pressures and temperatures at inlet and outlet manifolds. For instance, at inlet manifold:

$$c_{pa} = \frac{\sum_{i=1}^{9} c_{pa}(T_{im,i}, p_{im,i}, y_{im,i})}{9} \quad \Rightarrow \quad c_{va} = c_{pa} - R^* \quad \Rightarrow \quad \gamma_a = \frac{c_{pa}}{c_{va}} \tag{2.5}$$

The Tab. 2.3 reports the mentioned parameters.

Later on, some of model closure parameters have been changed:

- *inlet manifold*: the mass flow entering the cylinders is function of the volu-

Tables 2.3: Ambient and geometrical engine tuning parameters

	Value
p_{amb}	101 325 Pa
T_{amb}	307.69 K
V_d	0.0129 m^3
r_c	17.7
n_{cyl}	6
γ_a	1.40269
γ_e	1.34462
c_{pa}	999.7 $J\,kg^{-1}\,K^{-1}$
c_{pe}	1115.9 $J\,kg^{-1}\,K^{-1}$
c_{va}	712.7 $J\,kg^{-1}\,K^{-1}$
c_{ve}	829.9 $J\,kg^{-1}\,K^{-1}$

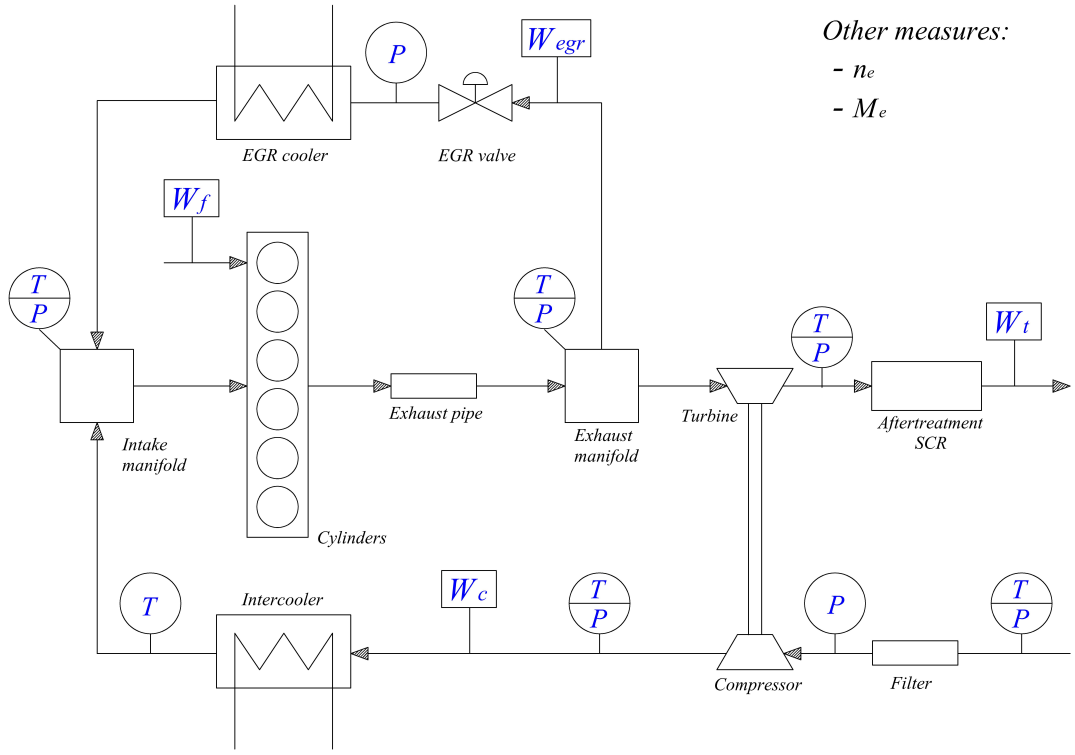

Figure 2.2: Available measures for engine model tuning

metric efficiency through the following equations:

$$W_{ei} = \eta_{vol} \frac{p_{im} V_d n_e}{R_a T_{im} 120} \tag{2.6}$$

$$\eta_{vol} = c_{vol1} \sqrt{p_{im}} + c_{vol2} \sqrt{n_e} + c_{vol3} \tag{2.7}$$

The closure parameters $c_{vol,i}$ have been tuned in order to match the measured mass flow W_{ei}, and the maximum relative deviation is 2.37%.

- *torque*: the engine efficiency is a function of the following set of equations:

$$\begin{cases} M_e = M_{ig} - M_p - M_{fric} \\ M_p = \dfrac{V_d}{4\pi} (p_{em} - p_{im}) \\ M_{ig} = \dfrac{u_\delta 10^{-6} n_{cyl} q_{HV} \eta_{ig}}{4\pi} \\ M_{fric} = \dfrac{V_d}{4\pi} 10^5 (c_{fric1} n_{eratio}^2 + c_{fric2} n_{eratio} + c_{fric3}) \\ n_{eratio} = \dfrac{n_e}{1000} \end{cases} \tag{2.8}$$

The tuning parameters are the mean indicated efficiency η_{ig} and the frictional torque coefficients $c_{fric,i}$, and they have been tuned in order to match the engine efficiency, deduced by experimental data. The maximum relative deviation is 2.4%.

- *cylinder*: the main cylinders section variable is the outlet temperature, which is a complex function of the Seiliger's cycle parameters (for the complete equations set see Appendix A). The two main closure parameters are the compensation factor for non ideal cycles η_{sc} and the total heat transfer coefficient h_{tot} that describes the temperature drop due to heat losses in the exhaust pipes:

$$\begin{cases} T_e = f(\eta_{sc}, \dots) \\ T_{em} = T_{amb} + (T_e - T_{amb}) \exp\left\{ -\frac{h_{tot} \pi d_{pipe} l_{pipe} n_{pipe}}{W_{eo} c_{pe}} \right\} \end{cases} \tag{2.9}$$

The parameters have been tuned to match the measured exhaust manifold temperature, and the maximum relative deviation is 8.5%.

- *compressor*: the compressor efficiency of the original model is given in Fig. 2.3. Assuming that the shape of the map did not change, it has been scaled

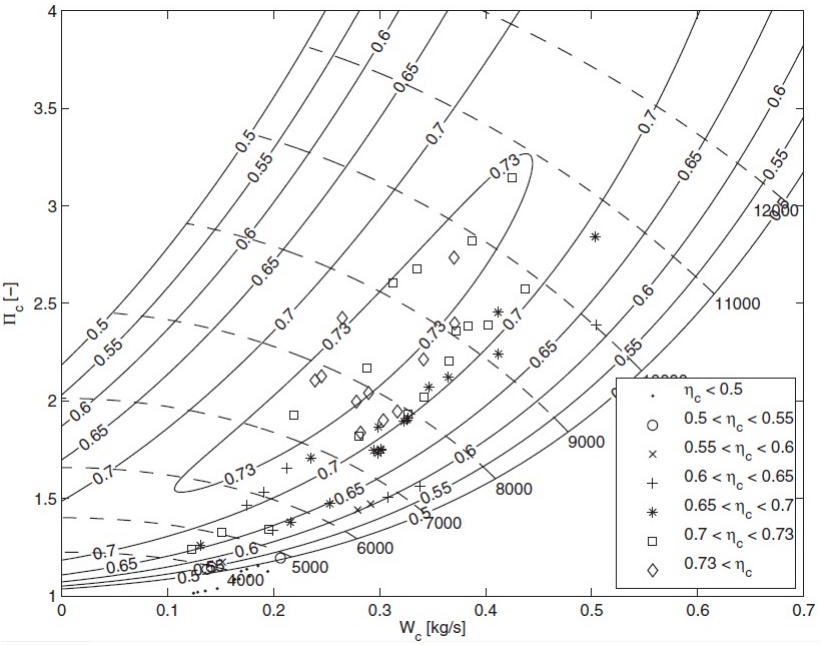

Figure 2.3: Compressor efficiency map

as a function of $\eta_{c,max}$, which appears in the following equation:

$$\eta_c = \eta_{c,max} - \boldsymbol{x}^T \boldsymbol{Q_c}\, \boldsymbol{x} \qquad \text{with} \quad \boldsymbol{Q} = \begin{bmatrix} a_1 & a_3 \\ a_3 & a_2 \end{bmatrix} \quad \text{and} \quad \boldsymbol{x} = \begin{pmatrix} W_c - W_{c,opt} \\ \pi_c - \pi_{c,opt} \end{pmatrix} \tag{2.10}$$

Through the experimental measures the compressor isentropic efficiency can be evaluated, so that $\eta_{c,max}$ has been tuned in order to match the actual value. The maximum relative deviation is 4.4%.

- *turbine*: together with the polytropic expansion index, which has been evaluated in the previous section, the turbine efficiency must be modelled. Since the definition of the isentropic efficiency can not be used due to heat losses during expansion, a different formulation should be adopted. At steady-state we can state that $P_t\, \eta_m = P_c$, so that another efficiency that is approximately equal to η_t can be calculated as:

$$\eta_{tm} = \frac{P_c}{P_{t,is}} = \frac{W_c\, c_{pa}\, (T_c - T_{amb})}{W_t\, c_{pe}\, T_{em} \left(1 - \Pi_t^{\frac{\gamma_e - 1}{\gamma_e}}\right)} = \eta_{tm,max} - c_m (BSR - BSR_{opt})^2 \tag{2.11}$$

As for the compressor, the tuning parameter can be $\eta_{tm,max}$, but the weighted

least-squares error minimization procedure leads to a very high deviation from experimental data. For this reason, $\eta_{tm,max}$ has been modeled as a squared function of the pressure ratio across the turbine, according to the following equation:

$$\eta_{tm} = tm_1 \left(\frac{1}{\Pi_t}\right)^2 + tm_2 \left(\frac{1}{\Pi_t}\right) + tm_3 \tag{2.12}$$

The coefficients tm_1, tm_2 and tm_3 are the tuning parameters and the maximum relative deviation is kept below 10%.

The last two parameters to be tuned are $A_{egr,max}$ and $A_{vgt,max}$. Since the actual effective area of the two valves and their flow characteristic is unknown, their value has been tuned assuming a 50% valve opening around the nominal operating point.

From a dynamic point of view, the main variables to be tuned are the manifolds volumes, which affect the pressure evolution, and the turbocharger moment of inertia. The experimental data of a transient test have been compared with the results of a simulation obtained with the same inputs, i.e. the valves positions, the engine rotational speed and the fuel flow rate. In particular, the pressures and turbocharger speed trends have been monitored, and the results are reported in Fig. 2.4, 2.5 and 2.6.

The offset between experimental and simulation data is due to the different valves characteristic: in particular, the VGT valve position has a strong influence

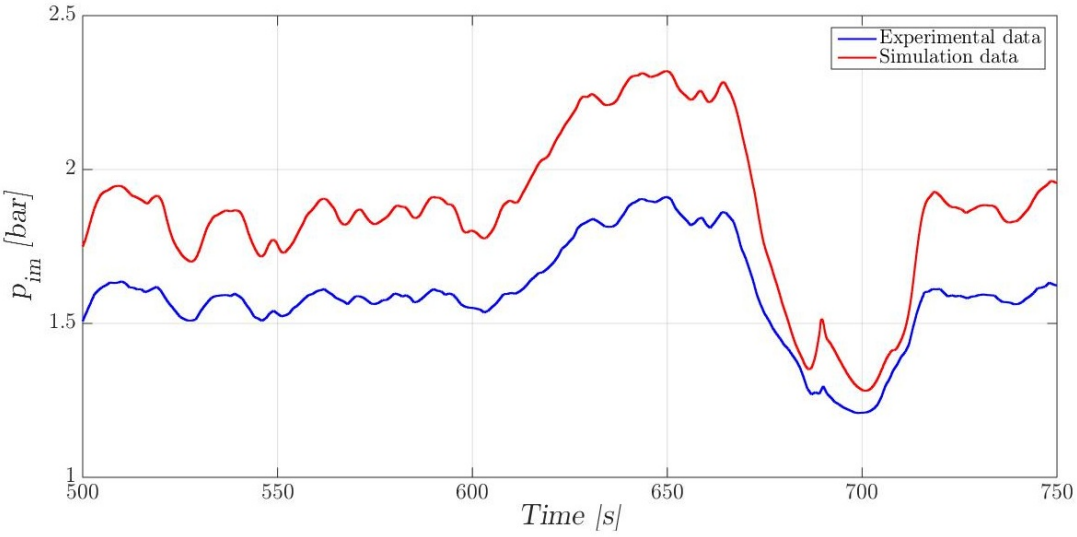

Figure 2.4: Pressure dynamic at the inlet manifold

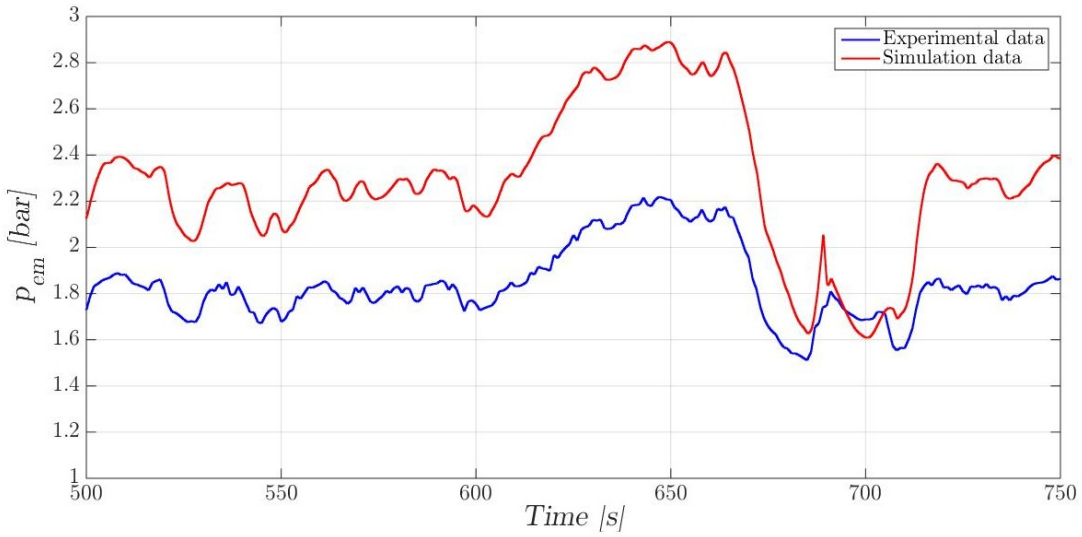

Figure 2.5: Pressure dynamic at the outlet manifold

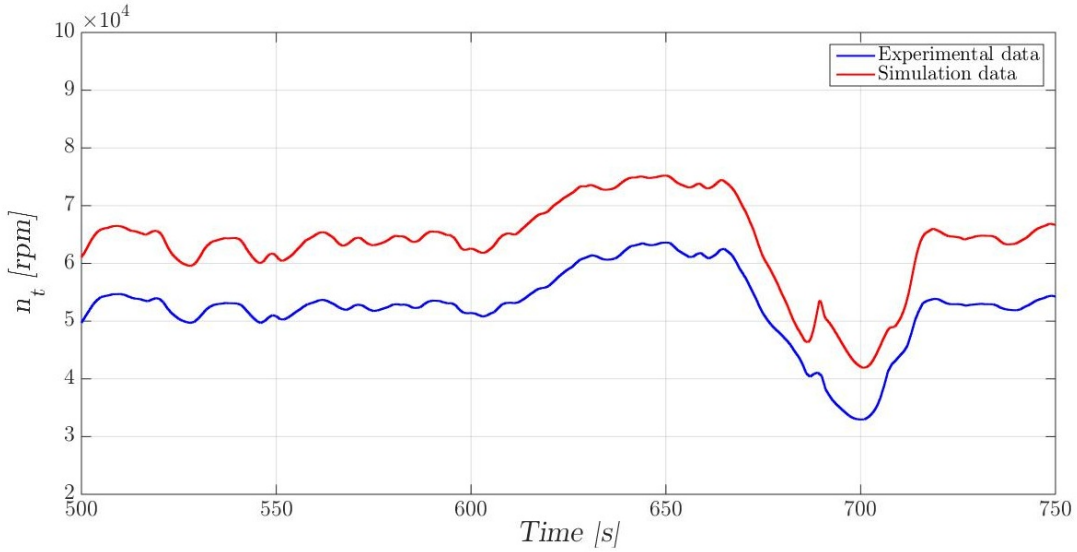

Figure 2.6: Turbocharger rotational speed dynamic

on the pressure level, but peaks and valleys are at the same position. We can conclude that the original model value for V_{im}, V_{em} and n_t are correct.

All the results are reported in Appendix A.

2.3 Control strategy

The engine model has four input variables, as stated in Eq. 2.1: the rotational speed, the fuel mass flow and the opening values of EGR and VGT valves. For this reason a control strategy of the ICE must be introduced.

The controlled variables are the engine torque M_e, the normalized oxygen/fuel ratio λ_{O_2}, the portion of recirculated gas x_{egr}, and turbocharger speed ω_t. The objective is to satisfy the request of the driver while maintaining low emissions, low fuel consumption, and suitable turbocharger speed, controlling EGR and VGT valves opening and modulating fuel injection.

The constraints that the control system has to comply with [16] are here summarized:

1. λ_{O_2} should be greater than a soft limit, a set-point $\lambda_{O_2,set\,point}$, which enables a trade off between emission, fuel consumption, and response time. A low value of λ_{O_2} can lead to a high fraction of unburnt fuel, which causes a high production of smoke and decreases the engine efficiency. $\lambda_{O_2,set\,point}$ is usually between 1.5 and 1.8 at full load and higher at partial load ([9],[13]).

2. λ_{O_2} is not allowed to go below a minimum limit $\lambda_{O_2,min}$, otherwise too much smoke would be produced. $\lambda_{O_2,min}$ is always smaller than $\lambda_{O_2,set\,point}$. A typical value for $\lambda_{O_2,min}$ is 1.3.

3. The set point for EGR-fraction $x_{egr,set\,point}$ is the result of a trade-off between smoke and NO_x production: there will be more NO_x if the EGR-fraction is too low and there will be more smoke if the EGR-fraction is too high. This phenomenon is shown in Fig. 2.7, noticing that the Air-to-Fuel Ratio is inversely proportional to EGR-fraction for a given amount of fuel.

   The value of $x_{egr,set\,point}$ is not univocal, because it depends on local emission limits and on engine design. Some recent studies ([10],[11],[12],[13]) report an optimal value between 10% and 20%, while if NO_x limit is more stringent a higher value is possible.

4. The turbocharger speed is not allowed to exceed a maximum limit, otherwise the turbocharger can be damaged.

5. The pumping loss M_p in stationary points must be minimized in order to decrease the fuel consumption.

In general, the EGR and VGT valves must be controlled together in order to fully utilize their joint effect on engine emission performance [8]. In fact the high pressure EGR loop is only applicable when the turbine upstream pressure is sufficiently higher than the boost pressure: a VGT can effectively provide the

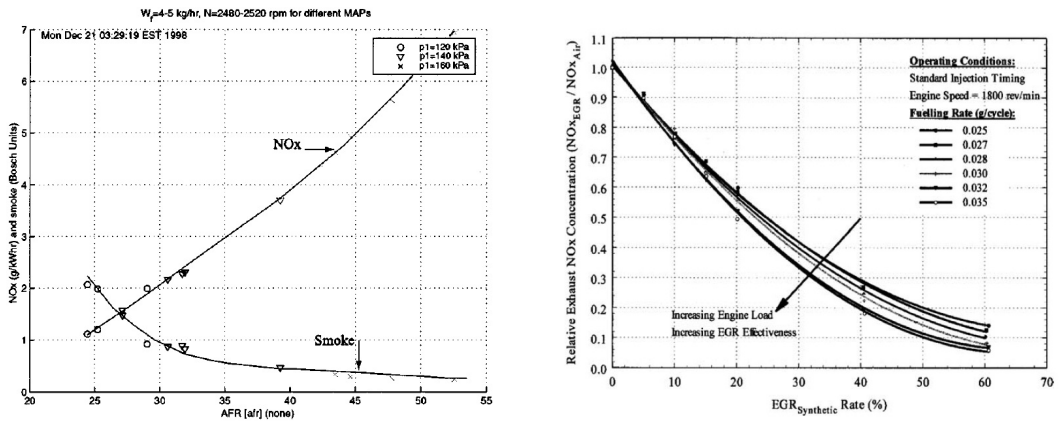

(a) Smoke and NO_x production vs. AFR (b) NO_x production vs. EGR

Figure 2.7: Trade-off between NO_x and smoke production

desired EGR driving pressure without substantially sacrificing the performance of the turbocharged engine. In such systems, the EGR control is closely tied to the VGT control: the shrinking of the flow passage of the turbine nozzles will increase the turbine upstream pressure (p_{em}) and reduce the boost pressure (p_{im}) (see Fig. 2.1) [9], but at the same time also the pressure ratio across the EGR valve.

The optimal point should be found taking into account the local NO_x emission limits: to reach the objectives described above it is possible to increases within the legislated limits the overall NO_x emissions during a defined driving cycle, increasing in this way the thermal efficiency of the engine and thus reducing the fuel consumption. At the same time, due to the monotonically decrease of the NO_x - smoke trade-off curve, this strategy leads to a minimization of the PM emissions as well, as shown in Fig. 2.8.

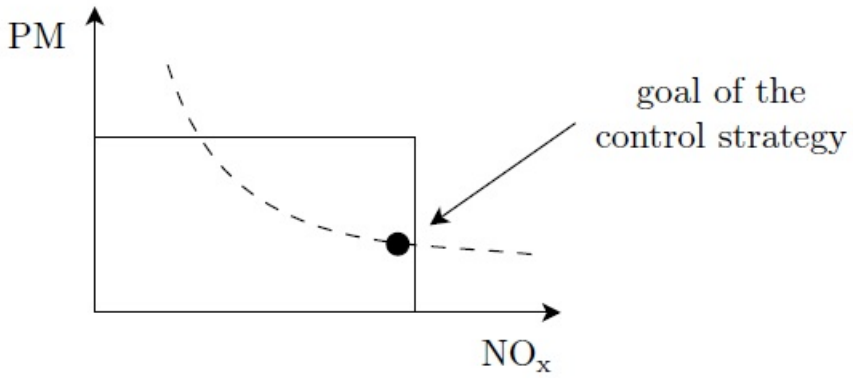

Figure 2.8: Control strategy based on the NO_x - smoke trade - off.

2.4 Engine map creation

The *Simulink* model of the engine is available in Ref. [37]. This model allowed the implementation of an optimization problem in *Matlab* which evaluates the optimal engine control strategy under certain operational constraints. The optimization problem has to be solved for all engine rotational speed and net torque values in the operating range of interest. It can be formulated as follow:

$$max \quad \eta_e\left(u_\delta, u_{egr}, u_{vgt}\right) \quad \text{such that} \quad \begin{cases} M_e = M_{e,req} \\ x_{egr} = x_{egr,opt} = 0.346 \\ \lambda_{O_2} \geq \lambda_{O_2,min} = 1 \\ 0.2 \leq u_{vgt} \leq 1 \\ 0 \leq u_{egr} \leq 1 \\ 0.1 \leq u_{delta} \leq 250 \end{cases} \tag{2.13}$$

Note that to guarantee the existence of an optimal solution that complies the constraints also at low rotational speed and high load (which is a rare situation) the minimum value of λ_{O_2} has been set equal to 1. Furthermore, the engine time constant values are around 1 s, so that the frequencies at which the engine control system works are higher than the frequencies at which ORC control system would work. For this reason the engine is considered as being ideally controlled and represented by algebraic equations, assuming all the variables equal to their set-points.

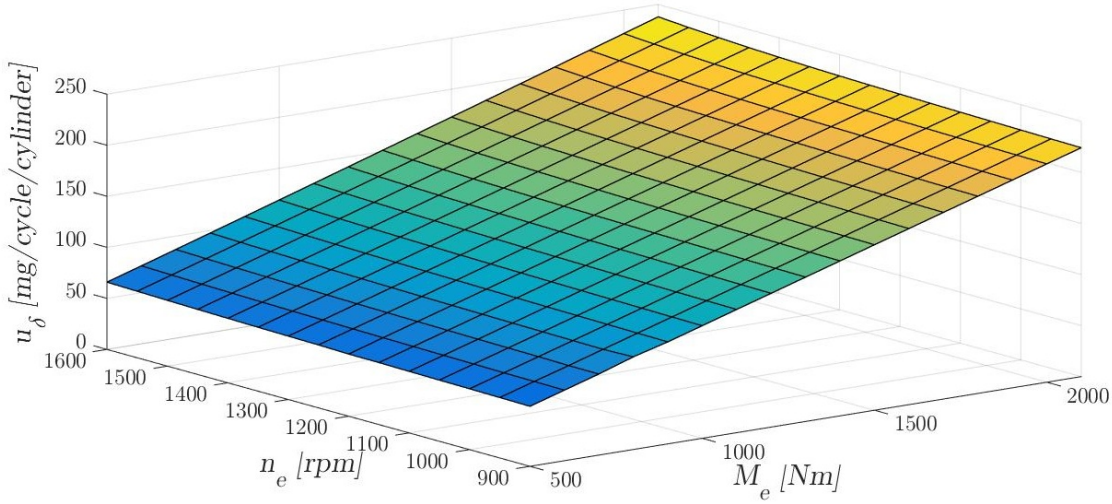

Figure 2.9: Fuel map

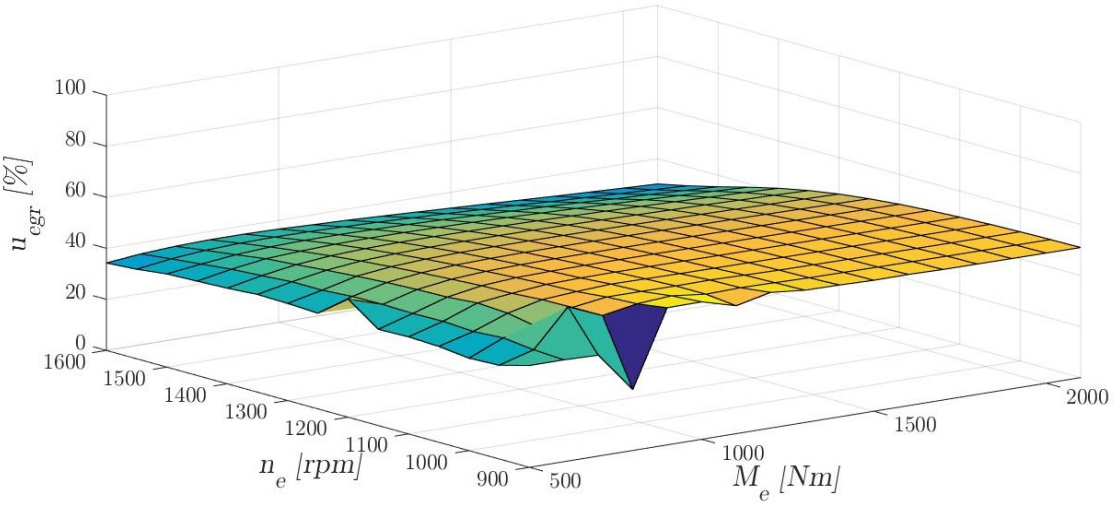

Figure 2.10: EGR valve map

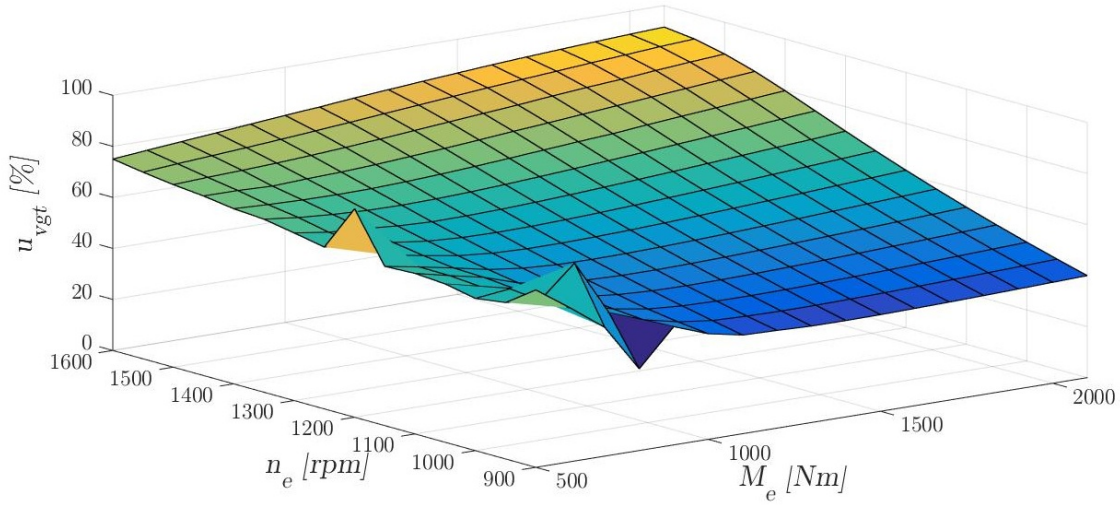

Figure 2.11: VGT valve map

The results of the optimization process are reported in Fig. 2.9, 2.10 and 2.11, while the values of λ_{O2} are reported in Fig. 2.12.

Tab. 2.4 reports the results of the model maps calibration and in particular it shows the relative error of the model predictions regarding the mass flow rates and the temperatures of interest. The maximum model relative error is 8.9%,

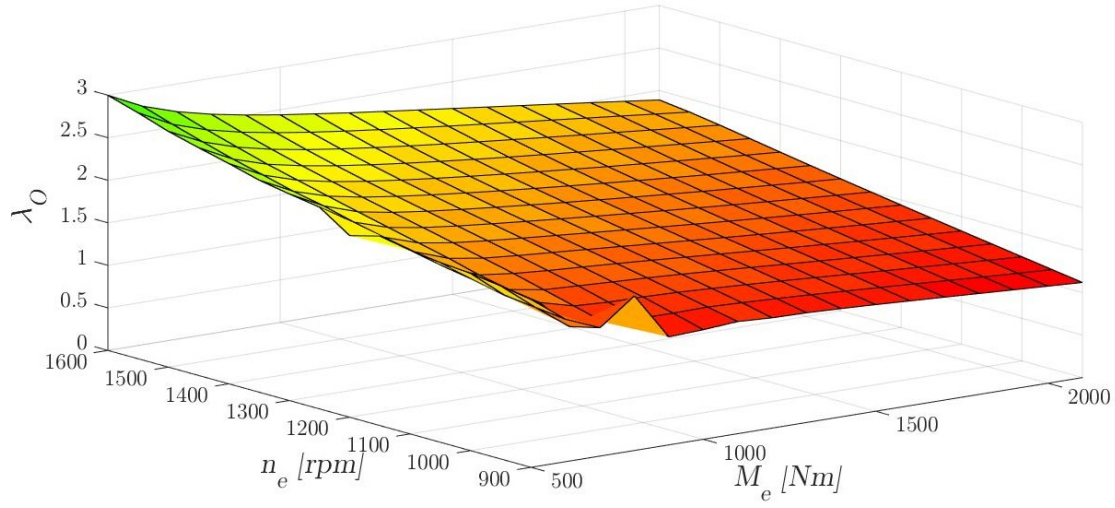

Figure 2.12: λ_{O2} values among the considered operational point

Tables 2.4: Model calibration at different operational points of the engine Paccar MX-13

Point	n rpm	M_e Nm	ΔW_{egr} %	ΔW_t %	ΔW_f %	ΔT_{em} %	ΔT_{es} %
1	1212	800	1.33	1.26	0.15	-5.87	-2.81
2	1212	914	0.99	0.94	0.03	-5.66	-2.66
3	1212	2142	2.40	2.26	0.05	-6.44	-4.03
4	1525	500	4.54	4.06	0.44	-8.93	-5.68
5	1212	500	0.66	0.67	-0.08	-7.22	-2.42
6	1350	583	2.62	2.73	0.16	-6.98	-4.22
7	1350	1070	1.29	1.21	0.08	-5.00	-3.24
8	1250	585	3.82	3.67	0.20	-6.52	-4.56
9	1350	2300	4.50	4.29	0.39	-8.01	-5.78
Δ_{max}	-	-	4.54	4.29	0.44	-8.93	-5.78
Δ_{mean}	-	-	2.46	2.34	0.15	-6.74	-3.93

while the mean error is 3.9%. Considering that the available experimental data are 9 operating points and the range of engine load is wide, the tuning process can be considered satisfactory. Moreover, the difference between the estimated fuel consumption and the actual measured values is much lower than 1%.

Chapter 3

Preliminary design of the WHR unit

This chapter reports the design process of the bottoming cycle. In particular it describes the choice of components, cycle configuration and working fluid, as well as the design of each component.

3.1 Components, cycle configuration and working fluid selection

In order to obtain a reliable estimation of the WHR unit performance a preliminary design of the system components is required. This means that first the cycle configuration must be decided, second an optimization must be performed to evaluate the optimal cycle parameters such as the evaporator pressure and the degree of superheating, and finally all components must be designed. An advanced ORC configuration has been adopted, whose main components are:

- *Evaporators*: the cycle configuration depends on the number of thermal sources that are exploited for heat recovery. In case of heat recovery from exhaust gases only a simple once-through evaporator is sufficient, while in case of heat recovery from both EGR and exhaust gases, the designer has to choose whether to place the two once-through evaporators in series or in parallel. Considering the improvement in ICE efficiency in the latest years, that has considerably decreased the temperature and mass flow of the engine exhaust, a parallel heat exchangers configuration has been preferred. As stated in Chapter 1, no other thermal sources are taken into account due to their low exergy content.

- *Turbine*: it is one of the most critical components of the system. Its design has been carried out simultaneously with the thermodynamic cycle optimization, and realised by means of an in-house mean line code [22]. An axial architecture has been implemented.

- *Condenser*: the rejection of the low grade heat of the ORC unit is a key feature to achieve high performance. The first option is to use the oversized engine water cooling circuit, that allows a condensation temperature of 100 °C. It is a simple but at the same time limiting solution: choosing an air-cooled condenser with a condensation temperature of 60 °C, the mechanical power output doubles. An intermediate solution has been thus adopted: the cooling water can be cooled down till 70 °C in the radiator, then sent to the ORC condenser and finally to the engine jacket. This permits to achieve a condensation temperature of 85 °C. Such a configuration has two main advantages: the mechanical power output of the bottoming cycle increases considerably thanks to a higher pressure ratio across the turbine, on the other end an external cooling circuit is not strictly required, thanks to the feasibility to exploit the oversized radiator [2], maintaining the whole system simple and less expensive. Moreover, the water temperature increase in the jacket is kept around 10 °C, in order to avoid high temperature gradients on the engine structure, that can cause thermal and mechanical stress [34, 574].
- *Regenerator*: as stated in Chapter 1, the adoption of a regenerative cycle with variable temperature thermal sources increases the cycle efficiency but at the same time reduces the heat recovery factor. Despite the cost of the additional PHE and the increase of complexity, a regenerator has been added only on the exhaust circuit due to the following reasons:
  - the EGR cooler should cool down the exhaust recirculating gases as much as possible in order to increase the density at the inlet manifold and so the mass flow entering the cylinders. Hence, the regeneration on this circuit could affect heavily the ICE performance.
  - the exhaust after treatment system (SCR) is a catalyzed reaction chain that reduces the NO_x concentration in the exhaust gases to fulfill the emission regulations. The conversion is mainly a function of the operating temperature of the catalyst and of the NO_2/NO_x ratio, as shown in Fig. 3.1 [14]. Assuming 200 °C as operative temperature and the adoption of noble metal-based high vanadium-content catalyst, a high NO_x conversion can be still reached, allowing at the same time to recovery a large amount of energy from the exhaust gases. Therefore, the aim of the regenerator is to keep the exhaust temperature at the evaporator outlet above 200 °C.
  - the exhaust pressure drop in the evaporator can be smaller due to the reduced heat exchangers area, so that the back pressure at the engine outlet is low.
- *Pump*: a diaphragm pump provides the pressure increase at condenser outlet.

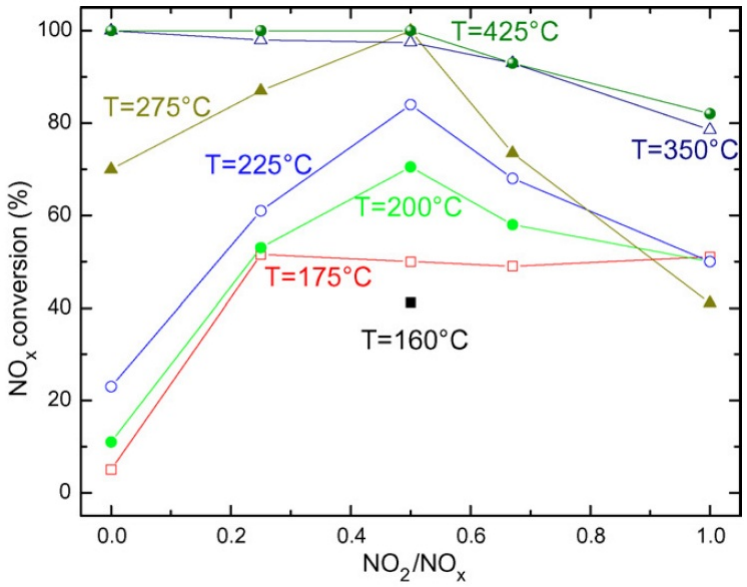

Figure 3.1: Steady state NO_x conversion at 160 °C (full squares), 175 °C (blank squares), 200 °C (full circles), 225 °C (blank circles), 275 °C (full triangles), 350 °C (blank triangles), 425 °C (spheres) vs. NO_2/NO_x feed ratio.

The variation of its rotational speed is a control variable of the ORC unit. During optimization process a constant isentropic efficiency of 65% has been adopted.

- *Tank*: a storage tank is essential during start-up and shut-down procedures. Moreover, it can decouple the high pressure side, i.e. the evaporators, from the low pressure side of the cycle, i.e. the condenser. This feature is fundamental during transient operations, because a variation on the hot or cold thermal source does not affect instantaneously the opposite side of the working fluid circuit.

About the heat exchangers type, once-through PHEs have been chosen in all cases because of their compactness and effectiveness.

An alternative solution could be the adoption of a 2 pressure levels cycle configuration, with two independent pumps. This layout would give a higher first principle efficiency but the small dimensions of the turbine do not allow the adoption of two different expanders or a dual admission expander.

About working fluid selection, the linear siloxane MM (esamethyldisiloxane) has been found as the most suitable for on-board waste heat recovery application. Its main advantages are:

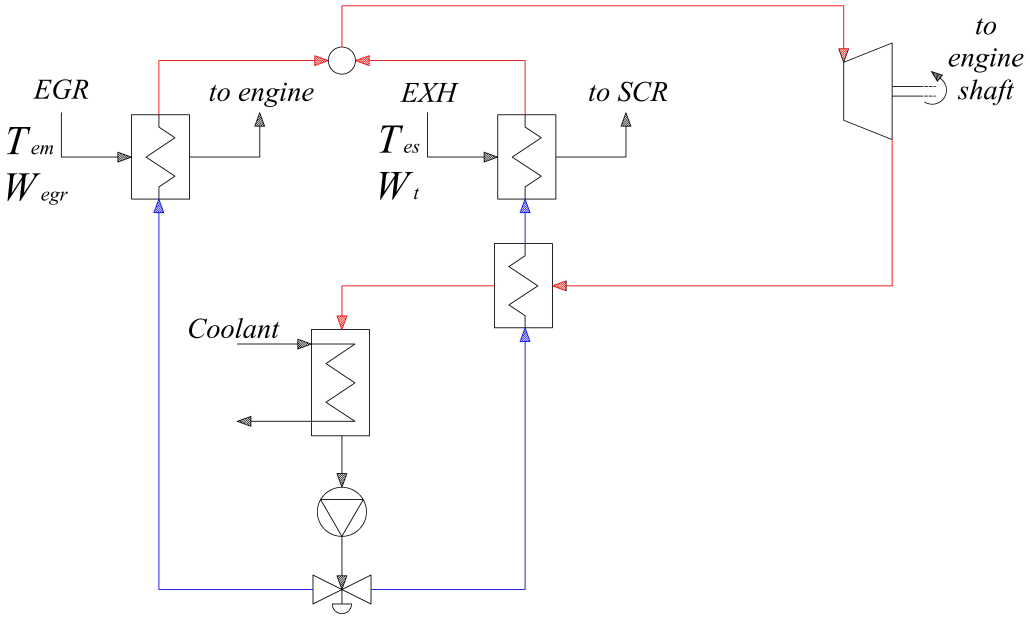

Figure 3.2: ORC components configuration

- low GWP and ODP values, so that it can be used on large scale;
- low inflammability and toxicity;
- lubricant properties, so that an external lubricant system is not required;
- high critical temperature, which allows to achieve higher cycle efficiency, as explained in Chapter 1;
- low critical pressure, in order to decrease the pump power consumption;
- positive slope of the saturated vapour line.

In the following sections the design procedure of all the ORC components will be illustrated.

3.2 ORC optimization

3.2.1 ORCHID_vpe

"ORCHID-vpe" is the acronym of Organic Rankine Cycle Hybrid Integrated Device-Virtual Prototyping Environment, an in-house software whose purpose is to optimize the design of a simple Rankine Cycle together with the turbine design. It has been developed at TU Delft and lately extended within the present work, in order to optimize the main parameters of the non-conventional cycle configuration presented in the previous section.

For a given set of hot sources and pressures, temperatures and geometrical bounds, the code attempts to find the cycle and turbine design that maximize the net mechanical power output, using the genetic algorithm as optimization tool.

The inputs of the design procedure are the following:

- $T_{cond} = 85\,°\text{C}$, condensing temperature;
- $T_{min,exh} = 200\,°\text{C}$, minimum temperature of the exhaust gases at the evaporator outlet;
- $\eta_{is,pump} = 65\%$, pump isentropic efficiency;
- $p_{max} = 18\,\text{bar}$, maximum evaporator pressure;
- $\Delta T_{sh,min} = 5\,°\text{C}$, minimum degree of superheating;
- $\Delta P/P = 1\%$, non dimensional pressure drop;
- $T_{egr} = 400\,°\text{C}$, inlet temperature of EGR thermal source;
- $W_{egr} = 0.066\,\text{kg}\,\text{s}^{-1}$, mass flow rate of the EGR thermal source;
- $T_{exh} = 314\,°\text{C}$, inlet temperature of the exhaust thermal source;
- $W_{exh} = 0.131\,\text{kg}\,\text{s}^{-1}$, mass flow rate of the exhaust thermal source;
- $\{y_{N_2} = 0.723774,\ y_{CO_2} = 0.133025,\ y_{H_2O} = 0.049952,\ y_{Ar} = 0.012266,\ y_{O_2} = 0.080985\}$, composition of the exhaust gases.

A minimum degree of superheating avoids the presence of liquid droplets at the turbine inlet, while the upper bound on the evaporators pressure does not allow a super-critical configuration ($p_{crit,MM} = 19.4\,\text{bar}$) and prevents the "peaking" phenomenon. The thermodynamic conditions of the thermal sources are taken from experimental data, and they correspond to a truck cruise speed of 85 km/h, with an engine load of 101.5 kW

About the expander, a 2 stages axial configuration has been chosen. Other turbine configurations have not been investigated, even if they allow to achieve a higher performance .

To avoid the creation of unfeasible design, the main geometrical/mechanical parameters of the turbine have to satisfy the following constrains:

- $15\,mm \leq D_{in} \leq 25\,mm$;
- $1.8\,mm \leq h_{in} \leq 2.2\,mm$;
- $90000\,rpm \leq \omega_t \leq 150000\,rpm$;

For a given set of optimization variables, the code evaluates as first step the vapour mass flow generated in the two evaporators. Then the external in-house software *"zTurbo"* is called [22], which attempts to design the turbine. If the design is not feasible or some geometrical/mechanical constraints are not satisfied, the solution is discarded.

Initially, multiple solutions are randomly generated by the genetic algorithm to form an initial population, in order to cover the entire range design domain. During each iteration, a portion of the existing population is selected to breed a new generation. When the maximum number of generations has been reached the best solution is selected. In WHR applications the aim of the system is to maximize the mechanical power, hence the cost function of the optimization process is the inverse of the mechanical power output.

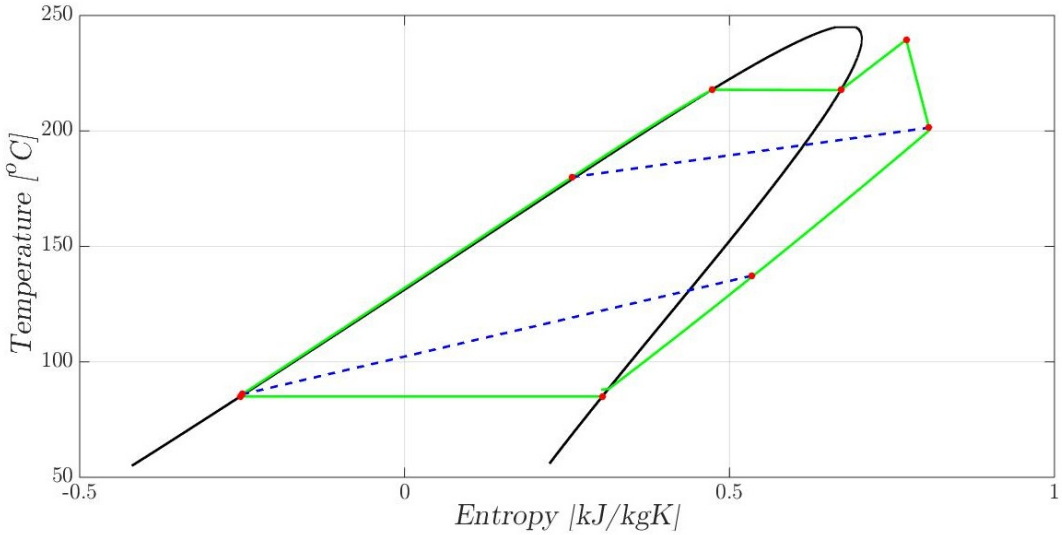

Figure 3.3: T-s diagram of the optimal cycle

It is worth noticing that by fixing a constant isentropic turbine efficiency, the optimal solution in this particular application and with MM as working fluid is to maximize the pressure and to minimize the superheating degree. This result is in agreement with the cycle design "guidelines" presented in Chapter 1, but due to turbine feasibility issues the maximum pressure is not reached, while the bound in the exhaust gases temperature forced the superheating degree to be much higher than the minimum bound.

3.2.2 Optimization results

The optimization process results are reported in Tab. 3.1, Fig. 3.3 and 3.4.

Tables 3.1: Optimization process results

$P_{net,orc}$	4.8	kW
$\eta_{is,tur}$	0.715	—
p_{eva}	12.67	bar
ΔT_{sh}	21.5	°C
w_{orc}	0.11	$\mathrm{kg\,s^{-1}}$
$Q_{eva,EGR}$	20.7	kW
$Q_{eva,EXH}$	15.6	kW

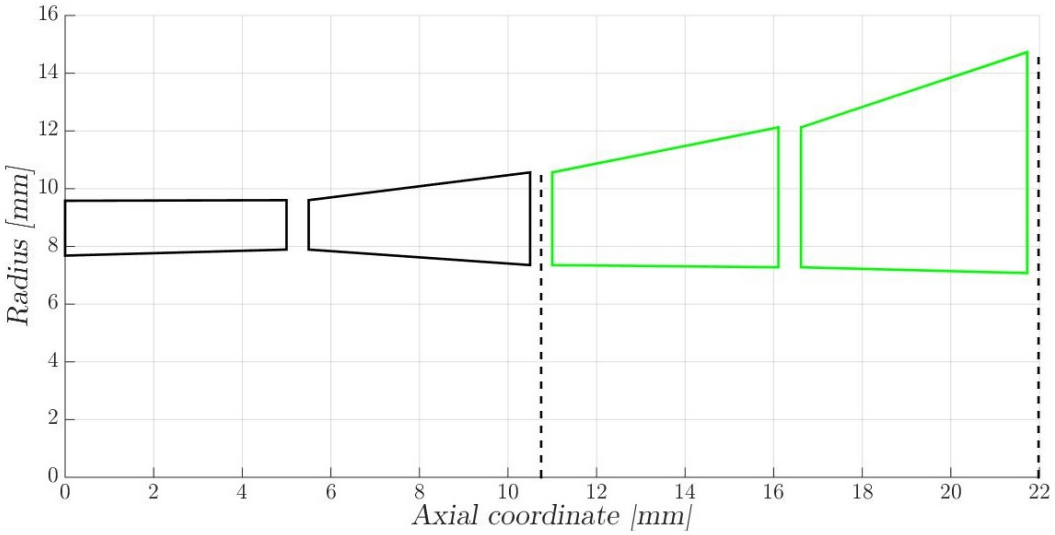

Figure 3.4: Meridian section of the turbine

3.3 Turbine - "OFF1D" code

To obtain a reliable evaluation of the system performance, the knowledge of the off-design behaviour of the turbine is required, due to the broad range of operating conditions. For this purpose, a big effort has been made to develop the "Off1D" code, in order to calculate the turbine efficiency and mass flow in conditions far from the nominal operating point. Currently a 2 stages axial flow architecture has been chosen, but future works will have to explore other solution, especially the radial configuration. According to the *"ORCHID_vpe"* code, the use of more than 2 stages has no influence on the recovered power, so the maximum number of stages is 2.

3.3.1 The structure of the off-design code

The main objective of the code is to evaluate the mass flow and the isentropic efficiency of an axial ORC micro turbine, given the inlet total pressure and temperature, outlet pressure and turbine geometry. The code computes the intermediate pressures between each blade cascade, equating the mass flow rate that flows through the different stages. All the equations are evaluated at the mean radius, and flow angles at the inlet, throat and outlet of each cascade. Hence, the code can be considered zero dimensional.

For instance, in the case of a 2 stages axial turbine, there is an intermediate pressure between the first and the second stage that matches the two mass flow rates. In Fig. 3.5 this case is represented: the working fluid is MM, the total

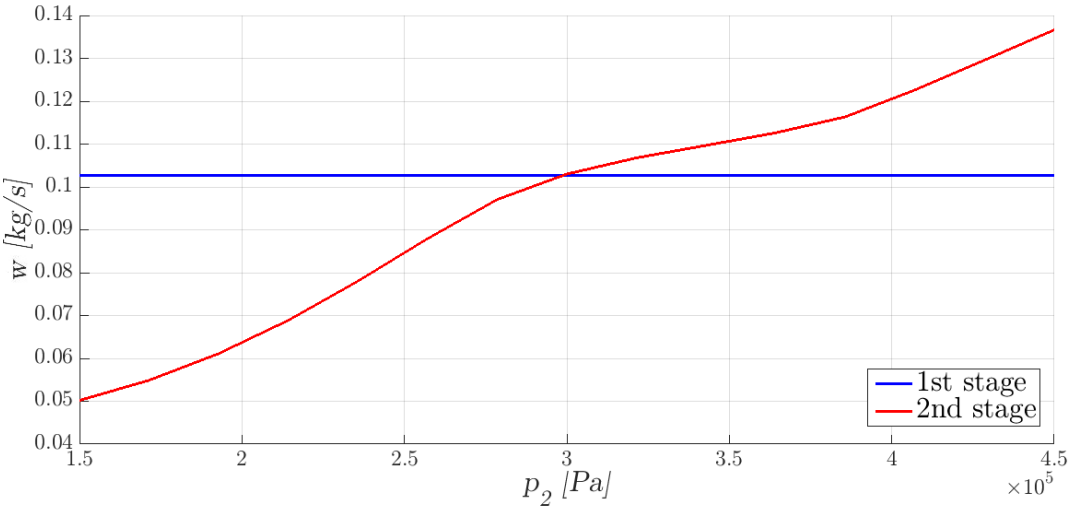

Figure 3.5: Example of the matching pressure

inlet pressure is 12.67 bar, the total inlet temperature is 239.7 °C and the outlet pressure is 0.7 bar. The plot represents the flow rate through the stages when the intermediate pressure changes. The first stage flow rate is constant, because the first stator is choked. Instead, the higher the intermediate pressure p_2, the higher the second stage flow rate, because at the inlet of second stage the density, which varies almost linearly with the pressure, increases.

As far as the turbine efficiency is concerned, a loss model must be implemented. By now, it is possible to set 4 different loss models:

- *isentropic expansion* - the expansion is considered isentropic. It has been implemented to test the correctness of the algorithm adopted;
- *constant loss coefficient* - a constant loss coefficient is given (default is 10%);
- *Craig & Cox* - the loss coefficient is computed according to the Craig & Cox's loss model [17];
- *Traupel* - the loss coefficient is computed according to the Traupel's loss model [18].

The loss coefficient, which includes profile, secondary, annulus, fan and leakage losses, is given as:

$$X_{tot} = 1 - \eta_{casc} = 1 - \frac{h_{in} - h_{out}}{h_{in} - h_{out,iso}} \tag{3.1}$$

The choice of the loss model seems to have a strong influence on the solution. According to [19, 1] the most accurate model for design purposes is the Craig & Cox's model, but for the off-design calculation the most suitable is the Traupel's model, because it varies the loss coefficient more regularly when the operating point changes.

The package contains two main scripts: `turbine_calculation_singlepoint.m`, that tries to calculate the performance for one specific point, and also plots the expansion in the T-s diagram and the velocity triangles for each turbine stage; `off1D.m`, that calculates the off-design performance varying the boundary conditions.

If the simulation fails at some point, a text file *"Error_report.txt"* is generated, with the description of the error.

It is important to underline that the geometry and the nominal inlet and outlet condition are given by the in-house tool *"zTurbo"* into a .txt file [22]. To keep the problem consistent, the loss model used by *"zTurbo"* should be the same set in *"Off1D"*.

The variation of the total inlet temperature seems to not influence so much the results of the off-design code, so only inlet and outlet pressure are changed,

while a mean temperature is assumed for each inlet pressure value. Moreover, the maximum and minimum rotational speed depends on the specific geometry. Finally, the code saves the results (flow rate, efficiency, inlet and outlet pressures, inlet temperature) for post processing.

3.3.2 The algorithm

The expansion points are referred as follow (see Fig 3.6):

- "t0" = total inlet condition;
- "1" = static condition between guide and runner of first stage;
- "2" = static condition between first and second stage;
- "3" = static condition between guide and runner of second stage;
- "4" = static outlet condition.

The logical procedure of the code is pretty simple: a Newton algorithm solves the equation $F(p_2) = w_{1st}(p_{t0}, p_2) - w_{2st}(p_2, p_4) = 0$, where w is the mass flow rate, starting from a guess initial value for intermediate pressure p_2. The mass flow through the single stage is calculated in the same way: the equations to be solved here are $F(p_1) = w_{guide}(p_{t0}, p_1) - w_{runner}(p_1, p_2) = 0$ for the first stage, and $F(p_3) = w_{guide}(p_2, p_3) - w_{runner}(p_3, p_4) = 0$ for the second stage.

The real core of the code are the functions `flow_guide.m` and `flow_runner.m`, which compute the mass flow through the guide and runner cascade, taking into account the loss model and the turbine geometry.

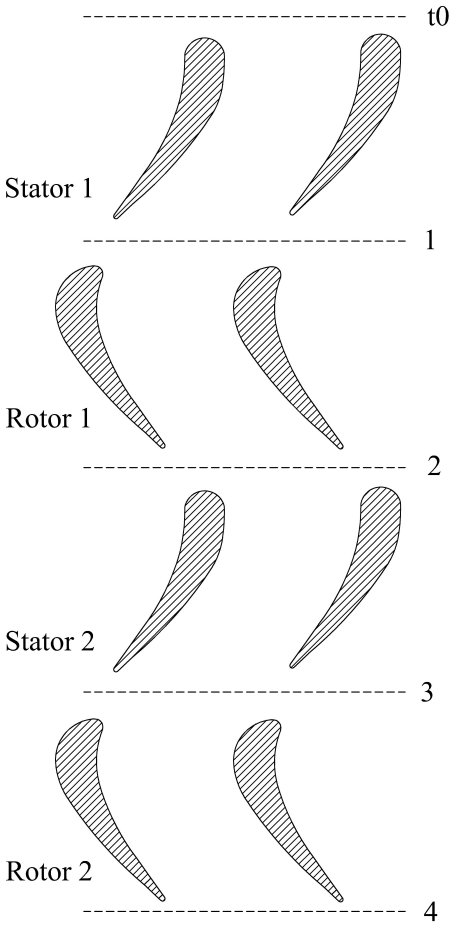

Figure 3.6: Axial turbine reference scheme

The `turbine_calculation.m` function

The `turbine_calculation.m` function is the top level function of the code, the one that `off1D.m` and `turbine_calculation_singlepoint.m` call. It takes as inputs the following information:

- *geometry*: is a structure variable containing all the geometrical data required;
- *n_stage*: defines the number of turbine stages;
- *pt_in*: defines the inlet total pressure;
- *Tt_in*: defines the inlet total temperature;
- *p_out*: defines the outlet pressure;
- *omega*: defines the rotational speed;
- *loss_model*: defines the loss model adopted;
- *p_init*: defines the initial guess for the intermediate pressure.

The function first gets the number of stages: if *n_stage* is equal to 1, it simply call the `stage_calculation.m` function, while if *n_stage* is equal to 2, the numerical algorithm that finds the intermediate pressure p_2 starts. The objective function `matching2st.m` is declared as sub-function, and returns the difference between the flow rate of the first and second stage, which must be equal to zero.

The numerical methods implemented are 2: bisection and Newton methods. As expected, the Newton algorithm is faster than the bisection one, but its effectiveness is highly dependent on the initial guess value.

It could happen that the code fails because of numerical errors. To prevent the code from stopping, in the Newton's algorithm a `try - catch` syntax is implemented.

If the "exitflag" of the numerical method is 1, the function calculates all the expansions point and efficiencies. Otherwise, an error is printed on Command windows and saved on the report file.

The `stage_calculation.m` function

The `stage_calculation.m` function works exactly as the `turbine_calculation.m` function but at a lower level. Through the Newton's algorithm, the intermediate pressure between guide and runner is computed, and then all the stage information are passed to the upper level function.

Function inputs are:

- *pt0*: total inlet pressure;
- *Tt0*: total inlet temperature;
- *p2*: static outlet pressure;
- *omega*: runner rotational speed;
- *guide_geometry*: structure with guide geometry details;
- *runner_geometry*: structure with runner geometry details;
- *loss_model*: defines the loss model adopted;
- *v0*: inlet velocity;
- *alpha0*: inlet fluid angle.

The last two input are actually used only if Traupel loss model is adopted.

The objective function `matching.m` is declared as sub-function at the bottom of the script, and returns the difference between the flow rate of guide and runner, which must be equal to zero. As in the latter function, if the "exitflag" variable equals 1, the correct expansion through the stage is computed, otherwise an error is printed on the Command window.

To help the convergence of the algorithm, the initial pressure value is calculated as follows:

$$x_0 = \sqrt{p_{t0}\, p_2} * initial\_coef \tag{3.2}$$

initial_coef is a tuning parameter that help the convergence of the algorithm. Typical values cover the range between 0.7 and 1.2, and are strictly dependent on the turbine geometry.

The `flow_guide.m` function

The `flow_guide.m` function evaluates the guide mass flow rate, given total inlet condition and outlet pressure. The subscript "b" refers to choked conditions in the throat, while subscript "a" refers to throat condition in general.

The code executes the following steps:

1. definition of isentropic expansion for initialization of loss model. According to the total inlet condition, the isentropic outlet condition are computed as follows:

$$h_{t0} = f\left(p_{t0}, T_{t0}\right) \qquad \Rightarrow \quad \text{EoS} \tag{3.3}$$

$$s_{t0} = f\left(p_{t0}, T_{t0}\right) \quad \Rightarrow \quad \text{EoS} \tag{3.4}$$

$$s_{1is} = s_{t0} \quad \Rightarrow \quad \text{Isentropic expansion} \tag{3.5}$$

$$h_{1is} = f\left(p_1, s_{1is}\right) \quad \Rightarrow \quad \text{EoS} \tag{3.6}$$

$$v_{1is} = \sqrt{2\left(h_{t0} - h_{1is}\right)} \quad \Rightarrow \quad \text{Energy equation} \tag{3.7}$$

$$c_{1is} = f\left(p_1, s_{1is}\right) \quad \Rightarrow \quad \text{EoS} \tag{3.8}$$

$$M_{1is} = \frac{v_{1is}}{c_{1is}} \quad \Rightarrow \quad \text{Mach number definition} \tag{3.9}$$

2. calculation of choking thermodynamic condition. The function `Mach_out_stat.m` calculates the throat pressure value which causes transonic condition in the throat, taking into account also the losses. In practice, a system is solved to calculate throat velocity and entropy when M = 1:

$$\begin{cases} c_b = f\left(p_b, s_b\right) & \Rightarrow \quad \text{EoS} \\ h_b = h_{t0} - \dfrac{v_b^2}{2} & \Rightarrow \quad \text{Energy equation} \\ v_b = c_b & \Rightarrow \quad \text{Mach number} = 1 \end{cases} \tag{3.10}$$

3. calculation of flow deviation, throat and outlet condition:

   - if $p_1 > p_b$, in other words if the guide is not choked, the deviation is computed with the function `out_dev_stat.m`. The throat conditions are calculated under the Joukowsky assumption, which says that throat and outlet pressure are the same. Once the pressure is fixed, the throat thermodynamic conditions and velocity can be evaluated applying the loss model again, as follows:

$$\begin{cases} p_1 = p_a & \Rightarrow \quad \text{Joukowsky condition} \\ (h_a,\, v_a) = f(\text{loss model, geometry, } p_{t,in},\, T_{t,in},\, p_a) \end{cases} \tag{3.11}$$

     The deviation value depends on the outlet Mach number, and is extrapolated from Fig. 3.7 [20].
     Then, outlet conditions are calculated solving continuity, energy and state equations between throat and trailing edge:

$$\begin{cases} \rho_1 = f\left(h_1, p_1\right) & \Rightarrow \quad \text{EoS} \\ h_1 + \dfrac{v_1^2}{2} = h_a + \dfrac{v_a^2}{2} & \Rightarrow \quad \text{Energy equation} \\ v_a\, \rho_a\, a = \rho_1\, v_1\, s \cos\alpha_1 & \Rightarrow \quad \text{Continuity equation} \end{cases} \tag{3.12}$$

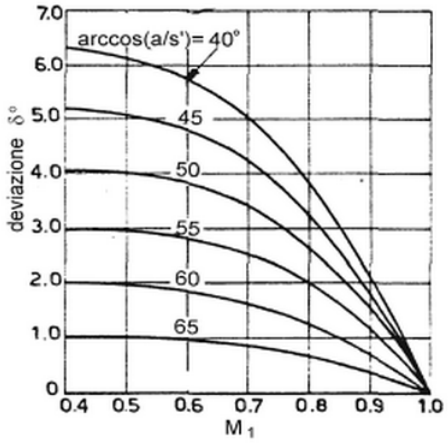

Figure 3.7: Outlet flow deviation from Osnaghi

- if $p_1 > p_b$ the throat is assumed to be choked, and its thermodynamic conditions are equal to those calculated with Eq. 3.10. The flow deviation is now calculated from the solution of the following system:

$$\begin{cases} \rho_a \, v_a \, a = \rho_1 \, v_1 \, s \cos \alpha_1 & \Rightarrow \quad \text{Continuity equation} \\ v_a^2 \, \rho_a + p_a = v_a \, \rho_a \, v_1 \, \cos \Delta\alpha + p_1 & \Rightarrow \quad \text{Momentum equation} \\ h_a + \dfrac{v_a^2}{2} = h_1 + \dfrac{v_1^2}{2} & \Rightarrow \quad \text{Energy equation} \\ \rho_1 = f\left(p_1, h_1\right) & \Rightarrow \quad \text{EoS} \\ \Delta\alpha = \alpha_a - \alpha_1 & \Rightarrow \quad \text{Deviation definition} \end{cases} \tag{3.13}$$

  In the case of subsonic flow, the loss coefficients are re-evaluated inside the function `out_dev_stat.m`, while in the case of supersonic flow they are computed by the choking function. Both the Craig & Cox's and the Traupel's model take into account the entropy increase caused by the post-expansion, because experimental measurements are taken far from the trailing edge. Considering that the latter system computes the post-expansion irreversibility in the supersonic regime, the loss model is used just from the leading edge to the throat, while the actual values for h_1 and v_1 are given by the solution of the Eq. 3.13.

4. output definition. The guide mass flow, the outlet and throat conditions and the loss coefficient are given as output.

The `flow_runner.m` function

The `flow_runner.m` function works similarly to the `flow_guide.m` function, but we have to consider the conservation of rotalphy, instead of total enthalpy. Moreover, in continuity and momentum equations absolute velocities must be replaced by relative velocities.

For instance, the system that computes the flow deviation becomes:

$$\begin{cases} \rho_a \, w_a \, a = \rho_2 \, w_2 \, s \cos \beta_2 & \Rightarrow \quad \text{Continuity equation} \\ w_a^2 \, \rho_a + p_a = w_a \, \rho_a \, w_2 \, \cos \Delta\beta + p_2 & \Rightarrow \quad \text{Momentum equation} \\ h_a + \dfrac{w_a^2}{2} = h_2 + \dfrac{w_2^2}{2} & \Rightarrow \quad \text{Energy equation} \\ \rho_2 = f\left(p_2, h_2\right) & \Rightarrow \quad \text{EoS} \\ \Delta\beta = \beta_a - \beta_1 & \Rightarrow \quad \text{Deviation definition} \end{cases} \tag{3.14}$$

3.3.3 Overview of the algorithm structure

For the sake of clarity, the scheme of the logical procedure for a 2 stages turbine is here represented. Subscripts refer to Fig. 3.6.

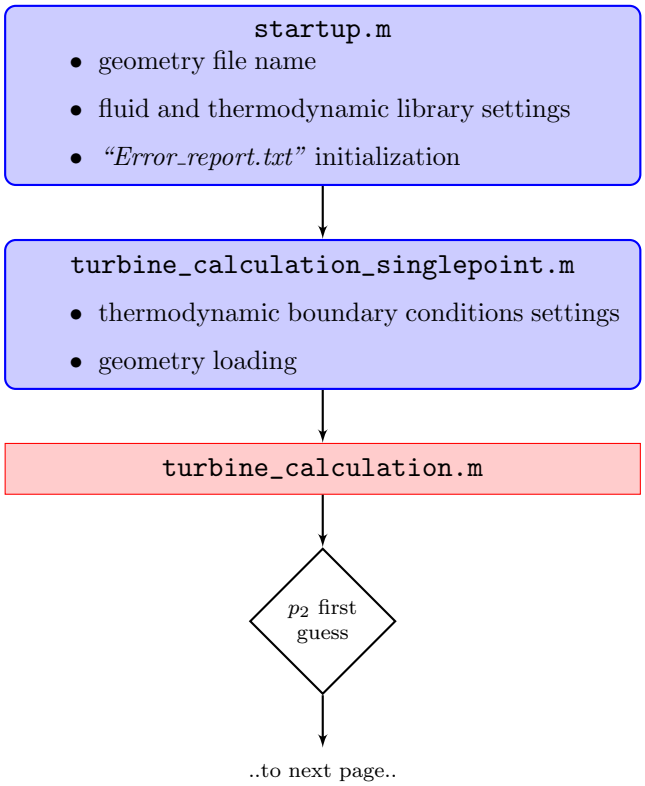

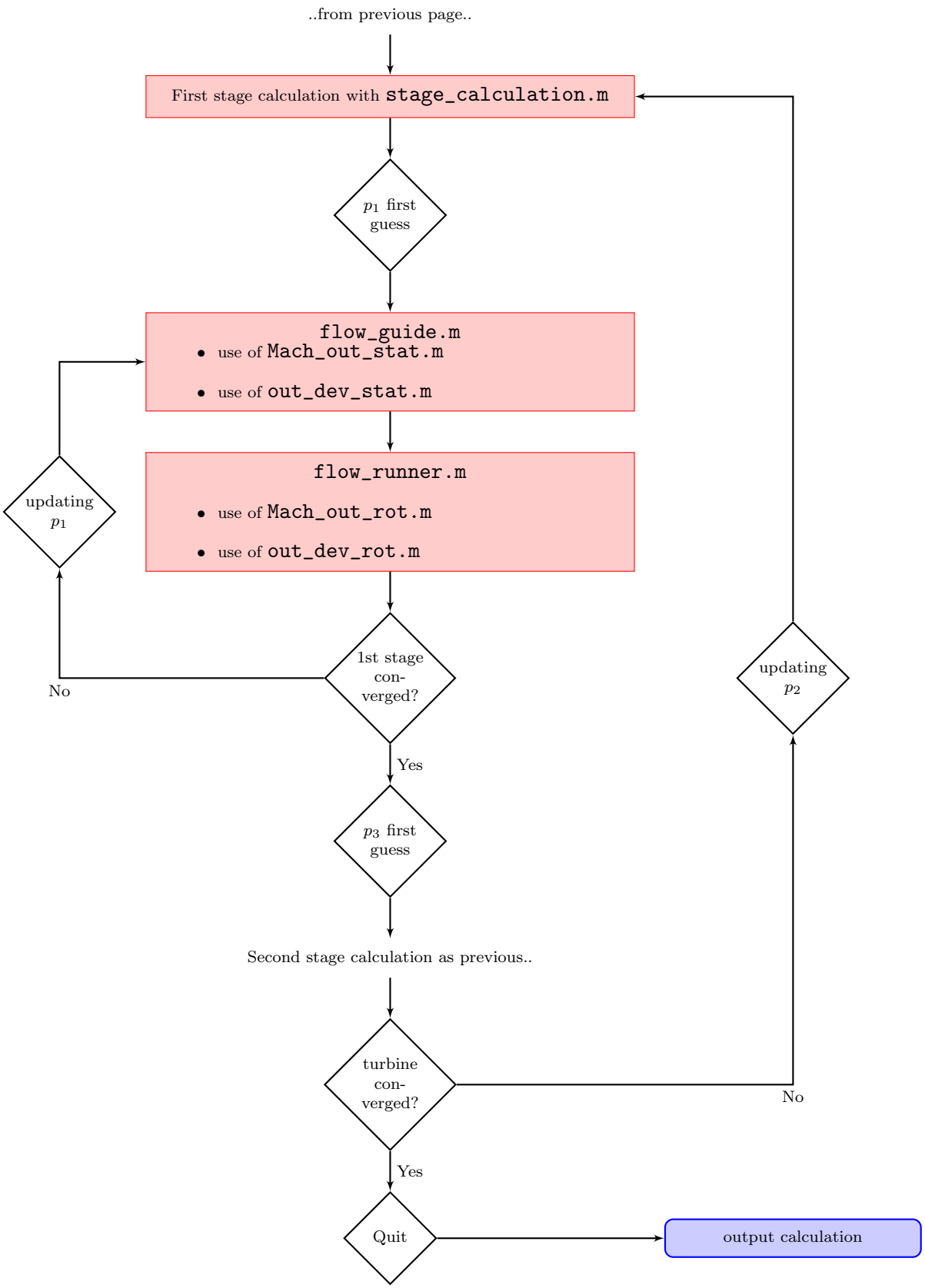
..from previous page..
First stage calculation with stage_calculation.m
p_1 first guess
flow_guide.m
use of Mach_out_stat.m
use of out_dev_stat.m
flow_runner.m
use of Mach_out_rot.m
use of out_dev_rot.m
updating p_1
1st stage converged?
No
Yes
p_3 first guess
Second stage calculation as previous..
turbine converged?
updating p_2
No
Yes
Quit
output calculation

3.3.4 Auxiliary functions

Some other functions are needed to run the main scripts. Probably the most important one is `read_geometry.m`. This function open and read the .txt file generated with *"zTurbo"* routine and gives as output cascade geometrical data (angles, radius, blade span, axial chord, chamber line, throat section, pitch, trailing edge thickness, tip clearance, number of blades). `design_expansion.m` and `design_veltriangle.m` draw the expansion on a T-s diagram and the velocity triangles.

3.3.5 Fluid properties

The fluid properties are computed via the external software *FluidProp - v3.01* [40]. A COM.server variable named "FP" is created with the global attribute, so that could be invoked from all the code subroutines. All the inputs must be in SI units. Note that the boundary condition are given in "normal units" (bar for pressure, °C for temperature..). Later, the code converts all the values in SI units, so that the equations do not involve "dangerous" conversion factors and they are consistent with *FluidProp* settings.

3.3.6 Results

Here the code results for the turbine of the ORC unit are reported. They have been obtained running the `off1D.m` script with the following boundary condition:

- the rotational speed range is ±15% from the nominal value, according to the engine rotational speed range;
- the total inlet pressure range is from 50% to 130% of the nominal value, which represent the expected bounds during "sliding pressure" operation;
- the outlet pressure range is ±20% from the nominal value. These bounds are closer if compared with the previous values because the presence of the tank soften the variation of the condenser pressure.

Fig. 3.8shows that the absolute mass flow increases with the total inlet pressure, while it remains constant as the outlet pressure decreases, independently from the rotational speed. This means, as expected, that the first stator is always choked.

If the mass flow is represented as a reduced mass flow [21], all the simulation points collapse on the same line, as shown in Fig. 3.9. This result is important from a theoretical point of view: even if the fluid conditions are far from the ideal state, because the expansion is close to the vapour saturation line, the Eq. 3.15 derived for ideal gases is still valid.

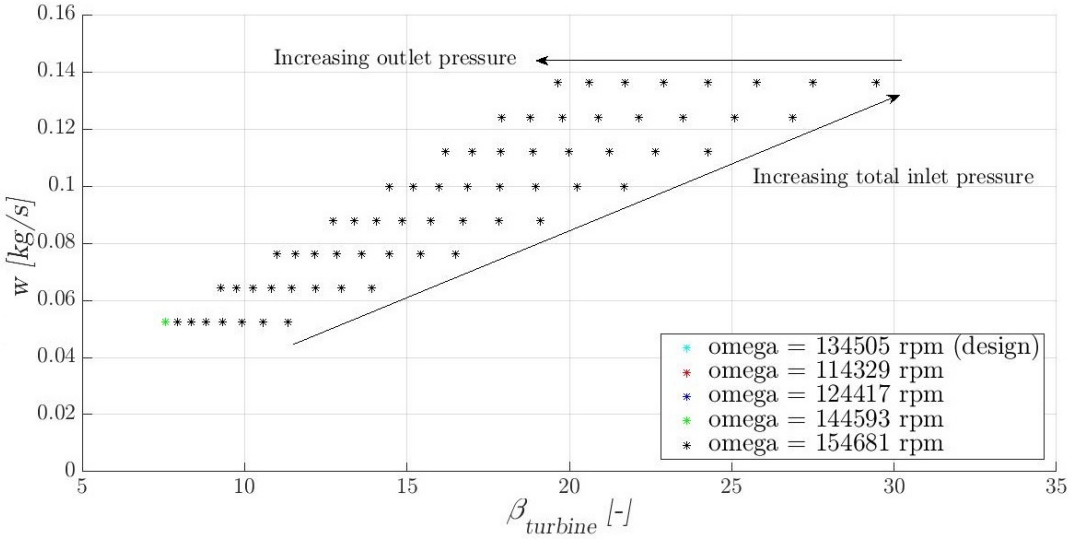

Figure 3.8: Turbine mass flow w vs. turbine pressure ratio β

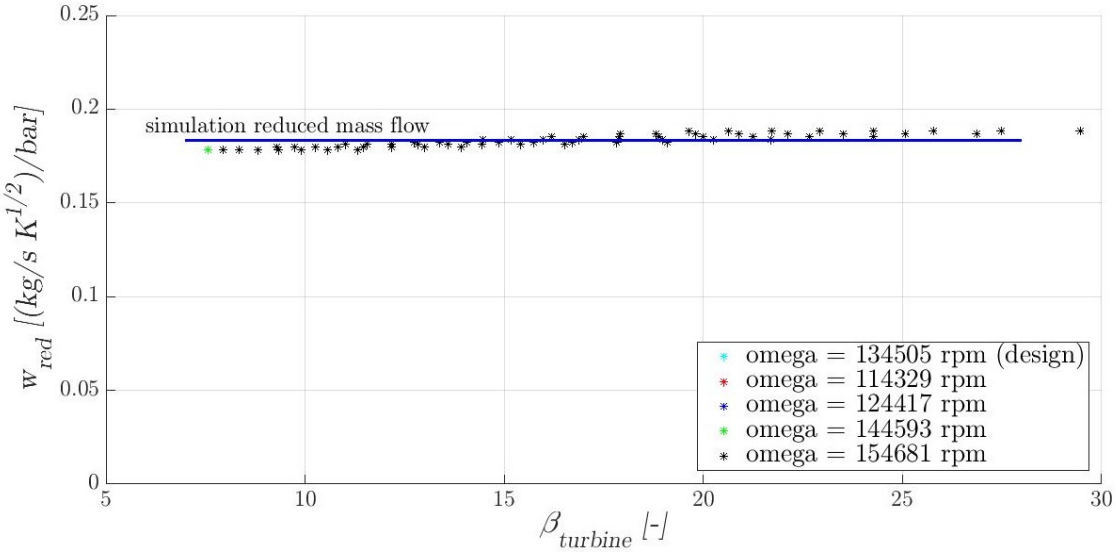

Figure 3.9: Turbine reduced mass flow w_{red} vs. turbine pressure ratio β

$$\frac{w\sqrt{T_{in}}}{p_{in}} = w_{red} \tag{3.15}$$

Finally, Fig. 3.10 represents the efficiency surface, as function of the rotational speed and of the pressure ratio across the turbine.

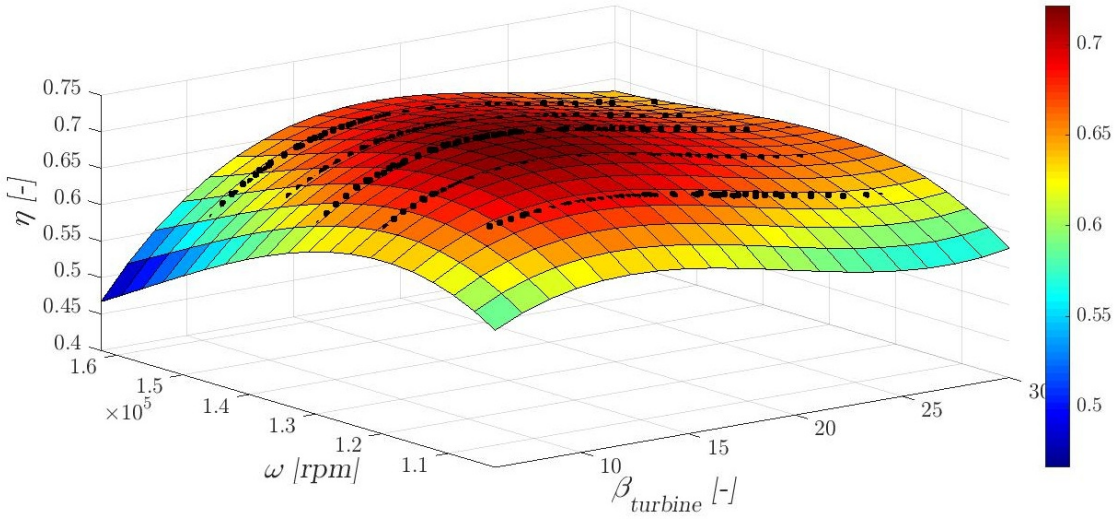

Figure 3.10: Turbine isentropic efficiency

The plotted surface is the result of a polynomial 2D interpolation, whose expression is:

$$\eta_{is} = p_{00} + p_{10}\,\beta + p_{01}\,\omega + p_{20}\,\beta^2 + p_{11}\,\beta\,\omega + p_{02}\,\omega^2 + p_{30}\,\beta^3 + p_{21}\,\beta^2\,\omega + p_{12}\,\beta\,\omega^2 + p_{03}\,\omega^3 \tag{3.16}$$

Tables 3.2: Turbine model coefficients

Coefficients	Value
w_{red}	0.1963027
p_{00}	-3.916
p_{10}	0.007538
p_{01}	$9.509e-05$
p_{20}	-0.001113
p_{11}	$1.558e-07$
p_{02}	$-6.555e-10$
p_{30}	$3.889e-05$
p_{21}	$-1.15e-08$
p_{12}	$1.44e-12$
p_{03}	$1.378e-15$

An important aspects of the previous results must be underlined: the loss model chosen is the Traupel's model [18], whose term regarding the tip clearance losses is strictly dependent on the reaction degree and on the load factor of the stage. Moreover, its value is much bigger if compared with profile and secondary loss terms. This fact leads to a non physical solution of the mass flow because the first stator mass flow is not constant for pressure ratio higher than the critical one, and to a huge amount of numerical problems during off-design calculation. For this reasons a new geometry without tip clearance has been used, and the simulation points have been tuned to match the nominal point performance, both in terms of reduced mass flow and isentropic efficiency.

All the closure coefficients obtained with the *OFF1D* code are reported in Tab. 3.2.

3.4 Heat exchangers

Heat exchangers are the components that most affect the dynamic behaviour of the WHR unit. While for pumps and turbines all mass and energy balances can be considered at steady-state due to the negligible volumes and fluid heat conductances, the heat exchangers mass and energy storage define the frequency response of the cycle, in other words its dynamic behaviour.

As stated before, plate heat exchangers have been selected because of their compactness and high efficiency. The design has been obtained with a commercial software that automates the design optimization process for a given set of process conditions. In particular the input are the thermodynamic conditions of cycle points, which result from the "ORCHID_vpe" optimization process.

The key factor of the PHE design is the maximum pressure drop allowed at the evaporators gas side. In fact, the ORC cycle should not affect the performance of the diesel engine, or at least have a small impact on it. A sensitivity analysis with the tuned model has been performed, in order to have an idea about the effect of the back pressure on the engine performance. Note that the effect of a pressure drop in the EGR evaporator does not affect the engine efficiency, because the EGR valve itself introduces a pressure drop definetely higher than the evaporator one.

For the design of the evaporators the exhaust gases pressure drop has been fixed equal to 5 kPa. In this way, the maximum difference in engine efficiency is lower than 0.5%, as shown in Fig. 3.11.

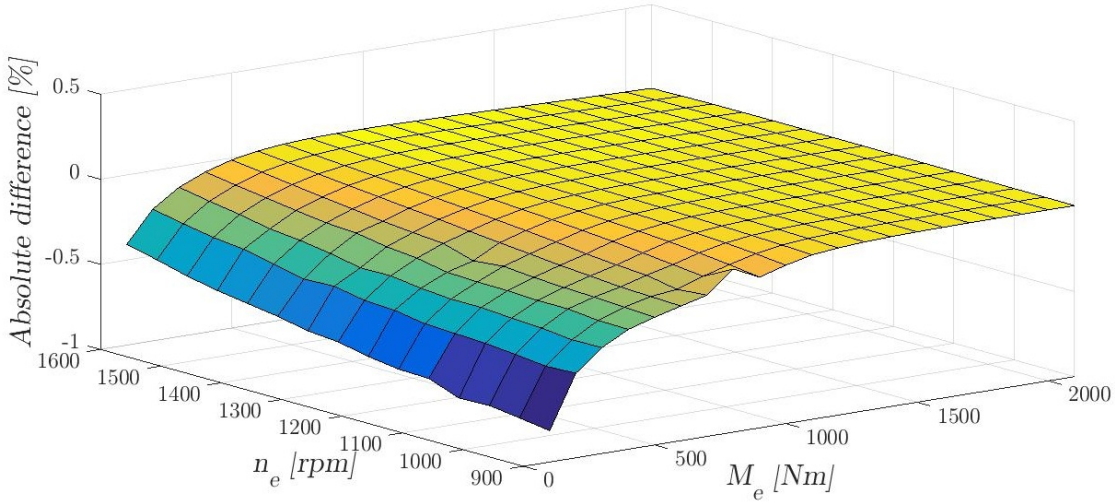

Figure 3.11: Effect of evaporator back pressure on engine efficiency

Tables 3.3: PHE design results

	EVA_{exh}	EVA_{egr}	REG	COND
$M\left[\mathrm{kg}\right]$	43.5	36.3	36.1	36.6
$V_{\mathrm{hot}}\left[\mathrm{m}^3\right]$	0.0113	0.007	0.0041	0.0068
$V_{\mathrm{cold}}\left[\mathrm{m}^3\right]$	0.0081	0.0041	0.0035	0.0068
$S\left[\mathrm{m}^2\right]$	6.1	5	3.1	5
$h_{\mathrm{ext}}\left[\mathrm{W\,m^{-2}\,K^{-1}}\right]$	140	130	–	4200
$h_{\mathrm{liq}}\left[\mathrm{W\,m^{-2}\,K^{-1}}\right]$	130	150	210	300
$h_{\mathrm{2ph}}\left[\mathrm{W\,m^{-2}\,K^{-1}}\right]$	1600	1600	–	2000
$h_{\mathrm{vap}}\left[\mathrm{W\,m^{-2}\,K^{-1}}\right]$	140	165	355	700

The heat exchangers masses, volumes, surfaces and heat transfer coefficients are reported in Tab. 3.3.

Note that the overall mass of the ORC system is around 150 kg, which represents an increase of 0.5% of the overall truck mass at full load.

We can conclude that the pressure drop in the evaporators does not affect significantly the engine performance at the design operational point.

3.5 Pump

The pump is the component that makes the organic fluid circulate and increase its pressure from condensation to the evaporation condition. The choice of the pump depends on the circuit mass flow and head. Since the former is small and the latter is large, a volumetric pump is the correct choice.

Among them, diaphragm pumps seem to be the most appropriate for the purpose. In order to obtain realistic results, a specific model has been chosen [39], while in Fig. 3.12 the adopted flow characteristic is reported.

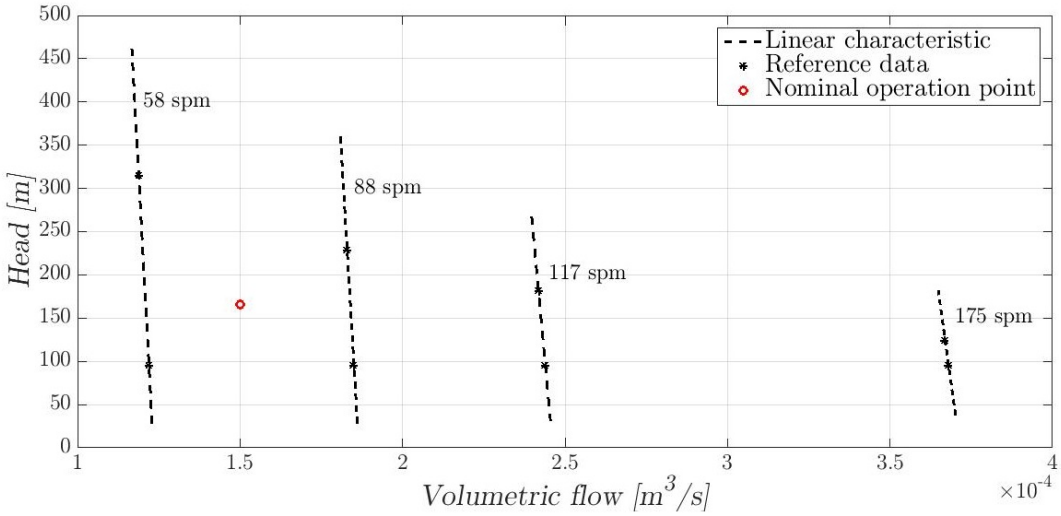

Figure 3.12: Diaphragm pump head vs. flow characteristic

Chapter 4

Dynamic modelling of the WHR unit - ICORC library

Since the combined system is not trivial, a complete dynamic model of the whole combined cycle is required in order to fully understand how the ORC unit responds to a variation of the heat input, i.e. of the primary engine load. Dynamic simulations can be used to support the choice of the the system configuration and equipments during the design phase, and to develop and test the control strategies as well as the design and tuning of the control system [30].

This chapter describes how the complete dynamic model has been built, using the modelling language Modelica. The first section is a quick description of the language main advantages, while the other parts present the components models and the dynamic model of the CC-powertrain.

4.1 Modelica language

Modelica is a tool-independent modelling language, developed by the non-profit Modelica Association since 1996, and represents one of the more advanced tool that allows to simulate the dynamic behaviour of multi physical systems consisting of mechanical, electrical, thermal and hydraulic components. First-principle, 0-dimensional and 1-dimensional models of each component can be written directly in terms of differential-algebraic equations (DAEs), while all the burden of solving those equations is shifted from the modeller to the simulation tool. At a higher level, plant models can be built by hierarchically connecting lower level models, thanks to the flexibility of the object-oriented approach.

The main advantages of this approach are [31]:

- *A-causal, declarative modelling*: boundary condition of each model are not necessarily declared a-priori as inputs or outputs. In fact, by a pure physical point of view, the model is always the same, irrespective of what is connected to it and if the flow variables enter or leave the component;

- *Code transparency*: the equations are coded as they can be written on a paper;
- *Encapsulation*: system components model are connected through rigorously defined interfaces or connectors. This is a key feature to re-use and to easily replace more or less detailed models, without affecting the rest of the system;
- *Inheritance*: model libraries can be structured in a hierarchical way, so that more complex models can be obtained from basic common models by adding specific variables and equations;
- *Multi-physics modelling*: within the Modelica language it is possible to straightforwardly combine physical models belonging to different domains;
- *Reusability*: at component level it is possible to re-use models provided by standard libraries, and to develop specific components wherever needed.

The model of the combined cycle powertrain uses both components from other libraries and components developed *ad hoc*. The ICORC library gathers all the models used. Its main components are described in the next sections.

4.2 Topping cycle - diesel engine

The aim of the topping cycle dynamic model is to compute the values of the variables of interest, i.e. temperatures and mass flows of heat sources, as function of the load of the diesel engine. The two main inputs are the engine torque and rotational speed, which can be directly supplied or evaluated solving the longitudinal dynamics of the truck. The first option is useful to test the input disturbances rejection of the control system.

4.2.1 Longitudinal dynamic of the truck

The control maps created in Chapter 2 require as input the rotational speed of the engine and the net torque it provides. The former is directly linked with the truck velocity through the transmission ratio of the gearbox:

$$n_e = \frac{30\,v}{\pi\,R\,\tau_i} \qquad n_e \text{ in rpm, v in km/h} \qquad \tau_i = \frac{n_{wheels}}{n_e} \tag{4.1}$$

τ_i depend on the inserted gear, and they have been freely extrapolated from [41]. The torque is evaluated as a function of truck velocity and acceleration, through a longitudinal momentum balance:

$$\frac{dv}{dt}\left[M+\frac{12\,J_w}{R^2}+\frac{\eta_d\,J_e}{\tau_i^2\,R^2}\right] = \underbrace{\frac{\eta_d\,(M_e+M_{orc})}{\tau_i\,R}}_{engine+ORC\,momentum} - \underbrace{M\,g\,f_v}_{rolling\,friction} - \underbrace{\frac{1}{2}\,C_x\,\rho_{air}\,S\,v^2}_{air\,friction} \tag{4.2}$$

Considering that the velocity v is an input, as well as the acceleration, the previous equation is algebraic, and the unknown is the torque that the ICE must supply to obtain the velocity set point. M is the total mass of the truck, J_w the wheels moment of inertia, R the wheels radius, η_d the transmission efficiency, τ the transmission ratio, J_e the engine shaft inertia, f_v the rolling friction factor, S the frontal section, and C_x the air friction factor.

The look-up tables that contain the control maps get as input the rotational speed and the torque needed, and give as output the control variables that are passed to the engine model. A mechanical interface connects the truck model to the engine model (see Fig. 4.1, white and grey filled circles): the former receives the actual value of the torque supplied by the ORC turbine, multiplied by an ideal gearbox, so that it can evaluate the net power required to the engine. At the same times it gives to the engine and to the turbine the actual value of the rotational speed.

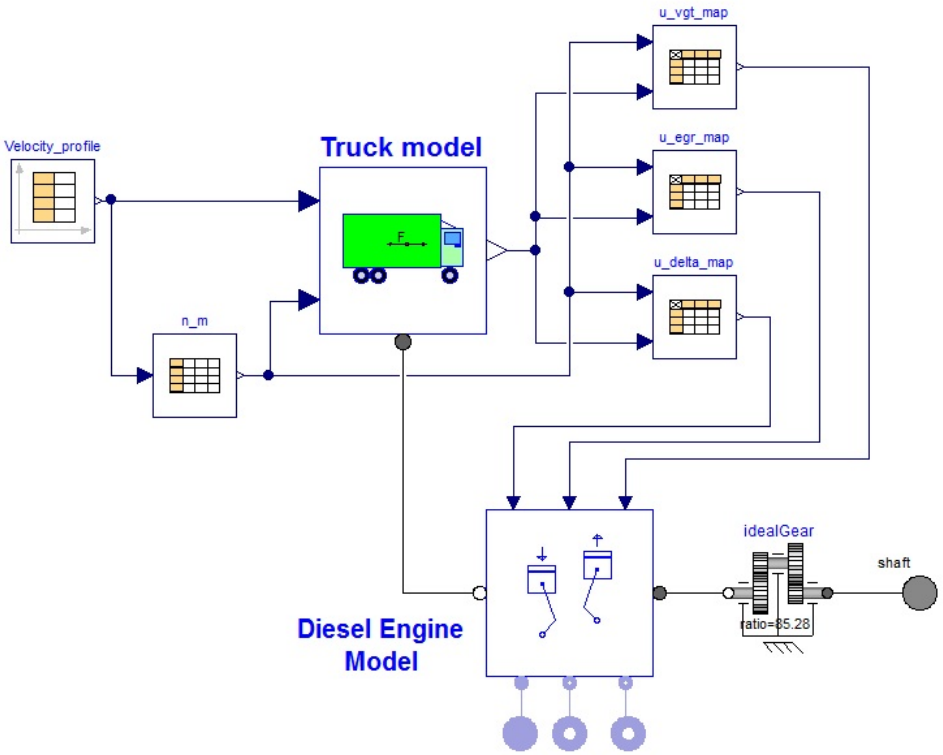

Figure 4.1: Object diagram of topping cycle

At the equilibrium point, given a specific velocity profile, for instance an European Driving Cycle, the truck model gives as output the net torque M_e required to the diesel engine, in a feed-forward controlled way.

4.2.2 Engine model

The model of the Diesel engine is exactly the transcription in Modelica language of the set of equations reported in Appendix A. The model of each component has been written as a submodel, so that it can be easily replaced by a more sophisticated one if necessary. Fig. 4.2 reports the object diagram of the engine.

With respect to the physical interfaces, two types of flanges have been used [27]:

- *mechanical ports*: starting from the cylinders model, they connect the ORC turbine shaft, the engine shaft and the truck momentum balance;
- *fluid ports*: the lilac filled (input) and empty (output) circles represent the connection of the exhaust gases and EGR circuit with the WHR unit. In particular, the intake manifold inlet and the EGR valve outlet are connected

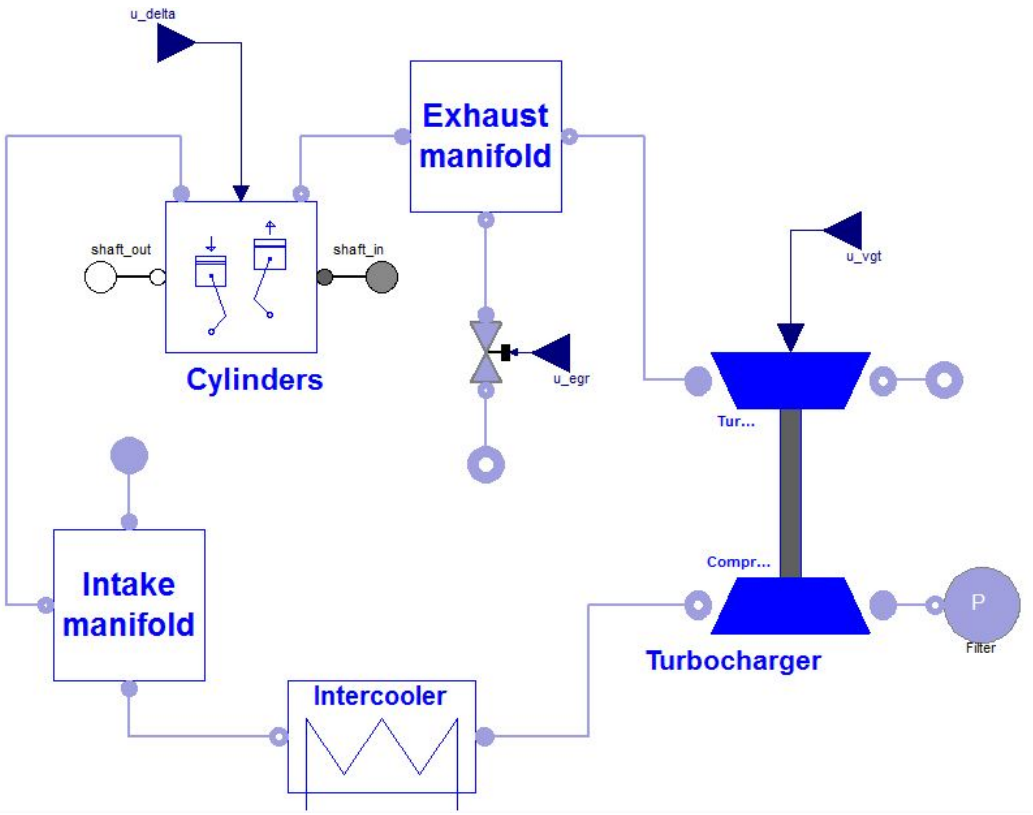

Figure 4.2: Object diagram of the engine

to the EGR evaporator, and the turbocharger outlet is connected to the exhaust gases evaporator (see Fig. 4.2 and 4.3).

4.3 Bottoming cycle - ORC

The ORC cycle has been built by connecting the submodels of its main component: heat exchangers, pump, turbine and tank. The inputs are the fluid ports that connect the evaporators to the engine and the position of the valve and the rotational speed of the pump, which represent the control variables.

The Modelica scheme of the ORC is reported in Fig. 4.3.

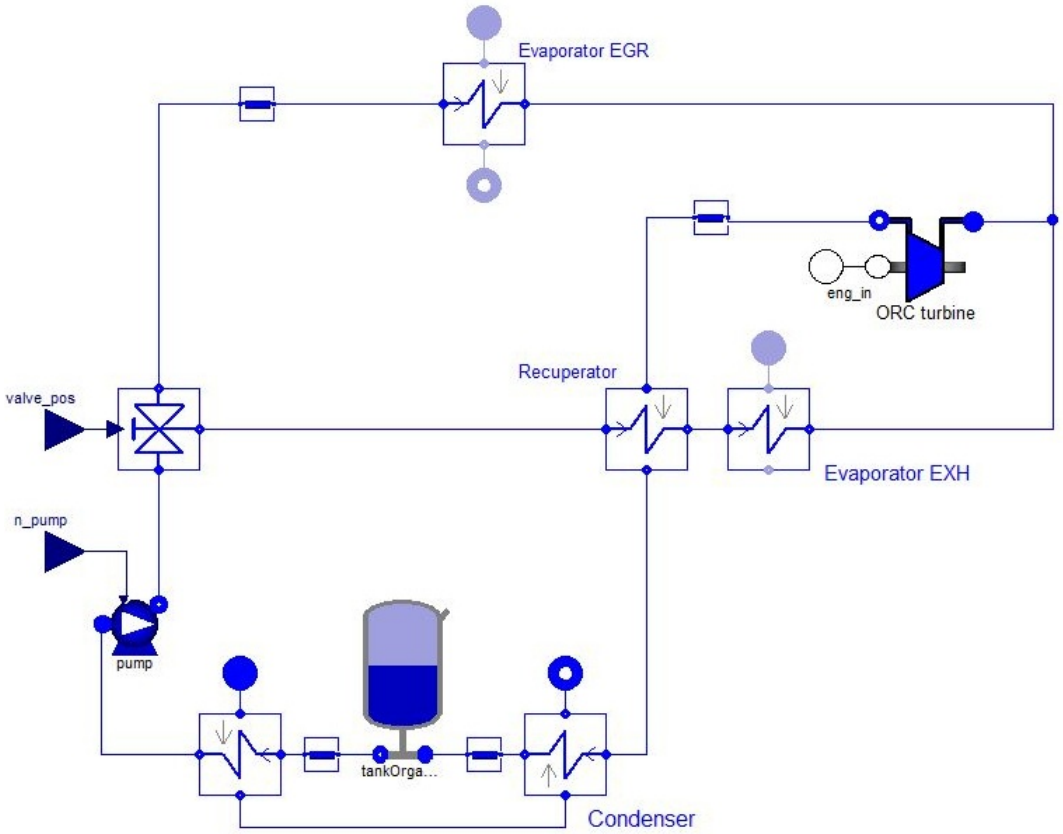

Figure 4.3: Object diagram of bottoming cycle

The blue fluid ports represent the connection with the truck radiator.

4.3.1 Turbomachinery

Both the pump and turbine model are described by pure algebraic equations. Indeed, from the system point of view, their dynamics are faster than PHE dynamics, so that a lumped steady-state model is enough to fully describe their behaviour. The equations here reported represent the design result of Chapter 3.

The pump model is basically composed by the so-called first and second characteristic: the first one describes the volumetric flow as a function of pump head, while the second one gives the efficiency, in other words the power consumption of the pump as function of the rotational speed and of the volumetric flow. Since the isentropic efficiency of the pump is not available from the technical datasheet and its variation does not affect significantly the global performance of the bottoming cycle, it has been considered constant and equal to the design value (65%).

The main equations of the pump model are reported below:

$$\begin{cases} q = \dfrac{\partial q}{\partial n}\,\Delta n + \dfrac{\partial q}{\partial H}\,\Delta H \\ P_{pump} = \dfrac{q\,\Delta p}{\eta_{is}} \end{cases} \tag{4.3}$$

The first equation describes the characteristic represented in Fig. 3.12: the term $\dfrac{\partial q}{\partial n}$ is the volume displaced, while $\dfrac{\partial q}{\partial H}$ represents the volumetric efficiency, which is a volumetric flow reduction due to the higher pressure at the delivery section. Their values are respectively $1.2764e-4\ m^3$ and $-1.456996e-8\ m^2/s$.

As for the pump, the turbine model is composed by a first and a second characteristic: the first one is the equation of a choked nozzle, the second one the polynomial interpolation of the surface that describes the isentropic efficiency as function of the rotational speed and the pressure ratio of the turbine.

$$\begin{cases} \dfrac{w\,\sqrt{T_{in}}}{p_{in}} = w_{red} \\ \eta_{is} = f\,(\omega,\,\beta) \\ h_{out} = h_{in} - \eta_{is}\,(h_{in} - h_{out,is}) \end{cases} \tag{4.4}$$

It is important to underline that in order to avoid numerical error, the evaluation of the polynomial expression of the isentropic efficiency is expressed in terms of nested multiplications using the Horner's scheme [32].

4.3.2 Heat exchangers

The modelling of the heat exchangers represents a key factor to describe correctly the dynamic behaviour of a power plant from a system-level point of view. In this context focusing on the detailed behaviour of single components, which belongs to the realm of CFD and FEM, is not worthy, because such complex models are

strictly dependent on the geometry of the specific application and implies much higher CPU time for simulation. Simplified 1D models with distributed parameters seem to be more suitable for simulation and analysis at system-level.

Thanks to the object-oriented modelling approach, all the PHE of the recovery cycle have been described using pre-existing, tested and validated 1D models [42] [43] based on the finite volume discretization method. The model of a generic heat exchanger is made of several submodels or classes: the model of the fluids, the model of the metal walls which separate the fluids, and the model of the heat transfer between the inner fluid and the metal, or between the metal and the outer fluid. The metal wall and the two fluid sides are divided into small volumes, whose thermal connection is defined by a specific heat exchanger topology, for instance the counter-current configuration.

The main parameters to be set are:

- *fluid model*: it has to be set on both the hot and cold side of the heat exchanger;
- *heat transfer topology*: since a PHE is essentially a counter-current heat exchanger, this configuration has been chosen;
- *number of volumes*: the optimal value is the result of a trade-off between accuracy and computational time. Generally, if there is a 2-phase zone a higher number of volumes is required: for this reason the two evaporators and the condenser have 15 volumes, while the recuperator has only 6 volumes;
- *PHE geometry and weight*: the total fluid volume and heat transfer surface, metal wall weight and specific heat capacity values have been taken from Tab. 3.3;
- *heat transfer model*: the heat transfer coefficient of both fluids varies according to the following equation:

$$\gamma = \gamma_{nom} \left(\frac{w}{w_{nom}} \right)^{\alpha} \tag{4.5}$$

  It is a simple but at the same time accurate expression, based on the assumption that in off-design condition the thermodynamic and transport properties are almost constant compared with the fluid velocity. In the end, the heat transfer coefficient is proportional to the actual mass flow raised to power of α, assumed equal to 0.8.

In case of a 2-phase heat exchanger the heat transfer coefficient varies according to the fluid phase, eventually corrected by the Eq. 4.5. If the values reported in

Tab. 3.3 are used to evaluate the heat transfer in the two evaporators, a numerical instability arises and causes unphysical oscillations in the solution. For this reason, a single heat transfer coefficient has been tuned so that the global heat exchanged in the PHE do not change both in on and off-design condition. This approximation is reasonable because the specific heat capacity of the liquid and vapour phases are almost equal, and the vaporization enthalpy is just a small part of the total enthalpy increase. In particular, the tuned values are $\gamma_{EGR} = 180\,\mathrm{W\,m^{-2}\,K^{-1}}$ and $\gamma_{EXH} = 220\,\mathrm{W\,m^{-2}\,K^{-1}}$

About the pressure drops that occur within the PHEs, they have been represented by simple pressure losses upstream the heat exchanger models, to avoid numerical problems. The flow dependency is guaranteed by the following equation, similar the Eq. 4.5:

$$\Delta p = \Delta p_{nom} \left(\frac{w}{w_{nom}} \right)^2 \tag{4.6}$$

Since the pressure drops are small, the last equation tuned on design values is enough to have a good accuracy.

4.3.3 Tank

For dynamic simulation purposes, a buffer tank between the condenser outlet and the pump inlet is required, in order to guarantee saturation conditions at the condenser outlet at all times, and to damp pressure fluctuations in the system, due to a variation of the working fluid density in the circuit during transient and start up. Without the buffer tank volume, an increase in the working fluid flow rate could cause the pump to run dry before the system can reach a new steady-state equilibrium, due to the inertia of the heat exchangers. Moreover, it represents the organic fluid reservoir when the add-on power unit is not in operation.

In normal operating conditions, the tank is supposed to be at vapour-liquid equilibrium at the condenser pressure and adiabatic. The set of equations describing such system is:

$$
\begin{cases}
M = M_l + M_v \\
M_l = A\, z_l\, \rho_l \\
M_v = A\,(h - z_l)\, \rho_v \\
V_l = A\, z_l \\
V_v = V - V_l \\
\alpha = \dfrac{V_v}{V} \quad \Rightarrow \quad \text{void fraction} \\
p_f = p_{sat} + \rho_l\, g\, z_l \\
\dfrac{dM}{dt} = w_{in} + w_{out} \\
E = V\left((1-\alpha)\,\rho_{ls}\,h_{ls} + \alpha\,\rho_{vs}\,h_{vs} - p_{sat}\right) \\
\dfrac{dE}{dt} = w_{in}\,h_{in}(p_{sat},\, T_{out,cond}) + w_{out}\,h_{out}(p_f,\, T_{sat})
\end{cases}
\tag{4.7}
$$

The tank design has to fulfill the following requirements:

- during transients the tank level should not reach neither its minimum, when the suction side of the pump becomes dry, nor its maximum, when the condenser gets flooded;
- his geometrical size and shape has to be compatible with its collocation on board of a truck.

Considering the fact that at steady-state the tank size does not affect the power output and the design of the ORC is at a preliminary stage, for simplicity it has been modelled as a cylinder with a diameter of 0.25 m and a height of 0.6 m.

From a numerical point of view, the presence of the tank facilitates the initialization of the models. Since a "full" steady-state initialization is not feasible due to the large size of the non-linear DAE's system, the saturation condition of the tank guarantees a correct enthalpy distribution in the condenser. This allows a correct distribution of the density, i.e. of the charge, also within all the heat exchangers.

Finally, another small heat exchanger between the tank and the pump sub cools the working fluid, preventing the pump from cavitation.

4.4 Combined cycle

Finally, the combined cycle is made by connecting the topping and the bottoming cycle, as shown in Fig. 4.4. The ORC model is linked to the hot sources, i.e. the diesel engine, and to the cold source, i.e. the radiator, through fluid ports. Moreover, a mechanical interface connects the turbine and the engine shaft. The two blocks on the left of Fig. 4.4 represent the control variables. The model is now complete and ready for the control implementation.

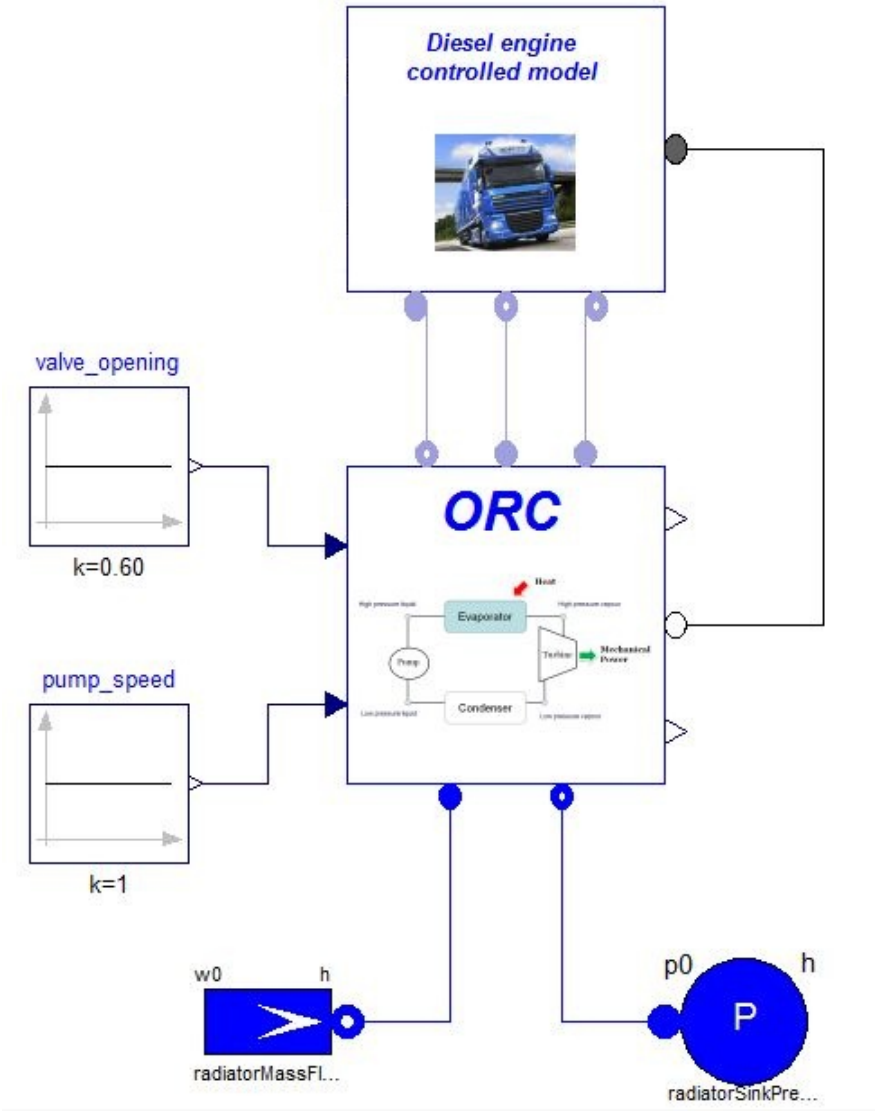

Figure 4.4: Object diagram of the complete system

Chapter 5

Optimal off-design operation

The final step of the design process is the definition of a control system for the ORC unit. To this purpose, first of all, it is necessary to define the control objectives and to perform an accurate analysis of the off-design operating conditions of the system. In fact, the optimal trend of the controlled variables can be derived by a first-principles approach, but since the plant configuration is not conventional, their optimal values is obtained through a model that considers all the physical bounds. Finally, some considerations concerning the results are reported.

5.1 Control objectives

The first step of the control design is the definition of the control objectives. The goals considered in this thesis are:

1. the exhaust gases temperature at the evaporator outlet must be kept above 200 °C so that the SCR after treatment can work properly;

2. the organic fluid temperature at the outlet of the two evaporators must be kept lower than a prescribed value, in order to avoid its thermal degradation. With a safety margin, the maximum fluid temperature has been set to 300 °C;

3. a minimum degree of superheating has to be guaranteed, in order to avoid the presence of liquid droplets at the turbine inlet;

4. the condenser pressure has to remain around its nominal value. When the engine load increases, as well as the heat recovered by the ORC evaporators, the amount of heat the condenser has to reject increases as well. This could lead to a higher condenser pressure, in order to provide a sufficient mean temperature difference for the heat transfer, but at the same time the pressure ratio across the turbine drops, and so its mechanical power output;

5. at the pump inlet the organic fluid has to be subcooled, in order to prevent pump cavitation;

6. the organic fluid has to cool down the EGR gas flow so that the engine efficiency does not decrease;

7. the evaporator pressure has to be kept subcritical to not compromise the mechanical integrity of the PHEs;

8. for any given thermal input, the ORC mechanical power output has to be maximized.

Considering that the available control variables are only two and the objectives are eight, it is impossible to satisfy all the goals with the control system. Hence, some of them have to be intrinsically satisfied.

The introduction of a tank and a small subcooler before the pump allows the system to satisfy items four and five. In fact, the tank decouples the high pressure side from the low pressure side of the ORC circuit, so that a variation of the heat input does not highly modify the mass distribution inside the condenser, and the organic fluid is always at saturation conditions at the condenser outlet. Moreover, the additional heat exchangers provides the temperature drop at the tank outlet which avoids the cavitation of the pump.

For simplicity, the condenser is not controlled, because the cold water circuit is not modelled. Hence, it is not possible to predict the inlet temperature of the cooling water at different engine loads. Considering that the radiator water pump is mechanically coupled with the engine shaft, whose rotational speed can be considered almost constant in this context, water temperature and mass flow have been assumed constant and equal to 70 °C and 0.8692 $\mathrm{kg\,s^{-1}}$.

5.2 Off-design analysis

The control system has to manipulate the control variables so that the mechanical power is maximized and the operating constraints are respected in each off-design condition. In order to guarantee this, we have to find out which is the optimal values of the controlled variables when different inputs and disturbances are applied. An off-design analysis that takes into account only steady-state operational points is enough. Since the two more stringent control objectives are ensuring the optimal operation of the SCR system and avoiding the organic fluid decomposition, we assume that the most suitable controlled variables are:

- $T_{gas,out,EXH}$: as stated in Chapter 3, it has to be kept above 200 °C so that the catalytic reactor works properly;

- ΔT_{sh}: considering that the critical temperature of MM is 245.6 °C, the control of the degree of superheating can prevent the working fluid from reaching dangerous temperatures, and on the other hand the injection of liquid droplets at the turbine inlet. Moreover, cycle efficiency depends on it.

5.2.1 First-principles approach

It is possible to find the optimal trend of the controlled variables set points with respect to the engine load through purely thermodynamic considerations.

Considering the gas exhaust temperature, it is obvious that in each operating condition the more the exhaust gases are cooled down, the higher the heat input for the ORC system and therefore its power output. When the engine load is higher than the nominal load and with a fixed mass flow rate through the EGR evaporator, the control system should increase the organic mass flow through the exhaust evaporator so that the heat recovery from the exhaust gases is maximized. On the other hand, at lower load the same mass flow has to be reduced, so that the limit on the minimum exhaust gases temperature, 200 °C, is satisfied.

This result can be justified if we consider the energy balance of the overall system: for a given fuel mass flow, i.e. thermal input, the heat fraction not recovered by the EGR evaporator represents a heat input for the diesel engine, as shown in Fig. 5.1, and do not leave the combined cycle domain.

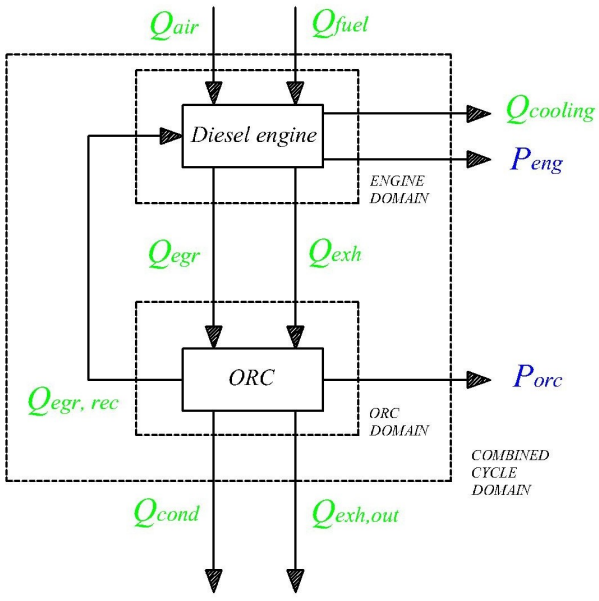

Figure 5.1: Control volume of the energy balances for the combined cycle and its subsystems

About the degree of super heating, it is not trivial to find its optimal value, and some further considerations have to be done. The mechanical power output is given by the following equation:

$$P_m = w_{orc}\,\eta_{is}\,\Delta h_{is} \tag{5.1}$$

Each term changes with the operating point. In particular, the global mass flow circulating inside the two evaporators is basically a function of the pump rotational speed, while the isentropic enthalpy drop of the turbine inlet conditions. The turbine isentropic efficiency depends on the pressure ratio and on the rotational speed.

Let us consider a constant and generic thermal source Q_{in}, higher than the nominal value, which makes the organic flow evaporate. There are two options concerning the control strategy:

1. the mass flow is kept constant. Therefore, the outlet temperature will be higher, together with the isentropic enthalpy drop;

2. the mass flow is increased. The degree of super heating is then kept constant, and the isentropic enthalpy drop as well.

Through the energy balances for a generic simple ORC configuration it is possible to determine which is the best option. For a given heat input, evaporator

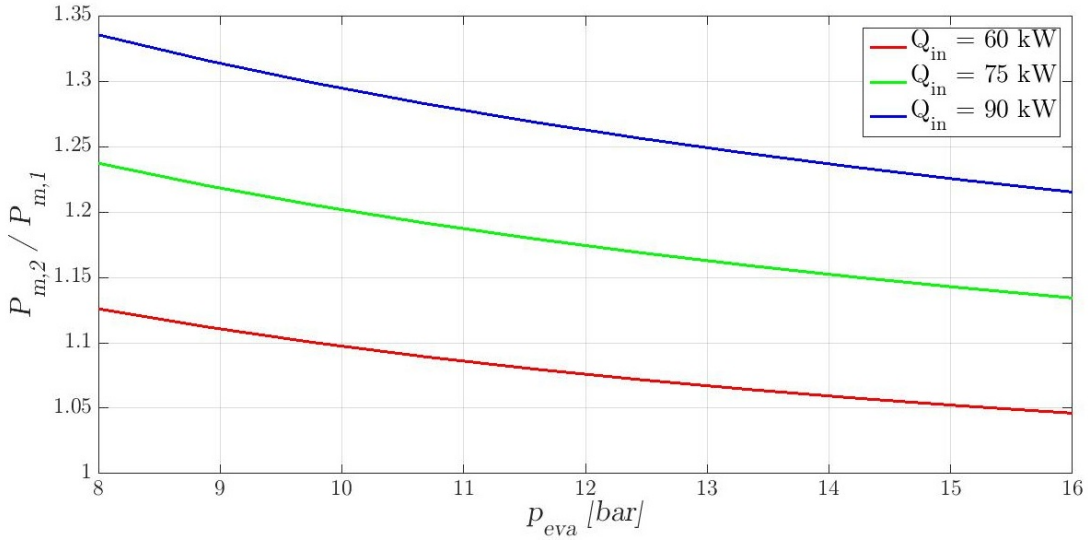

Figure 5.2: Power output ratio between first and second case

and condenser pressure and pump outlet temperature, it is possible to evaluate the power output for the first option as follows:

$$\begin{cases} w_{orc} = \text{const} \\ h_{out} = h_{in}\left(p_{eva},\, T_{out,pump}\right) + \dfrac{Q_{in}}{w_{orc}} \\ TIT = f(p_{eva},\, h_{out}) \\ \Delta T_{sh} = TIT - T_{sat} \\ \Delta h_{is} = f\left(TIT,\, p_{eva},\, p_{cond}\right) \\ P_{m,1} = w_{orc}\, \eta_{is}\, \Delta h_{is} \end{cases} \tag{5.2}$$

In the second case the equations are:

$$\begin{cases} \Delta T_{sh} = \text{const} \\ TIT = T_{sat} + \Delta T_{sh} \\ h_{out} = f\left(p_{eva},\, TIT\right) \\ w_{orc} = \dfrac{Q_{in}}{h_{out} - h_{in}} \\ \Delta h_{is} = f\left(TIT,\, p_{eva},\, p_{cond}\right) \\ P_{m,2} = w_{orc}\, \eta_{is}\, \Delta h_{is} \end{cases} \tag{5.3}$$

The numerical result shows that the relative increase of the mass flow in the second case is higher than the relative increase of the isentropic enthalpy drop in the first one. Fig 5.2 shows the power output ratio between the first and the second approach as a function of the evaporator pressure and of the heat input. All the values are greater than one, in other words it is always better to minimize the degree of superheating. Fig. 5.3 shows the relative variation of the organic mass flow and of the isentropic enthalpy drop with regard to the nominal point. The solid line, i.e. the mass flow variation, is almost always above the dashed line, i.e. the isentropic enthalpy drop variation. Hence, the influence of the mass flow rate on the power output is in general higher than the influence of the isentropic enthalpy drop.

Making the hypothesis that the influence of the isentropic efficiency variation is negligible, we can conclude that the optimal set point of the degree of superheating is ideally zero. However, it has to be fixed to a value that makes the system respect all the constraints.

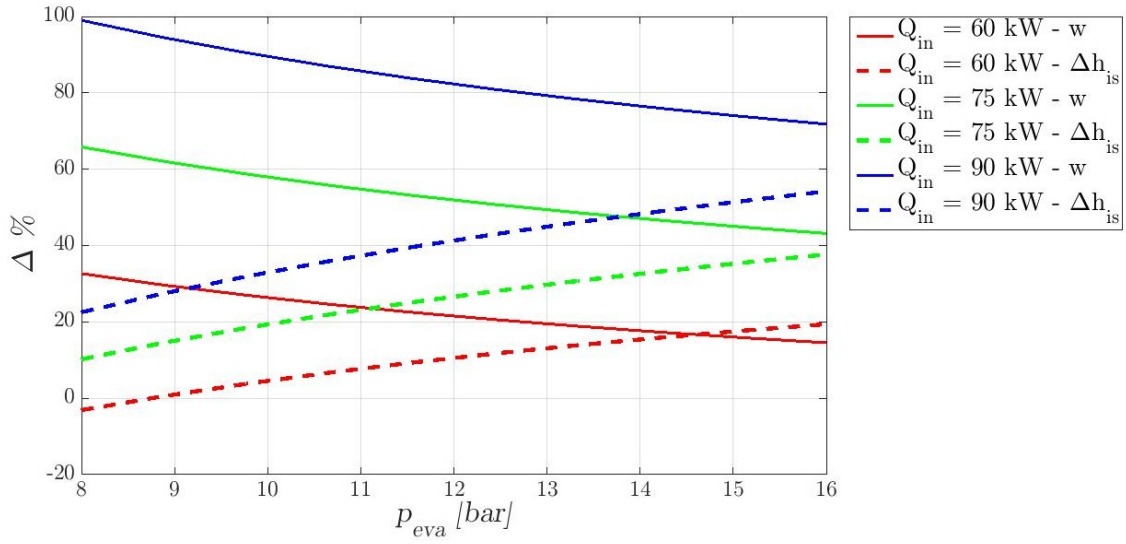

Figure 5.3: Relative variation of the mass flow and the isentropic enthalpy drop

5.2.2 Model-based approach

In order to check if the previous results still apply to the complete combined cycle powertrain, a Modelica model has been used to scan all the feasible steady-state operating point in order to investigate how the mechanical power output changes as a function of the control variables.

The model has 6 inputs and 2 outputs. Therefore, the number of input/output pairs to be evaluated is high and the post processing hard to handle. In order to simplify the analysis, the number of input variables of the engine model can be reduced to only 2: the rotational speed and the net torque required. Since the engine is controlled through the maps created in Chapter 3, it is possible to use the *Simulink* model of the engine and the maps to evaluate the mass flows and temperatures of the thermal sources for each combination of torque and rotational speed. With this approach, the problem dimension is split in half and the handling and visualization of the results is easier. Moreover, we can avoid to use the engine model and reduce the integration time.

The aim of this section is to find the optimal set-point of the controlled variables so that the mechanical power is maximized: for a specific set of combination between engine torque and rotational speed, the control space has been mapped using a series of steps and trapezoidal waves with a very low slope so that the ORC system is always at quasi steady-state conditions, as shown in Fig. 5.4.

For ten different positions of the three way valve, from 1 to 0.1 per unit, a positive or negative ramp on the pump speed is performed. The actual value of the pump speed is kept constant when one of the following conditions is verified:

- *upper bounds*: the pump speed increases too much so that the thermodynamic condition at the turbine inlet enters the two-phase region, or the maximum pressure allowed is reached;

- *lower bounds*: on the other hand, the pump speed decreases too much so that the temperature at the evaporators outlet reaches its maximum, or the organic flow rate its minimum.

The bounds have been chosen as follows: the maximum temperature is set to 350 °C, the maximum pressure to 19 bar and the minimum mass flow to $0.03\,\mathrm{kg\,s^{-1}}$. It is worth noticing that these are not physical but "simulation" bounds, in order to prevent the simulation from failing because one of the variables leaves the range of validity of the equations of state.

The values of the disturbance variables used to explore the state space are the following:

- $n_e = \{900,\ 1000,\ 1100,\ 1200,\ 1300,\ 1400,\ 1500\}\,rpm$;

- $M_m = \{500,\ 800,\ 100,\ 1200,\ 1400,\ 1600\}\,Nm$;

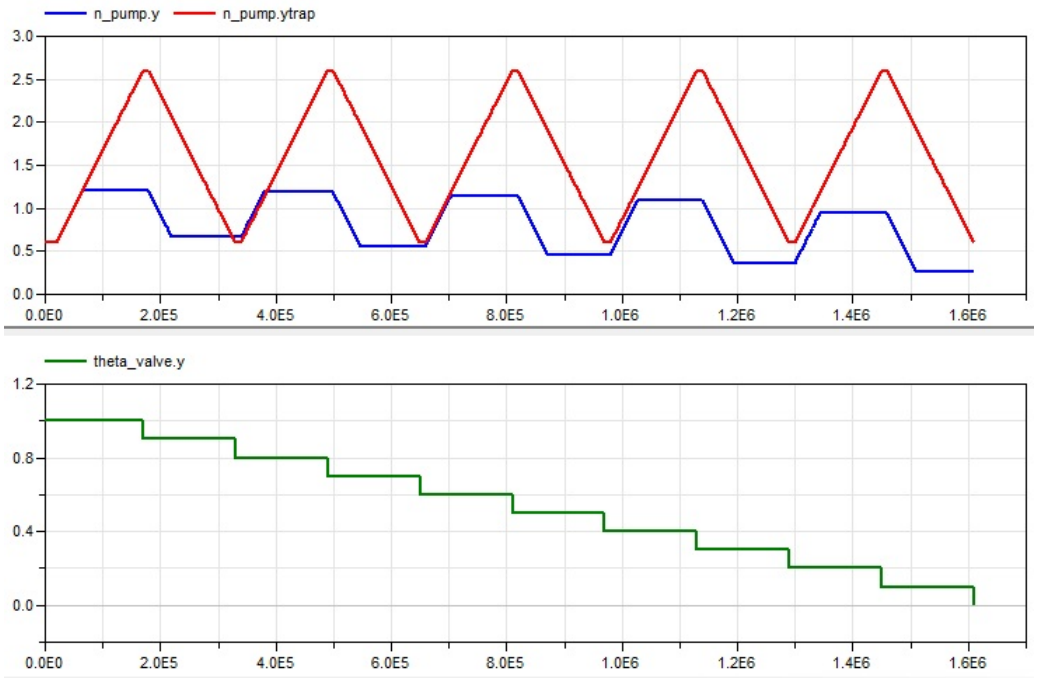

Figure 5.4: Temporized control variables: pump speed on the top, valve position on the bottom graph, both in pu

For each combination of the previous variables, the simulation data have been filtered, in order to eliminate the transient part and the operating points which do not satisfy the constraints listed in Sec. 5.1. Lately, they have been grouped according to the value of w_{TOT} or $\frac{w_{EXH}}{w_{TOT}}$.

Fig. 5.6 show the trend of the mechanical power of the ORC as a function of a specific diesel engine load and of the total organic fluid mass flow. For each value of the flow rate w_{TOT} the mechanical power increases when the degree of superheating at the end of the evaporators increases. At the same time, the mechanical power is maximized when the value of w_{TOT} is maximum. This result confirms both the trends exposed in the previous section and in Chapter 1.

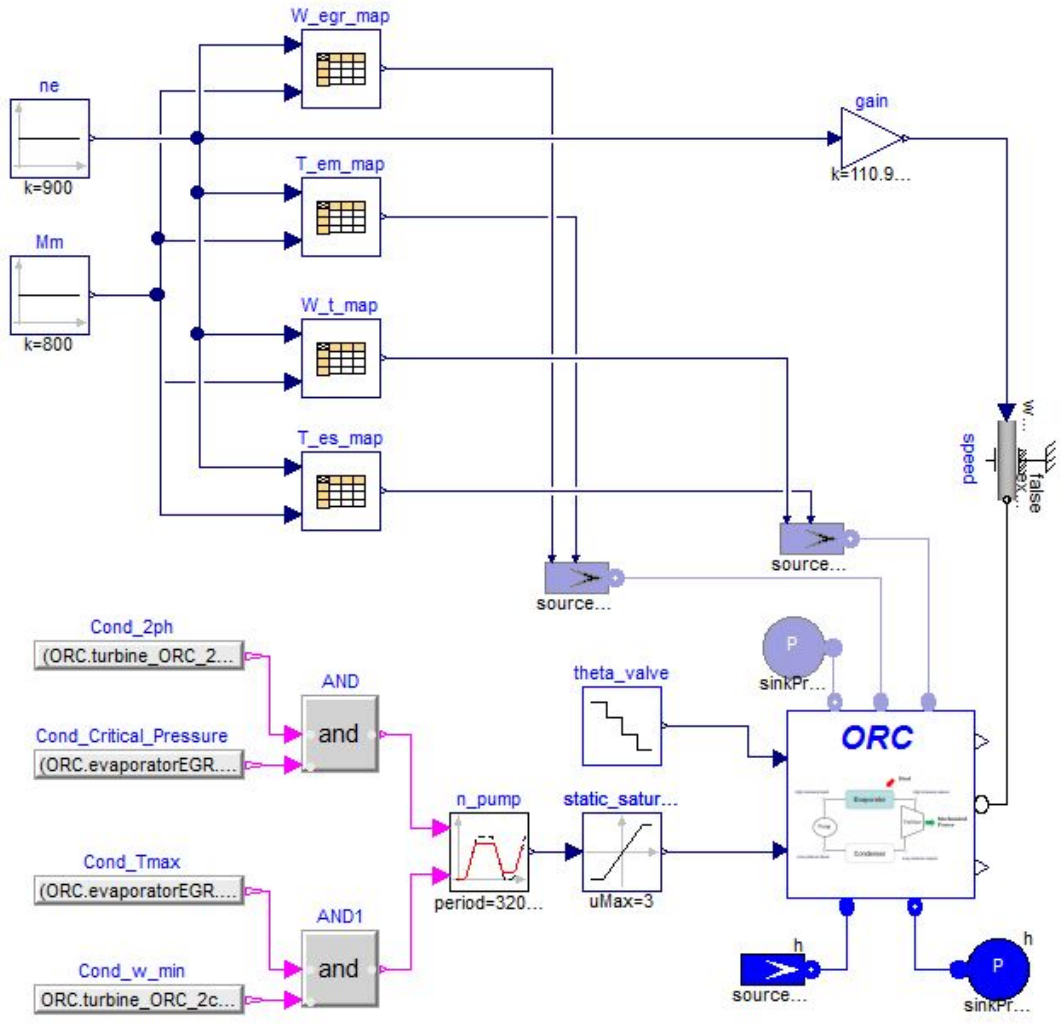

Figure 5.5: Object diagram of the control set points optimization

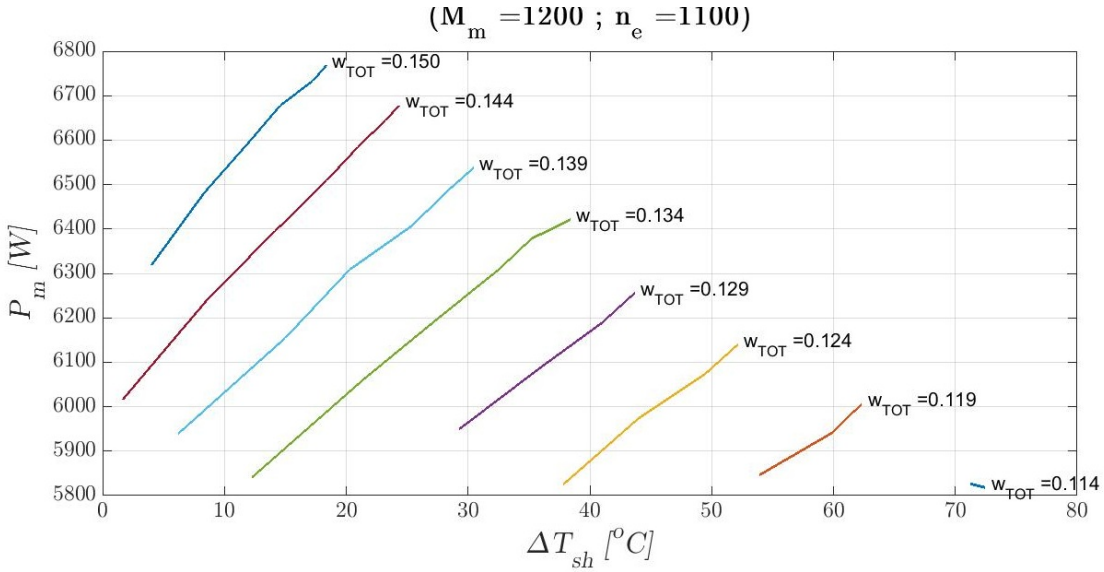

Figure 5.6: Mechanical power output of the ORC unit as function of degree of superheating and total mass flow

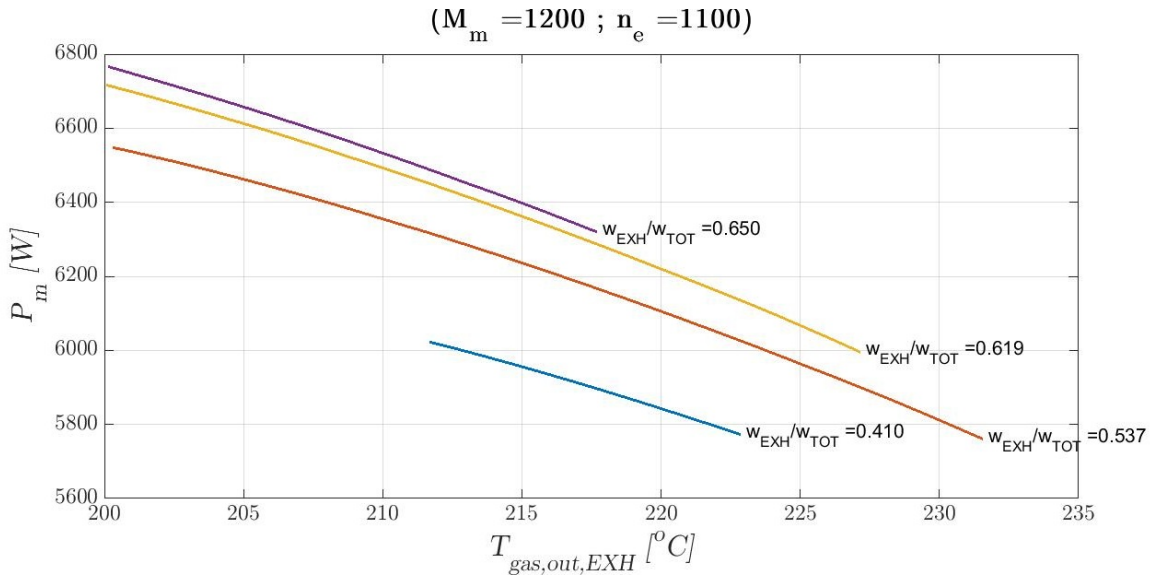

Figure 5.7: Mechanical power output of the ORC unit as function of exhaust gases outlet temperature and $\frac{w_{EXH}}{w_{TOT}}$

Moreover, the simulations give also the additional information concerning the feasible range of the degree of superheating: n has to be bounded so that total mass flow is between $0.114\,\mathrm{kg\,s^{-1}}$ and $0.150\,\mathrm{kg\,s^{-1}}$, and for instance for $w_{TOT} = 0.139\,\mathrm{kg\,s^{-1}}$ the degree of superheating has to be greater than 7 °C and lower than

30 °C.

Fig. 5.7 confirms as well what stated in the previous subsection: if all the physical bounds are respected, it is better to cool down the exhaust gases as much as possible, so that the heat recovery factor is higher. The maximum value of P_m is reached with the higher value of the ratio between w_{EXH} and w_{tot}.

5.3 Optimal set points

It is important to underline that the optimal value of the controlled variables is not unique, but it changes according to the engine load. This is due to the control objectives: for instance, at high load and with a fixed pump rotational speed, the higher the valve opening, the higher the mass flow through the exhaust evaporator and the lower the exhaust gas temperature, but at the EGR evaporator outlet the organic fluid temperature could be higher than its upper bound because the mass flow is decreased. Thus, the optimal set point of the exhaust gases temperature is not its minimum value, as shown in Fig. 5.9. On the other hand, at low load the degree of superheating has to be high, so that the exhaust gas temperature is kept above 200 °C, as reported in Fig. 5.8.

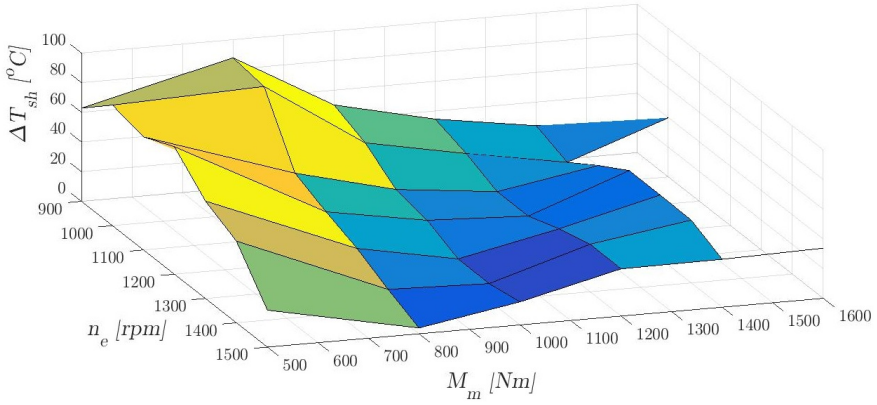

Figure 5.8: Optimal set points of the degree of superheating

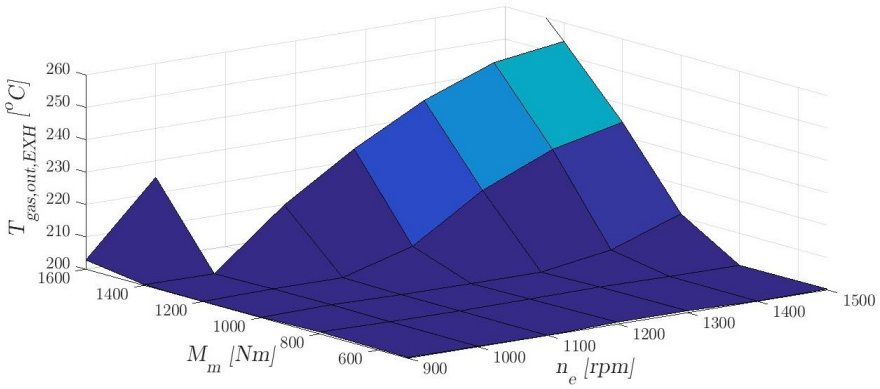

Figure 5.9: Optimal set points of the exhaust gases temperature

Fig. 5.8 and Fig. 5.9 report the optimal values of the controlled variables as function of the engine torque and rotational speed.

5.4 Control saturation

One of the main outcome of the previous simulations is the maximum value of the pump rotational speed. In Fig. 5.8 and 5.9 it can be noticed that at the maximum load considered ($M_m = 1600\,Nm$) there are no feasible operational points for the ORC system. This is due to the fact that it is not possible to keep the organic fluid maximum temperature under the value of 300 °C without a super critical cycle. This phenomenon is well explained by the turbine reduced mass flow equation:

$$\frac{w\sqrt{T_{in}}}{p_{in}} = w_{red} \tag{5.4}$$

When the pump rotational speed increases the previous equation implies that the evaporators pressure has to increase as well. Since a supercritical operating condition should be avoided, it results that for a certain value of turbine inlet temperature there is a maximum value of mass flow rate: considering that the nominal evaporators pressure is around 12.5 bar and the critical pressure is around 19 bar, the total mass flow could increase approximately of the 50%. This results is confirmed by the value of the pump speed normalized with respect to the nominal point, as shown in Fig. 5.10.

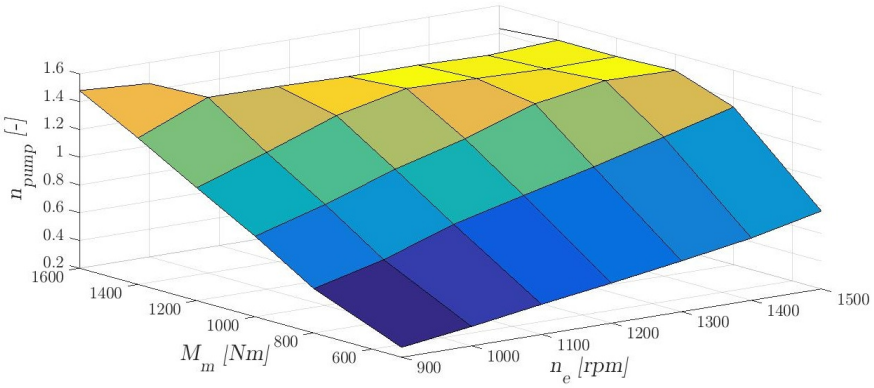

Figure 5.10: Optimal values of the pump rotational speed

For high values of n_e and M_m the pump speed saturates around a value of 1.4
.

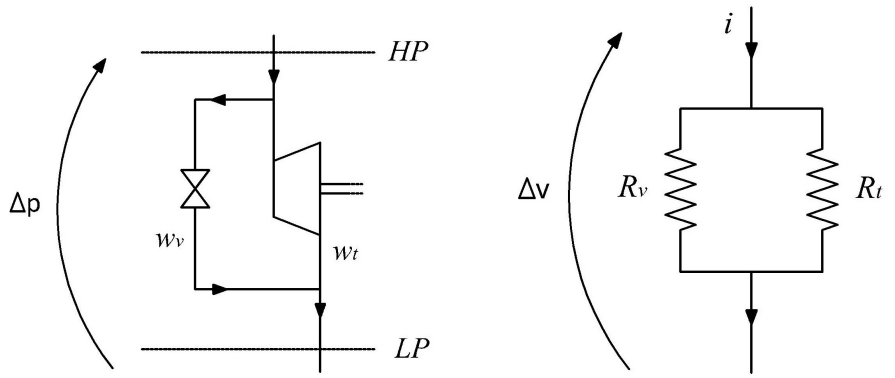

(a) Physical scheme (b) Electrical scheme

Figure 5.11: Scheme of the electrical analogy

This saturation does not represent a problem during normal truck operation, but when the requested torque is higher than 1500 Nm a safety device has to keep the cycle pressure subcritical. There are two options:

- *turbine by-pass*: a by-pass valve in parallel configuration with the turbine could be opened when the critical pressure is reached. Its operating principle is well explained in Fig. 5.11: using the electrical analogy, it is possible to evaluate the equivalent resistance of the circuit with the equation:

$$R_{eq} = R_v \parallel R_t = \frac{R_v\, R_t}{R_v + R_t} \quad \Rightarrow \quad i = \frac{\Delta V}{R_{eq}} \tag{5.5}$$

  If the equivalent resistance decreases, i.e. the by pass valve is opened, the mass flow rate can be higher, while the pressure drop is constant. This solution can guarantees the cooling of the EGR system but part of the heat recovered from the engine is rejected through the condenser.

- *evaporator by-pass*: a by-pass on the gas side of the exhaust evaporator can reduce the heat recovery, so that the ORC system can operate in the safety region. The condenser is therefore less overloaded.

The first option seems to be more attractive, even if the condenser is then overloaded: indeed, at a high engine load there is always a large amount of heat to be rejected, so that the radiator is in any case almost at full load. Moreover, the design thermal load of the radiator is much higher than its nominal load, so that the additional heat coming from the ORC condenser does not affect its performance.

Chapter 6

Control system design

At this point, it is useful to distinguish between manipulated and disturbance variables. The process inputs can be divided as follow:

- *2 manipulated variables*: pump rotational speed n, expressed as the ratio between the actual and the nominal value, and valve opening θ, expressed in per unit;
- *2 disturbance variables*: variations of engine torque and rotational speed, which change according to the current velocity and acceleration of the truck.

Therefore, the system is MIMO.

The main purpose of this final analysis is to check the feasibility of a simple control system that respects the operating constraints and at the same time guarantees the optimal performance of the WHR unit. About the control architecture, the first and simpler option is a decentralized controller. This solution is doable if the mutual interaction between the two control loops is not too strong: this is verified through the RGA matrix. If the interaction is high a decoupling method has to be implemented, and the controller becomes centralized. In the next sections, the identification of a linearised model and of the corresponding transfer functions is performed. Once the control architecture is defined, two PI controllers are tuned and tested with a realistic truck velocity profile as simulation input.

6.1 System linearisation

The first step of control design is the linearisation of the system around the nominal operating point and a limited number of off-design conditions. In particular 5 conditions have been chosen in order to explore the state-space around the nominal point. They are identified by a combination of engine torque and rotational speed (see Tab. 6.1).

Tables 6.1: Operating points considered in the linearisation process

Point	Torque Nm	Rotat. speed rpm
1	600	1000
2	600	1400
3	900	1200
4	1200	1000
5	1200	1400

A generic time-invariant dynamic system can be described by non-linear ordinary differential equations derived from first-principle laws, i.e. mass, momentum and energy balances. Typically, it is presented in "state-space" form as:

$$\begin{cases} \dot{x} = f(\, x(t),\, u(t)\,) \\ y = g(\, x(t),\, u(t)\,) \end{cases} \tag{6.1}$$

where $x \in \mathbb{R}^n$ is the state variables vector, $u \in \mathbb{R}^m$ is the inputs vector and $y \in \mathbb{R}^p$ is the outputs vector. Assuming that we want to make use of linear multivariable control theory, the non-linear system has to be linearised around a certain equilibrium point. The main hypothesis behind this theory is the superposition principle, which is valid for linear systems. It implies that a change in an output variable (y) can simply be found by adding together the separate effects resulting from the variation of the different input variables $(u_1,\, u_2,\, \ldots,\, u_n)$ considered independently from one another. Using a first order Taylor's series approximation, we can write:

$$\begin{cases} \Delta\dot{x} = f(\, \overline{x},\, \overline{u}\,) + \dfrac{\partial f}{\partial x}\Delta x + \dfrac{\partial f}{\partial u}\Delta u + \text{h.o.t.} \\ \overline{y} + \Delta y = g(\, \overline{x},\, \overline{u}\,) + \dfrac{\partial g}{\partial x}\Delta x + \dfrac{\partial g}{\partial u}\Delta u + \text{h.o.t.} \end{cases} \tag{6.2}$$

Considering that at the equilibrium point $f(\, \overline{x},\, \overline{u}\,) = 0$ and $\overline{y} = g(\, \overline{x},\, \overline{u}\,)$, and neglecting the second-order terms:

$$\begin{cases} \Delta\dot{x} = \dfrac{\partial f}{\partial x}\Delta x + \dfrac{\partial f}{\partial u}\Delta u \\ \Delta y = \dfrac{\partial g}{\partial x}\Delta x + \dfrac{\partial g}{\partial u}\Delta u \end{cases} \quad \Rightarrow \quad \begin{cases} \Delta\dot{x} = A\Delta x + B\Delta u \\ \Delta y = C\Delta x + D\Delta u \end{cases} \tag{6.3}$$

All the signals are then deviation variables, and the symbol Δ is usually omitted. The last system is called "tangent linearised system", and the coefficients A, B, C and D are the Jacobian matrices evaluated at the equilibrium.

The Jacobian matrices can be obtained through the "Linearize" command of Dymola: for a given set of variables values at equilibrium, the software numerically evaluates the Jacobian and stores the results in a $(n+p) \times (n+m)$ matrix which can be lately manipulated. n is the system order, i.e. the number of state variables, p the number of outputs and m the number of inputs.

For control design purposes it is convenient to work in the frequency domain, where the evaluation of stability properties of the process and of bandwidth and peaks of closed-loop transfer functions is easier. Applying the Laplace's transform at Eq. 6.3 and neglecting the transient part linked to the initial conditions, the transfer function, or the matrix of transfer functions in case of a MIMO system, between input and output can be derived as follows:

$$Y(s) = P(s)\,U(s) \quad \Rightarrow \quad P(s) = [\,C\,(s\,I - A)^{-1}\,B + D\,] \tag{6.4}$$

The combined cycle composed by the Diesel engine and the ORC has 4 inputs and 2 outputs. Hence, the matrix $P(s)$ has size 2×4. In order to reduce the non-linearities of the system, it is convenient to use as virtual control variables the two dimensionless mass flow rates of the evaporators, defined as their deviation with respect to their equilibrium values. Given these values, the controller can determine the pump speed and the valve opening through some suitable algebraic transformations.

If we distinguish between control variables and disturbances, the matrix $P(s)$ can be splitted in two different parts:

$$G(s) = \begin{bmatrix} \dfrac{\Delta(\Delta T_{sh})(s)}{\delta w_{EGR}(s)} & \dfrac{\Delta(\Delta T_{sh})(s)}{\delta w_{EXH}(s)} \\ \dfrac{\Delta T_{scr}(s)}{\delta w_{EGR}(s)} & \dfrac{\Delta T_{scr}(s)}{\delta w_{EXH}(s)} \end{bmatrix} = \begin{bmatrix} G_{11}(s) & G_{12}(s) \\ G_{21}(s) & G_{22}(s) \end{bmatrix} \tag{6.5}$$

$$H(s) = \begin{bmatrix} \dfrac{\Delta(\Delta T_{sh})(s)}{\delta M_m(s)} & \dfrac{\Delta(\Delta T_{sh})(s)}{\delta n_e(s)} \\ \dfrac{\Delta T_{scr}(s)}{\delta M_m(s)} & \dfrac{\Delta T_{scr}(s)}{\delta n_e(s)} \end{bmatrix} = \begin{bmatrix} H_{11}(s) & H_{12}(s) \\ H_{21}(s) & H_{22}(s) \end{bmatrix} \tag{6.6}$$

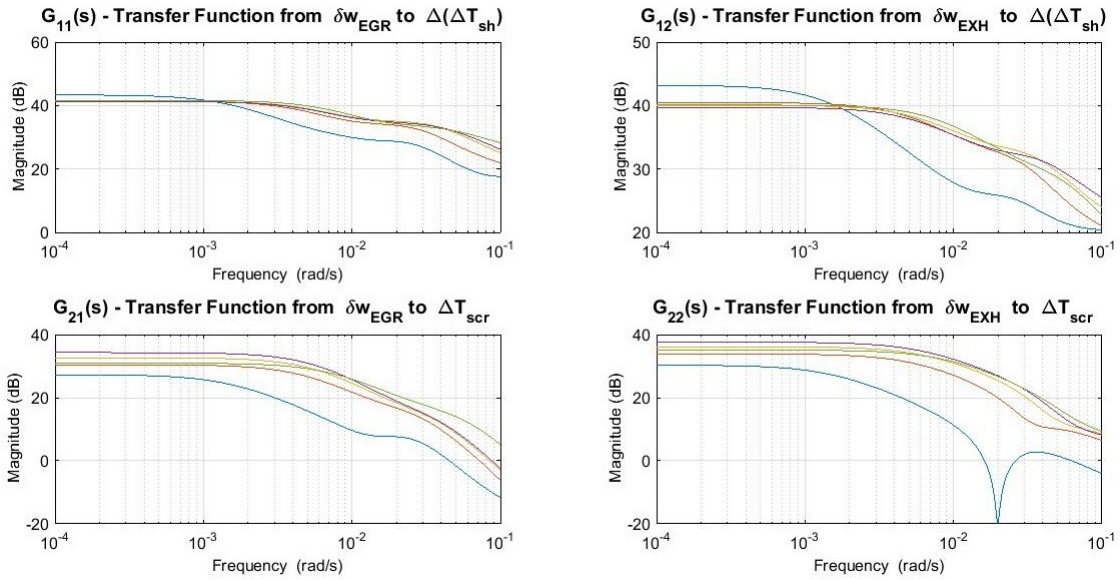

Figure 6.1: Magnitude diagrams of G(s)

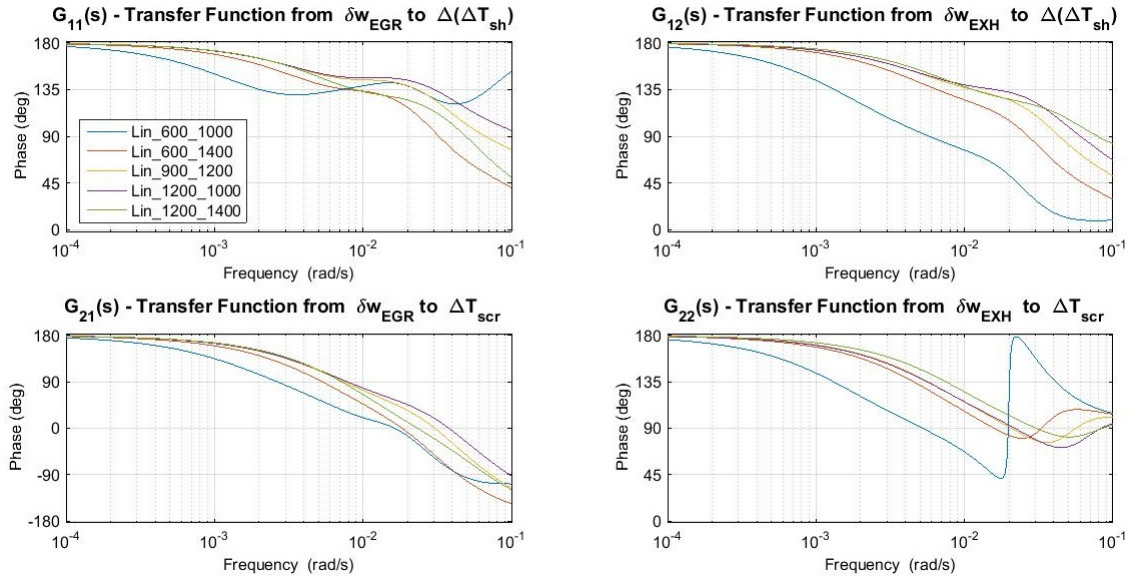

Figure 6.2: Phase diagrams of G(s)

Thanks to a specific *MATLAB* commands it is possible to obtain the Bode plots of the matrix of transfer functions G(s) within the range of interest. The minimum frequency has been set to $0.0001\,\mathrm{rad\,s^{-1}}$, while the maximum frequency to $0.1\,\mathrm{rad\,s^{-1}}$. The latter value is the higher crossover frequency we can expect for

the closed-loop controllers.

Fig. 6.1 shows the magnitude values and Fig. 6.2 the phase values: apart from the simulation number 1 (Lin_600_1000, see Tab. 6.1), the matching between the magnitude and phase curves is good till $\omega = 0.01\,\mathrm{rad\,s^{-1}}$. This means that the change in the control variables choice reduces the non-linearities, leading to a more robust behaviour of a fixed-parameter linear controller. For sake of simplicity we use as reference the linearisation number 3 (Lin_900_1200), which is close to the nominal operating point.

6.2 Control architecture

The control architecture mainly depends on the mutual interaction between the controlled and control variables. This analysis can be done through the evaluation of the Relative Gain Array (RGA) matrix, an analytical tool used to determine the optimal input-output variable pairings for a MIMO system. In other words, the RGA is a normalized form of the gain matrix that describes the impact of each control variable on the outputs, compared to each control variable impact on other variables. The closer the diagonal values to one, the better the couplings choice.

It can be evaluated for a generic system $n \times n$ as follows:

$$\Lambda = G(0) \otimes (G(0)^T)^{-1} = \begin{bmatrix} \lambda_{11} & \lambda_{12} & \dots & \lambda_{1n} \\ \lambda_{21} & \lambda_{22} & \dots & \lambda_{2n} \\ \vdots & \vdots & \ddots & \vdots \\ \lambda_{n1} & \lambda_{n2} & \dots & \lambda_{nn} \end{bmatrix} \tag{6.7}$$

For a 2×2 system the latter formula becomes:

$$\Lambda = \begin{bmatrix} \lambda_{11} & 1-\lambda_{11} \\ 1-\lambda_{11} & \lambda_{11} \end{bmatrix} \quad \text{with} \quad \lambda_{11} = \frac{1}{1 - \dfrac{g_{12}\, g_{21}}{g_{11}\, g_{22}}} \tag{6.8}$$

Fig. 6.3 shows the values of λ_{11} for each linearisation. The mean value is around 2.5: this means that the system is strongly coupled, while the highest influence is between $\Delta(\Delta T_{sh})$ and δw_{EGR} and between ΔT_{scr} and δw_{EXH}.

Therefore it is necessary to design non-interacting or decoupled control schemes. Essentially, the role of decoupler is to decompose a multivariable process into a series of independent single-loop sub-systems. If such a situation can be achieved, then complete or ideal decoupling occurs and the multivariable process can be controlled using independent loop controllers [36].

Referring to Fig. 6.4, the process matrix $G(s)$ is replaced by a pseudo-process

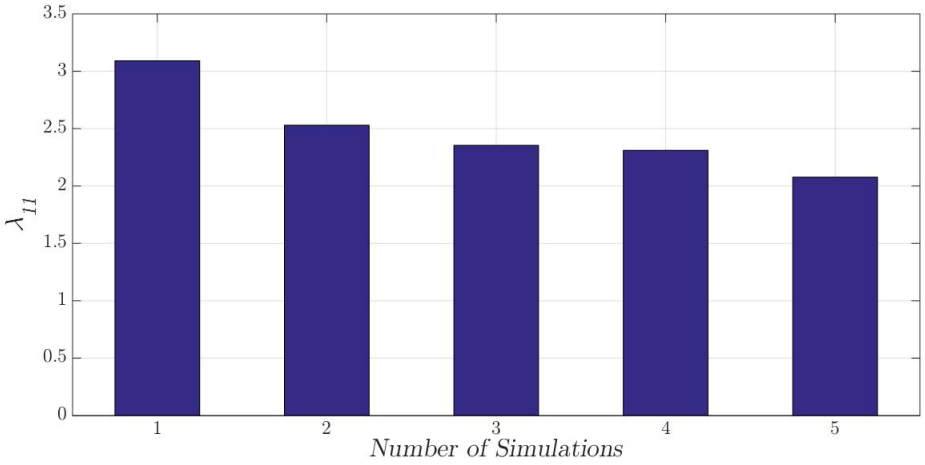

Figure 6.3: Value of λ_{11} for each linearisation

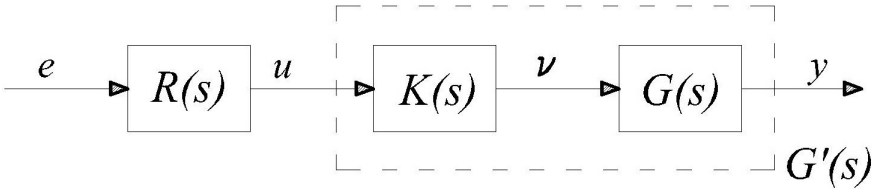

Figure 6.4: Reference scheme for decoupling procedure

matrix $G(s)\,K(s) = G'(s)$, diagonal by construction. This condition is expressed by the following system:

$$\begin{cases} G_{11}(s)\,K_{12}(s) + G_{12}(s)\,K_{22}(s) = 0 \\ G_{21}(s)\,K_{11}(s) + G_{22}(s)\,K_{21}(s) = 0 \\ K_{11}(s) = 1 \\ K_{22}(s) = 1 \end{cases} \tag{6.9}$$

Since the number of diagonality conditions is 2 and the number of unknowns 4, i.e. the elements of the matrix $K(s)$, we have to introduce other two equations to close the system. Arbitrarily the trace of $K(s)$ is set to 1. The solution is:

$$\begin{cases} K_{11}(s) = 1 \\ K_{12}(s) = -\dfrac{G_{12}(s)}{G_{11}(s)} \\ K_{21}(s) = -\dfrac{G_{21}(s)}{G_{22}(s)} \\ K_{22}(s) = 1 \end{cases} \Rightarrow G'(s) = \begin{bmatrix} G_{11}(s)\big(1 - K_{12}(s)\,K_{21}(s)\big) & 0 \\ 0 & G_{22}(s)\big(1 - K_{12}(s)\,K_{21}(s)\big) \end{bmatrix} \tag{6.10}$$

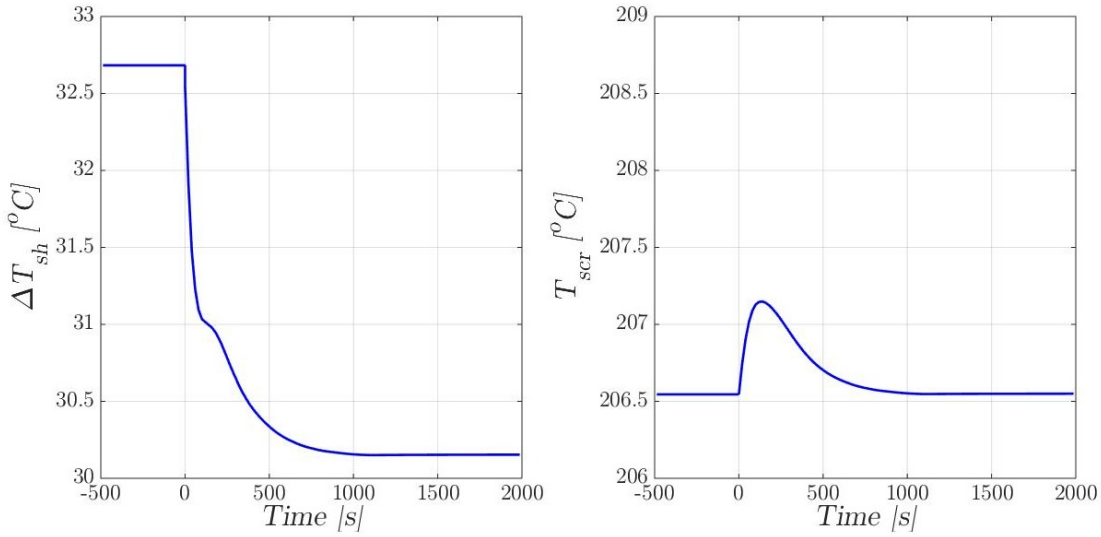

Figure 6.5: Step response of controlled variables for a 5% increase of w_{EGR}

Since the linearised model has a high number of states, the resulting dynamic decoupler is often not physically feasible and it might also be unstable. Hence, a static decoupling scheme is implemented, which guarantees a good static performance. The matrix of the pseudo-process at steady-state becomes:

$$G'(0) = \begin{bmatrix} G_{11}(0)\big(1 - k_{12}\,k_{21}\big) & 0 \\ 0 & G_{22}(0)\big(1 - k_{12}\,k_{21}\big) \end{bmatrix} \quad \text{with} \quad k_{ij} = -\frac{g_{ij}}{g_{ii}} \tag{6.11}$$

Concerning dynamic performance, it has to be tested in order to evaluate how much a controlled variable moves against a step change of the non-coupled control variable. Fig. 6.5 and 6.6 show the results of a step response of the two controlled variables when the EGR and the exhaust mass flow are respectively increased of

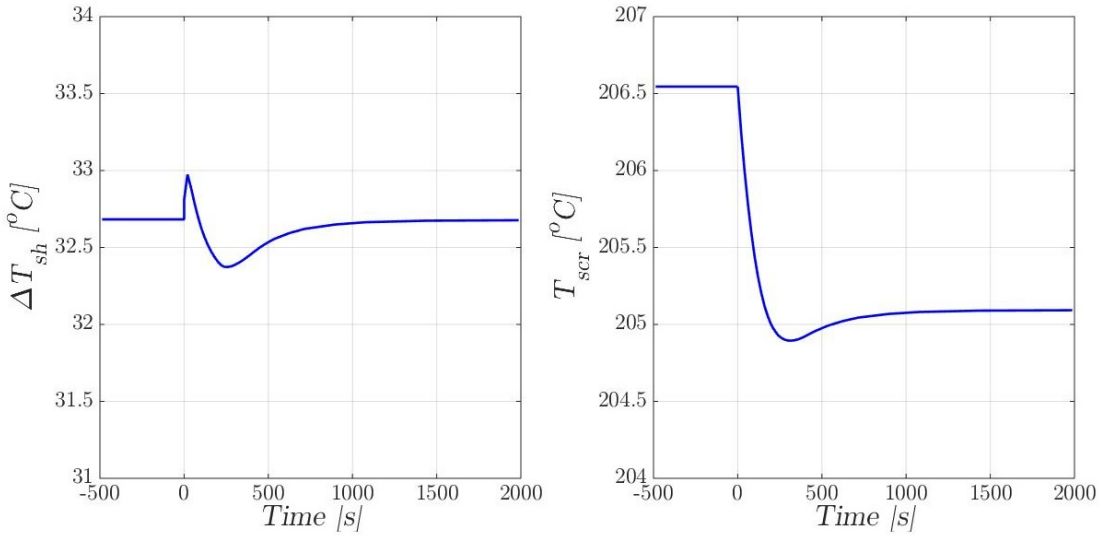

Figure 6.6: Step response of controlled variables for a 5% increase of w_{EXH}

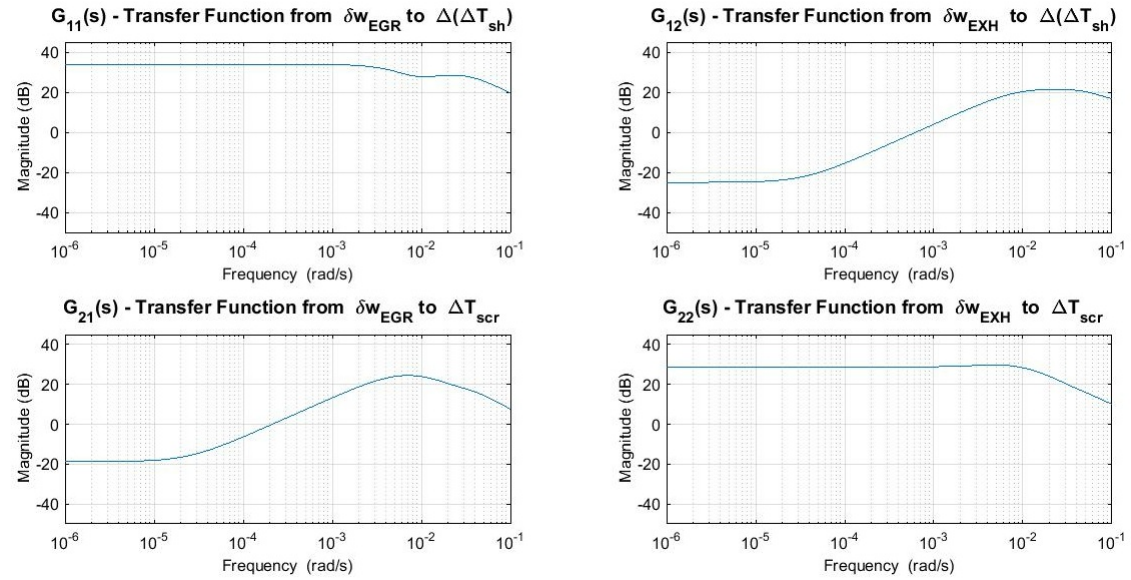

Figure 6.7: Magnitude diagrams of G'(s)

5%. The steady-state error of the uncoupled variables is practically zero, and the response overshoot is small if compared with the steady-state value.

At this point the "Linearize" feature of Dymola is used on the decoupled system, in order to check the correctness of the decoupling procedure. Fig. 6.7 shows the magnitude of the transfer functions matrix $G'(s)$: as expected the gain of the

anti-diagonal components is lower than 0 dB, so that at low frequencies their effect is negligible. Moreover, the value of λ_{11} is equal to 1, confirming the correct coupling.

6.3 Identification of the transfer functions

Since the order of the system, in other words the dimension of matrix A or the number of states, is high, the model might be unnecessarily complex for the purposes of controller design. Model order reduction may overcome some of these difficulties: simplification of the model usually results in a model of lower complexity which is easier to handle, especially during advanced control design, but it is quite possible that model reduction causes a significant loss of accuracy.

Balanced realisation The first step of model reduction is to obtain a balanced realisation, or representation, of the LTI system. A balanced realization is an asymptotically stable minimal realization in which the controllability and observability Gramians are equal and diagonal [35, 482]. Defined n the order of the system, the controllability Gramian is a squared matrix of order n used to define whether a state is controllable or not. State controllability condition implies that it is possible, by admissible inputs, to steer the states from any initial value to any final value within some finite time window. A continuous time-invariant linear state-space model defined by matrices (A,B,C,D) is controllable if and only if:

$$rank \begin{bmatrix} B & AB & A^2B & \dots & A^{n-1}B \end{bmatrix} = n \tag{6.12}$$

In a similar way it is possible to define the observability Gramian, which defines if a state is observable or not. Observability is a measure for how well internal states of a system can be inferred by measuring its external outputs. In this case, a continuous time-invariant linear state-space model defined by matrices (A,B,C,D) is observable if and only if:

$$rank \begin{bmatrix} C \\ CA \\ C^2A \\ \dots \\ C^{n-1}A \end{bmatrix} = n \tag{6.13}$$

The evaluation of the controllability and observability Gramians of the LTI system obtained from the linearisation process allows a partial order reduction: in fact, the rank of the two matrices defined above is lower than n. Therefore we can

eliminate all those states which are neither controllable nor observable, and obtain the minimal realisation of the system.

It is important to underline two aspects:

- one of the state is the angular position of the engine shaft. Unfortunately, its equation is a pure integrator in Laplace domain, thus unstable by definition. In fact:

$$\frac{d\varphi}{dt} = \omega \quad \overset{\text{Laplace transform}}{\Rightarrow} \quad \varphi(s) = \frac{\omega(s)}{s} \tag{6.14}$$

  This formalism is strictly necessary within the Modelica language. Once the position φ is defined during initialization, angular velocity and angular acceleration can be uniquely defined with a numerical derivative calculation, while the opposite procedure depends on a constant. Since the state φ is neither controllable nor observable, it is erased from matrix A during the minimization process, and does not influence the system stability.

- another state closed to be a pure integrator is the tank internal energy. Its dynamic is described by the following equations:

$$\begin{cases} E = V\left((1-\alpha)\,\rho_{ls}\,h_{ls} + \alpha\,\rho_{vs}\,h_{vs} - p_{sat}\right) = f\left(T_{sat}\right) \\ \dfrac{dE}{dt} = w_{in}\,h_{in}(p_{cond},\,T_{out,cond}) + w_{out}\,h_{out}(p_f,\,T_{sat}) \end{cases} \tag{6.15}$$

  The pole related to E has $\mathbb{R}(p) \simeq 10^{-14}$, which means zero up to machine precision. If the tank level remains within its minimum and maximum value, this pole will not affect the controlled variables, because its is neither controllable nor observable. Thus, the dynamic of E can be neglected for our purpose.

At the end of the minimization procedure, the system has to be balanced. Any minimal realization of a stable transfer function can be balanced by a simple state similarity transformation which scale the matrix A so that the controllability and observability Gramians of the minimized system are equal and diagonal. This transformation does not affect the matrix D, i.e. the influence of the inputs on the outputs, but allows to properly compare states whose absolute values are large, for instance the pressures and enthalpies, with other states whose absolute values are small, for instance the temperatures. The similarity transformation replaces each state with an appropriate combination of other states, called modes of the system.

Reduced model Once the state-space system is in balanced form, an order reduction procedure based on this form may be applied.

The most important degree of freedom is the desired order of the reduced model. It is the result of a trade-off between accuracy and simplicity: the higher the order, the harder the handling of the model. The best choice is the order that minimize the error between reduced and non-reduced model within the control bandwidth, and can be evaluated on the basis of the Hankel singular values analysis. In fact, they provide a measure of energy for each mode of a system: during balanced model reduction high energy states are retained while low energy states are discarded. At the same time the reduced model retains the important features of the original model.

Hankel singular values are calculated as the square roots of the eigenvalues of the product between the controllability Gramian, W_C, and the observability Gramian, W_O.

$$\{\sigma_i \geq 0,\, i = 1, \ldots, n\} = eig\,(W_C \times W_O) \tag{6.16}$$

Fig. 6.8 shows the Hankel singular values for the 5 operational point chosen for the linearisation. It can be easily inferred that the first six states are the ones with the highest energy level. Hence, the reduction order is 6.

Given the observability/controllability Gramian Σ with the sorted Hankel singular values on the diagonal ($\sigma_1 \geq \sigma_2 \geq \cdots \geq \sigma_n$), the minimised and balanced realisation can be decomposed into two main subsystem: the first one gathers the

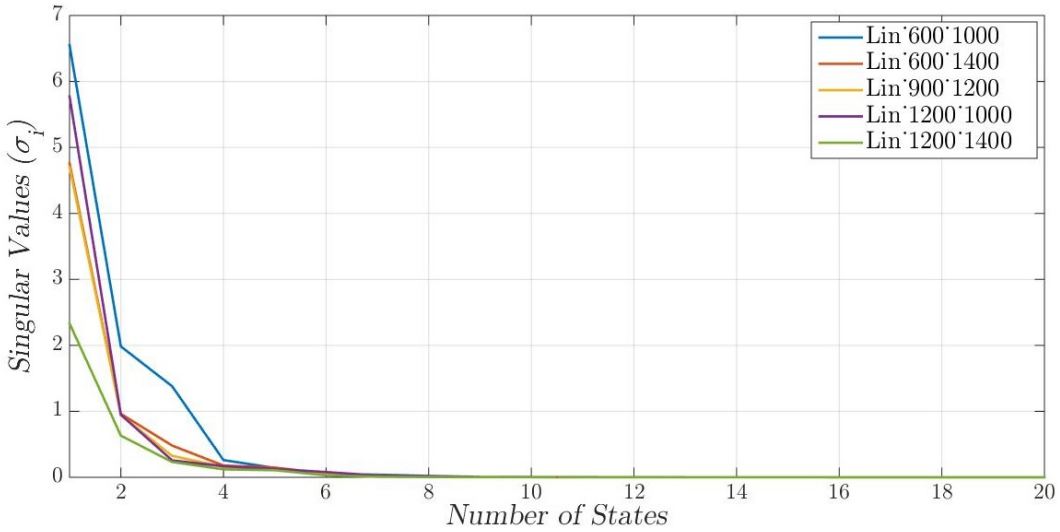

Figure 6.8: Hankel singular values of the balanced realisations

first six states with the related highest six Hankel singular values; the second one gathers all the other states. More formally:

$$\Sigma_1 = diag(\sigma_1 \geq \cdots \geq \sigma_k), \quad \Sigma_2 = diag(\sigma_{k+1} \geq \cdots \geq \sigma_n) \quad \Rightarrow \Sigma = \begin{bmatrix} \Sigma_1 & 0 \\ 0 & \Sigma_2 \end{bmatrix} \tag{6.17}$$

where k is the reduced system order. Therefore the Jacobian matrices become:

$$A = \begin{bmatrix} A_{11} & A_{12} \\ A_{21} & A_{22} \end{bmatrix} \quad B = \begin{bmatrix} B_1 \\ B_2 \end{bmatrix} \quad C = \begin{bmatrix} C_1 & C_2 \end{bmatrix} \tag{6.18}$$

where the elements with subscript 1 refer to Σ_1 and the elements with subscripts 2 to Σ_2. Among all the reduction methods, the three most common are [35, 483]:

- *Balanced truncation*: it discards all the information related to the states whose Hankel singular values are lower than σ_k. Hence, the reduced order model is given by $G_a = (A_{11}, B_1, C_1, D)$. The truncated model G_a is equal to the linearised model G at high frequencies, but the gain values can be different;
- *Balanced residualisation*: it sets $\dot{x}_2 = 0$. Therefore the influence of the low energy states is preserved at low frequencies, so that the gain are matched, but causes a low accuracy at high frequencies;
- *Optimal Hankel norm approximation*: it finds a reduced order model $G_a^k(s)$ of degree k such that the Hankel norm of the approximation error $\| G(s) - G_a^k(s) \|$ is minimized. This method tries to find a reduced model which has a good accuracy both at high and low frequencies.

Applying the reduction algorithms on the decoupled linearised system $G's$ and comparing the Bode diagram within the frequency range of interest, the conclusion is that the best reduction method is the optimal Hankel approximation, as shown in Fig. 6.9: indeed, at each frequency the gap between the linearised model and the Hankel model is low, concerning both the magnitude and the phase.

Another check of the good quality of the model is the comparison between the real simulation data, the linearised and the reduced models for a step response. The result is shown in Fig. 6.10: as expected, the linearised model is the best one, both statically and dynamically, while the Hankel method has the better accuracy compared with the other reduction method. The gain value is not perfectly matched, as the time step response and the Bode diagram at low frequency show, but the reduced model is closed to the linearised one at mid frequency.

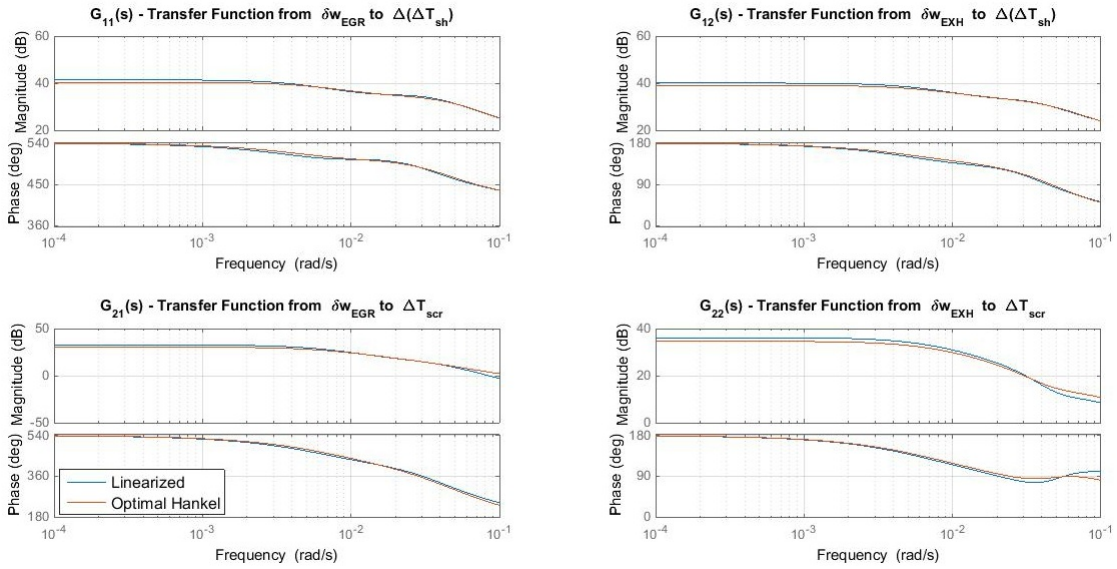

Figure 6.9: Comparison between linearised and Hankel model

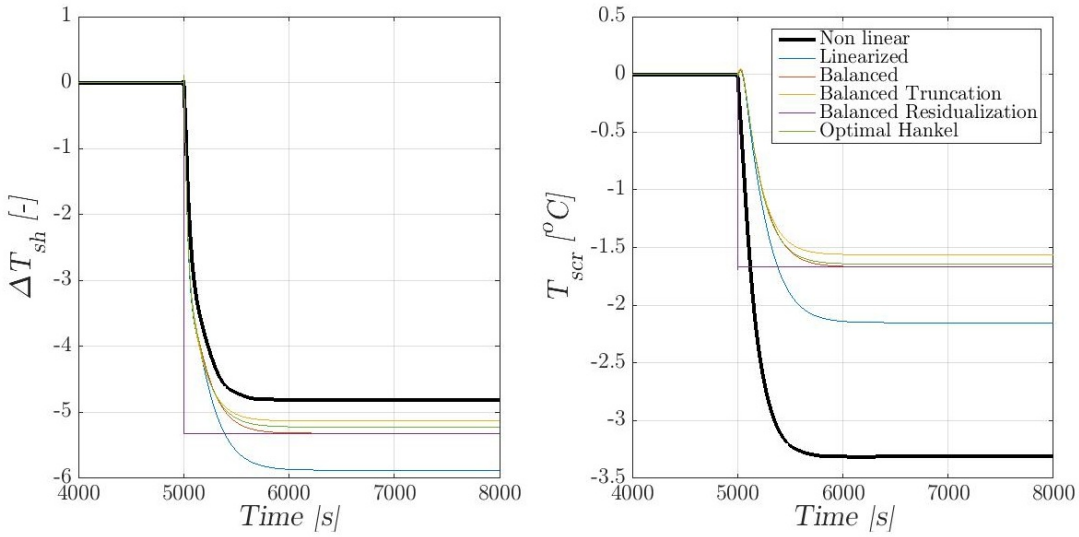

Figure 6.10: Comparison between step responses of controlled variables for a 5% increase of w_{EGR}

6.3.1 Transfer function definition

The transfer functions provide a basis for determining important system response characteristics, especially in gain - time constant form. In particular it is useful to

analyse $G'_{11}(s)$ and $G'_{22}(s)$, on which the control loops will be closed. In particular:

$$G'(s)_{11} = \frac{\Delta(\Delta T_{sh})}{\delta w_{EGR}} = \mu \frac{(1+\tau_1 s)(1+\tau_2 s)}{(1+T_1 s)(1+T_2 s)(1+T_3 s)(1+T_4 s)} \frac{\left(1+\frac{2\xi_{z1}}{\omega_{z1}}s+\frac{s^2}{\mu_{11}\omega_{z1}^2}\right)\left(1+\frac{2\xi_{z2}}{\omega_{z2}}s+\frac{s^2}{\omega_{z2}^2}\right)}{\left(1+\frac{2\xi_{p1}}{\omega_{p1}}s+\frac{s^2}{\omega_{p1}^2}\right)} \tag{6.19}$$

$$G'(s)_{22} = \frac{\Delta T_{scr}}{\delta w_{EXH}} = \mu \frac{(1+\tau_1 s)(1+\tau_2 s)(1+\tau_3 s)}{(1+T_1 s)(1+T_2 s)(1+T_3 s)(1+T_4 s)} \frac{\left(1+\frac{2\xi_{z1}}{\omega_{z1}}s+\frac{s^2}{\omega_{z1}^2}\right)}{\left(1+\frac{2\xi_{p1}}{\omega_{p1}}s+\frac{s^2}{\omega_{p1}^2}\right)} \tag{6.20}$$

The transfer functions parameters are reported in Tab. 6.2.

The most important information is the presence of complex conjugate poles and zeros around the desired crossover frequency, which can cause oscillations in the time response.

If a system has a pair of complex conjugate poles with a low damping factor the magnitude of the frequency response has a peak, or resonance, at frequencies in the proximity of the pole. Moreover, it is possible to evaluate the sensitivity transfer function, i.e. the transfer function between the output variable and the disturbance, as:

$$S(s) = \frac{1}{1+L(s)} = \begin{cases} 1 & \text{for} \quad \omega \gg \omega_c \\ \dfrac{1}{L(s)} & \text{for} \quad \omega \ll \omega_c \end{cases} \tag{6.21}$$

This means that if the open-loop transfer function $L(s)$ has complex conjugate zeros they become complex conjugate poles in the sensitivity function. As a consequence, the time response up against a disturbance step has a dip or notch in its magnitude function at frequencies near the natural frequency. This is a key information for control tuning process, because this effect can not be cancelled out and strongly limits the control bandwidth.

Tables 6.2: Transfer functions gains, time constants, natural frequencies and damping factors

	Parameter	$G'_{11}(s)$	$G'_{22}(s)$
	μ	-45.23	-27.22
denominator	T_1	$138.9\,\mathrm{s}$	$138.9\,\mathrm{s}$
	T_2	$108.4\,\mathrm{s}$	$108.4\,\mathrm{s}$
	T_3	$41.7\,\mathrm{s}$	$41.7\,\mathrm{s}$
	T_4	$3.0\,\mathrm{s}$	$3.0\,\mathrm{s}$
	ξ_{p1}	0.979	0.979
	ω_{p1}	$0.041\,\mathrm{rad\,s^{-1}}$	$0.041\,\mathrm{rad\,s^{-1}}$
numerator	τ_1	$57.3\,\mathrm{s}$	$215.7\,\mathrm{s}$
	τ_2	$12.1\,\mathrm{s}$	$20.4\,\mathrm{s}$
	τ_3	–	$1.4\,\mathrm{s}$
	ξ_{z1}	0.668	0.927
	ω_{z1}	$0.33\,\mathrm{rad\,s^{-1}}$	$0.029\,\mathrm{rad\,s^{-1}}$
	ξ_{z2}	0.655	–
	ω_{z2}	$0.01\,\mathrm{rad\,s^{-1}}$	–

However, since the damping factors values reported in Tab. 6.2 are high, we can conclude that the presence of complex poles/zeros pairs is not critical.

6.4 PID tuning and performances evaluation

6.4.1 PID tuning

PID controller is by far the most widely used control algorithm in the process industry, thanks to his simplicity and proven robustness. It has three principal control effects: the proportional (P) action gives a change in the input (manipulated variable) directly proportional to the control error; the integral (I) action gives a change in the input proportional to the integrated error, and its main purpose is to eliminate the offset error once the transient is over; the less commonly used derivative (D) action is used in some cases to speed up the response or to stabilize the system, and it gives a change in the input proportional to the derivative of the controlled variable. In this case we will use a PI configuration, which is enough to guarantee good control performances, thanks to the limited phase shift of the process transfer functions. Fig. 6.11 shows the reference control scheme.

The controllers parameters to be tuned are the proportional gain K_p and integral time constant T_i. Given a minimum phase closed-loop transfer function

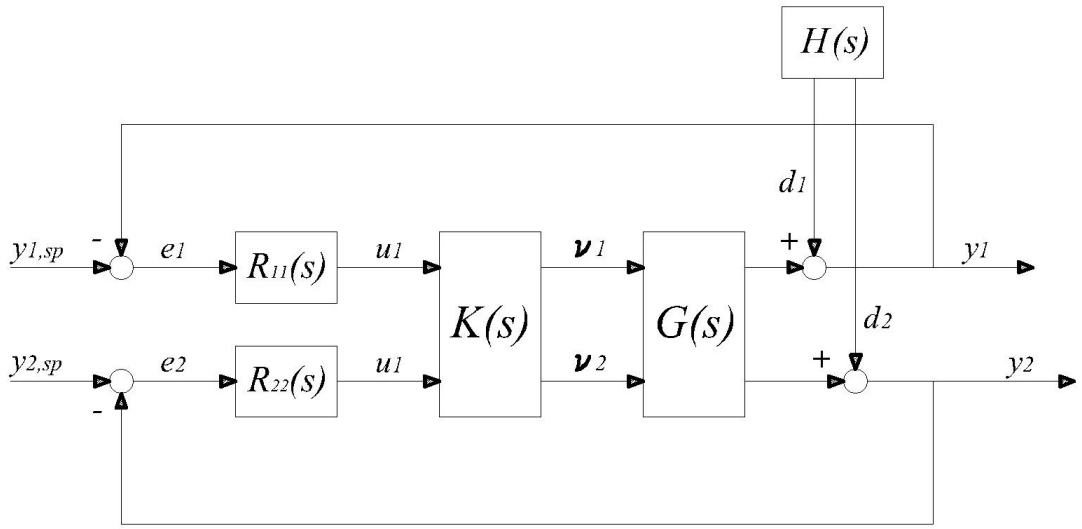

Figure 6.11: Reference control scheme

$L(s) = R(s)\,G'(s)$ with $\mathbb{R}(p) \leq 0$ and $\mid L(j\,\omega_c) \mid = 1$, the Bode criterion states that the controlled system is asymptotically stable if and only if:

- $\mu_L > 0$
- $\varphi_m > 0$

ω_c, i.e. the crossover frequency, defines the control bandwidth: this means that a control input signal with a frequency higher than ω_c will have a low impact on the output variables.

As first attempt the crossover frequency is set to $0.01\,\mathrm{rad\,s^{-1}}$. Moreover, the phase margin is set to 80°. The controller parameters are the solution of the following system:

$$\begin{cases} \mid L(j\,\omega_c) \mid = 1 \\ \varphi_m = 180° - \mid \varphi_c \mid = 80° \end{cases} \tag{6.22}$$

The results are reported in Tab. 6.3.

It is worthy underlining that the controllers gain is negative, so that $\mu_L = K_p\,\mu_{ii} > 0$. Hence, the Bode criterion is satisfied.

Fig. 6.12 and 6.13 shows the Bode plot of the open-loop transfer functions.

Tables 6.3: Controllers tuned parameters

Controller	K_p [−]	T_i [s]
R_{11}	−0.008845	22.07
R_{22}	−0.020803	64.89

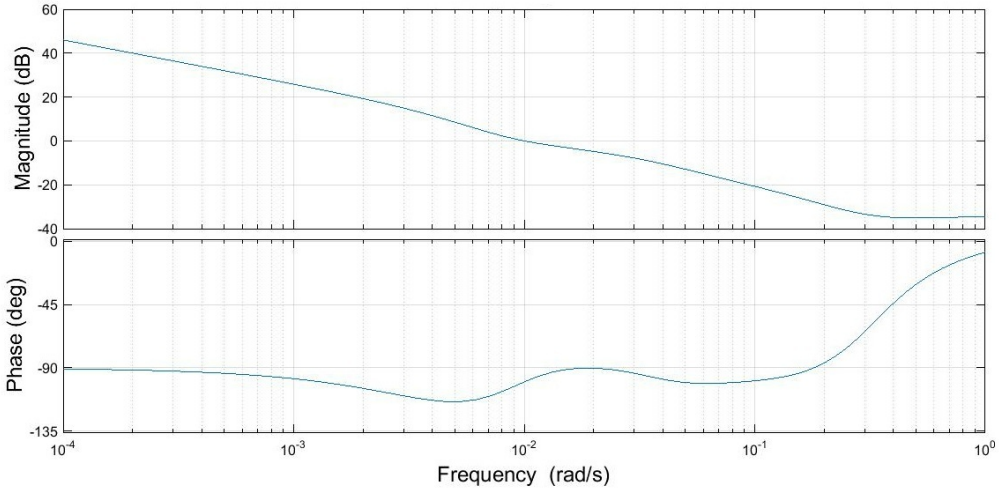

Figure 6.12: Bode plot of $L_{11}(s)$

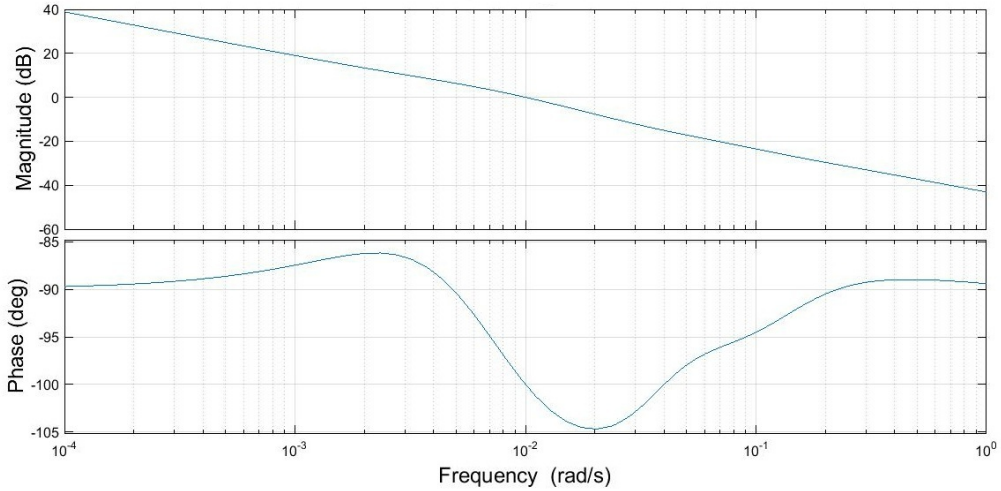

Figure 6.13: Bode plot of $L_{22}(s)$

6.4.2 Performance evaluation

The control performance has to be evaluated both from static and dynamic point of view. Good static performance is guaranteed by the presence of the integral action, which ensures that the set point error is zero at steady-state.

Without considering output disturbances due to measurement noise, the dynamic performances are good if:

$$\begin{cases} Y(s) = F(s)\, Y^{sp}(s) & \Rightarrow \quad F(s) \simeq 1 \\ Y(s) = S(s)\, D(s) & \Rightarrow \quad S(s) \simeq 0 \end{cases} \tag{6.23}$$

The first condition implies that the controlled variables follow a variation of their set-point. This is confirmed by Fig. 6.14. Moreover, the decoupled variables do not move at the end of the transient.

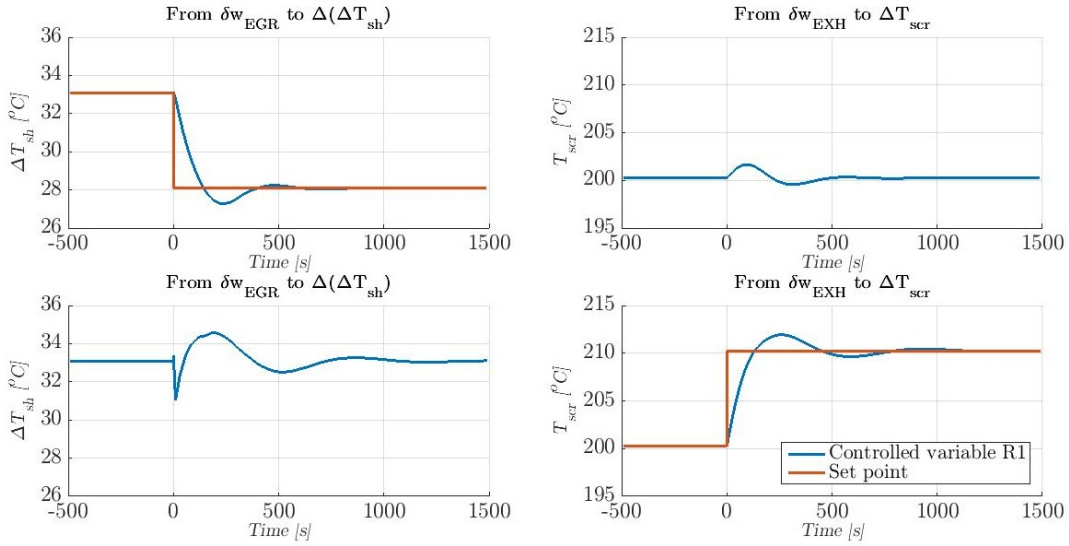

Figure 6.14: Step response of $F(s)$

The second condition implies that the control system rejects the disturbances effectively. This is confirmed by Fig. 6.15, whose result are obtained with a 5% step of each disturbance.

6.5 Tests of the control system

Once the control system is designed, it has to be tested for virtual drive-test. The first test (case A) consists of a series of slow velocity ramps, shown in Fig. 6.16,

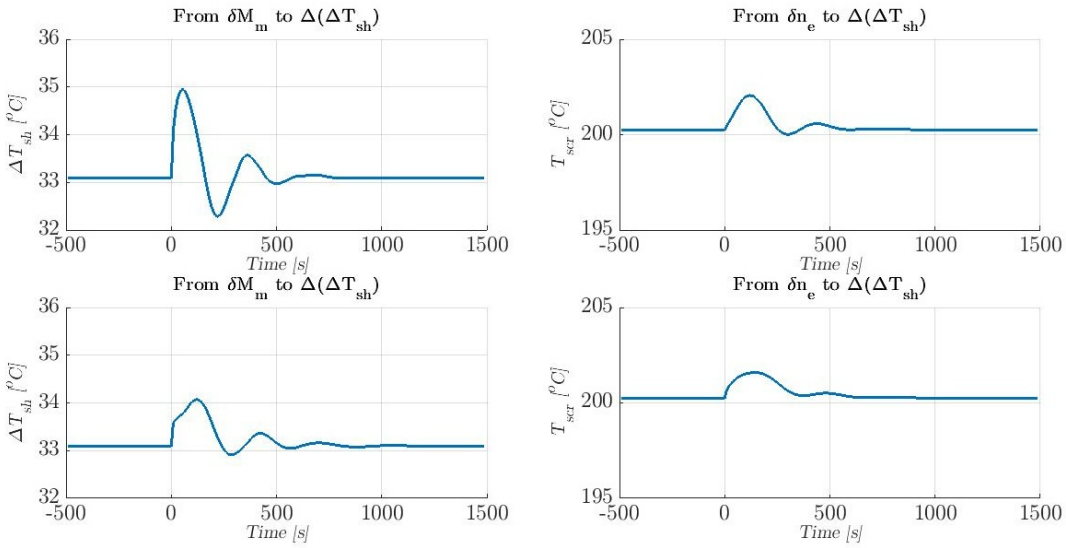

Figure 6.15: Step response of $S(s)$

i.e. a disturbance whose main component in the frequency domain is around ω_c.

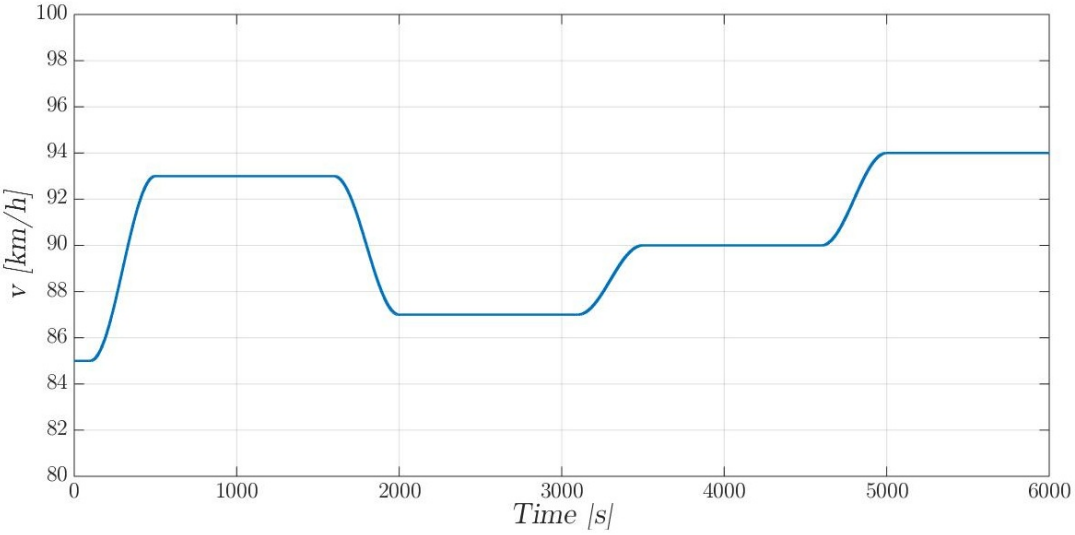

Figure 6.16: Velocity profile - case A

Fig. 6.17 and Fig. 6.18 show that the matching between controlled variables and their set-points is good, both statically and dynamically. The optimal value of degree of superheating changes according to the engine load, and its actual value follows the set-point with quite small over and undershoots. On the other hand,

the optimal value of the exhaust gases temperature is almost constant, while the actual values over and undershoots are within the range of ±5 °C.

Fig. 6.19 and Fig. 6.20 show the maximum temperature of the working fluid close to the wall of both evaporators: apart from the first ramp, the thermal decomposition is avoided. Moreover, Fig. 6.21 and Fig. 6.22 prove the increase of performance due to the positive effect of the WHR unit: in fact, the first principle efficiency of the combined cycle is 2% higher on average than the engine efficiency. Concerning the power output, at the cruise speed of 85 km h^{-1} the nominal engine power is 101.5 kW. With the add-on system, the engine power is 96.8 kW while the ORC power is 4.7 kW, so that the global power output is the same. The ratio between the ORC and the engine power is 4.9%, really close to the break-even point of 5%, which makes the investment interesting from the economical point of view.

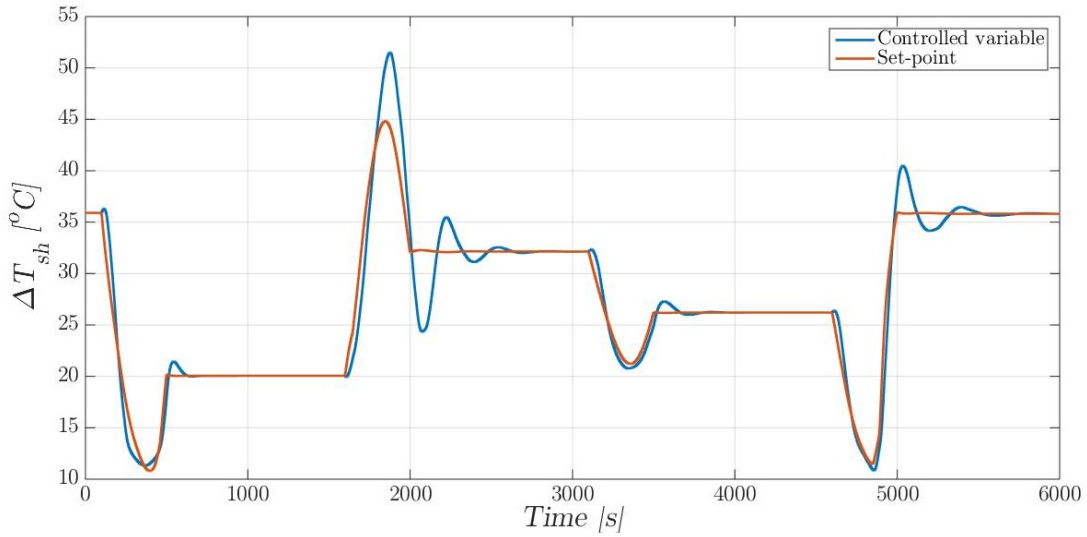

Figure 6.17: Degree of superheating - case A

The second test is performed with a real highway velocity profile, with a strong initial acceleration which causes a fast variation of the energy content and mass flows of the flue gases, i.e. the disturbance variables for the control system of the WHR unit. In this case the disturbances act at a frequency higher than the crossover frequency of the open-loop transfer function. Therefore, the results in terms of control objectives are not good: as shown in Fig. 6.23, 6.24 and 6.25 the output variables do not follow their set-point because the controlled process response is slower than the disturbance variation. Furthermore, the EGR maximum temperature is sensibly higher than the value at which thermal decomposition takes place.

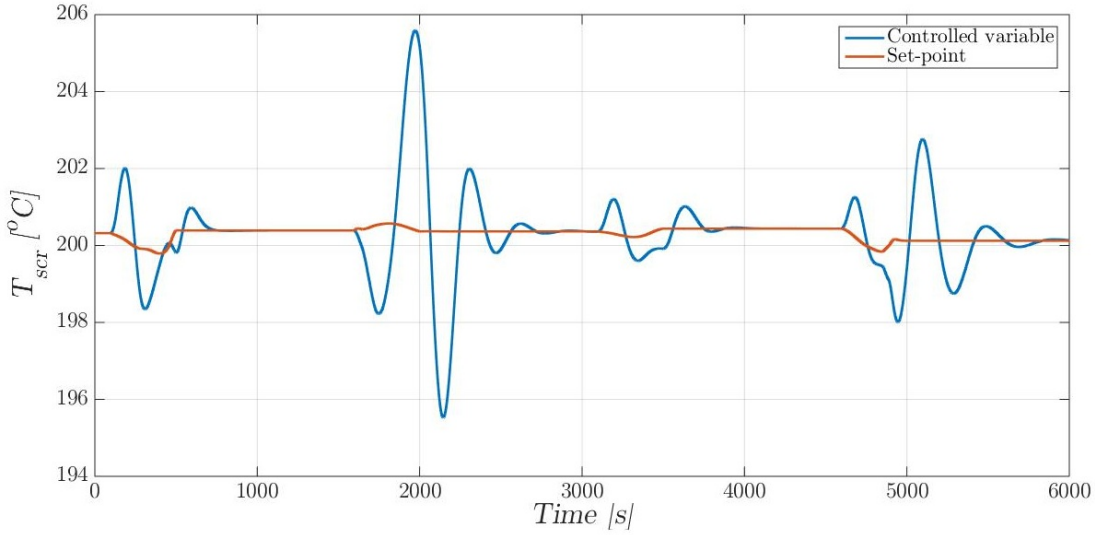

Figure 6.18: Exhaust gases temperature - case A

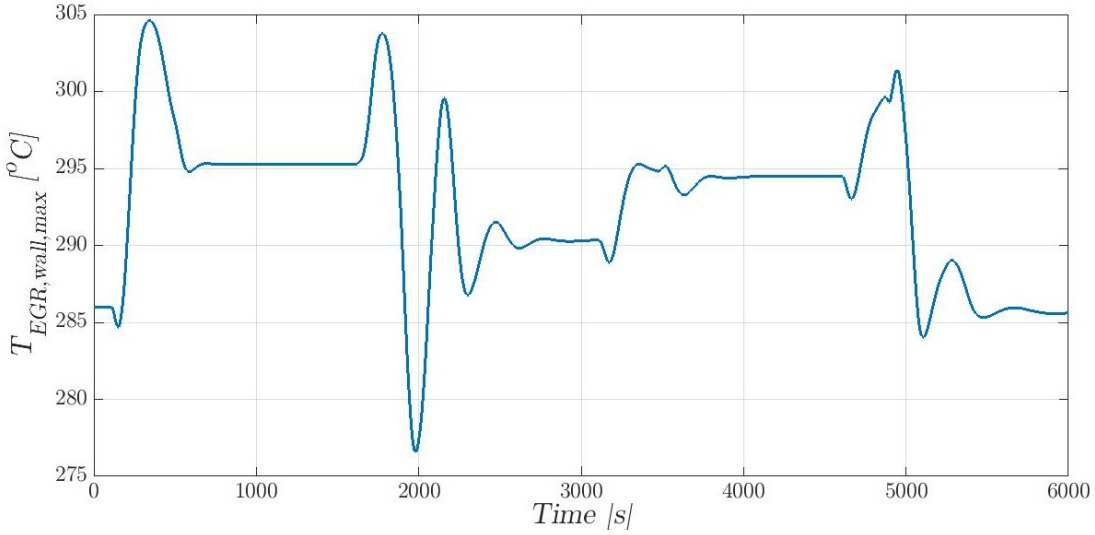

Figure 6.19: Maximum temperature of the working fluid in the EGR evaporator - case A

Therefore, the crossover bandwidth has to be increased to obtained satisfying performance during real operation. Unfortunately, setting a higher crossover frequency causes higher oscillations, even if the phase margin of the open-loop functions is high.

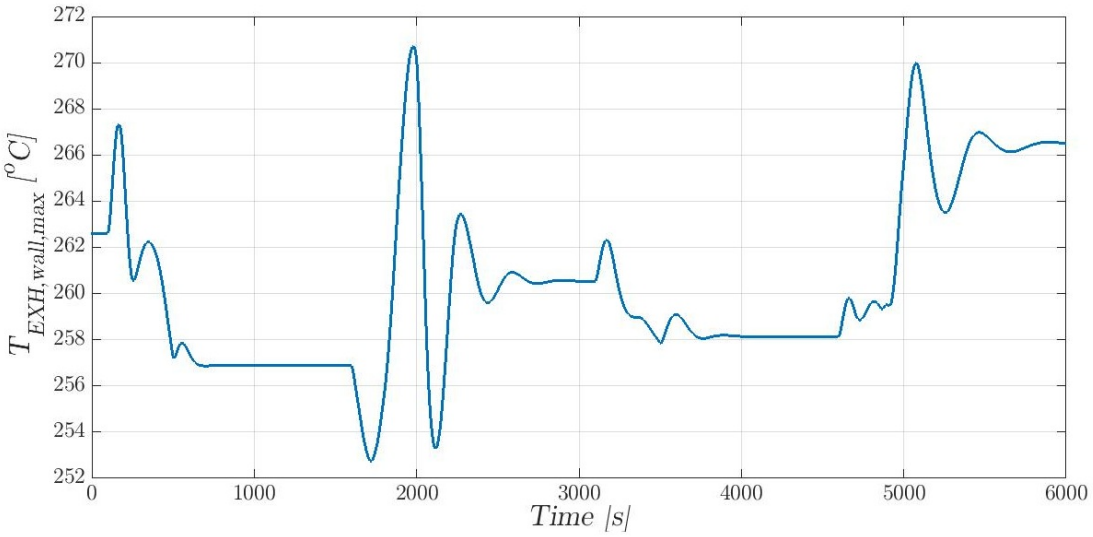

Figure 6.20: Maximum temperature of the working fluid in the EXH evaporator - case A

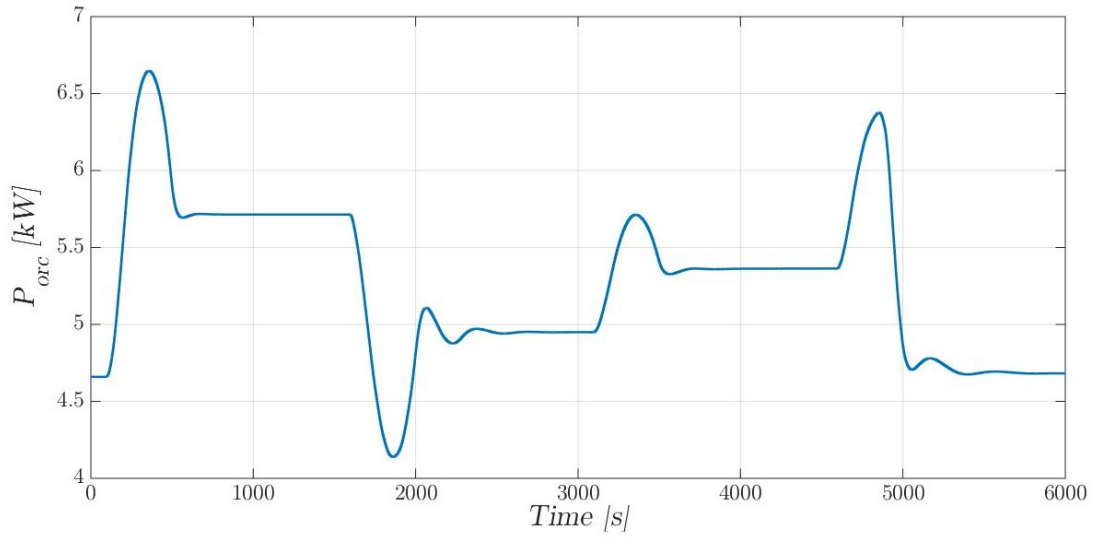

Figure 6.21: ORC power output - case A

We can conclude that the choice of a static decoupler is not satisfactory. From the dynamic point of view, indeed, there is still a strong coupling between the control loops, as shown in Fig. 6.7. The more evident consequence is the presence of oscillations in the controlled variables, due to a reduction of the real open-loop transfer functions phase margin, which is probably lower than 40°. In order

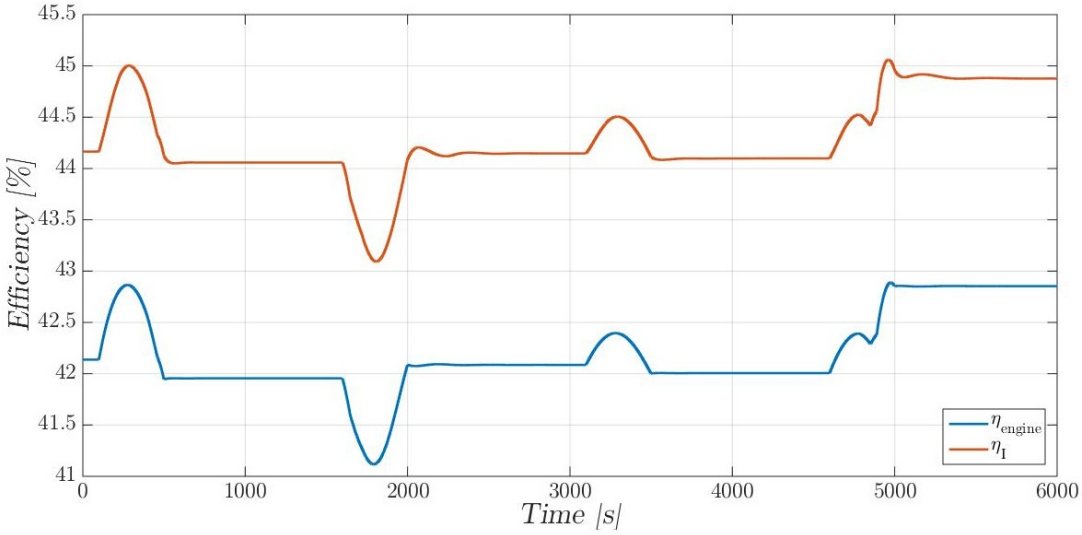

Figure 6.22: Efficiencies - case A

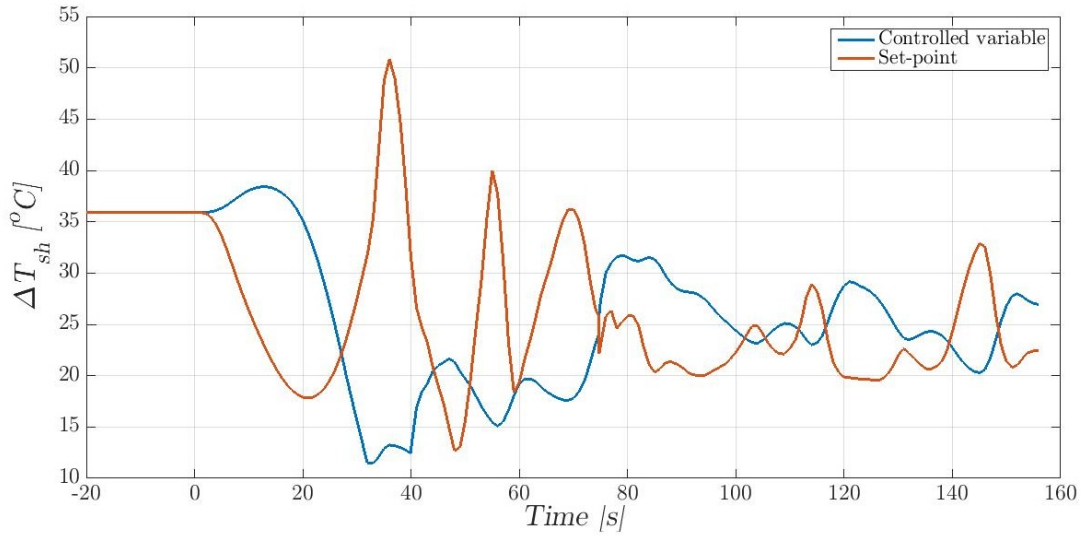

Figure 6.23: Degree of superheating - case B

to improve the performance of the control system, a dynamic decoupler has to be developed, so that the magnitude of the out-of-diagonal transfer functions is much lower than 0 dB not only at low frequencies but also around the crossover frequency. Moreover, a feed-forward compensation could improve the promptness of the control system.

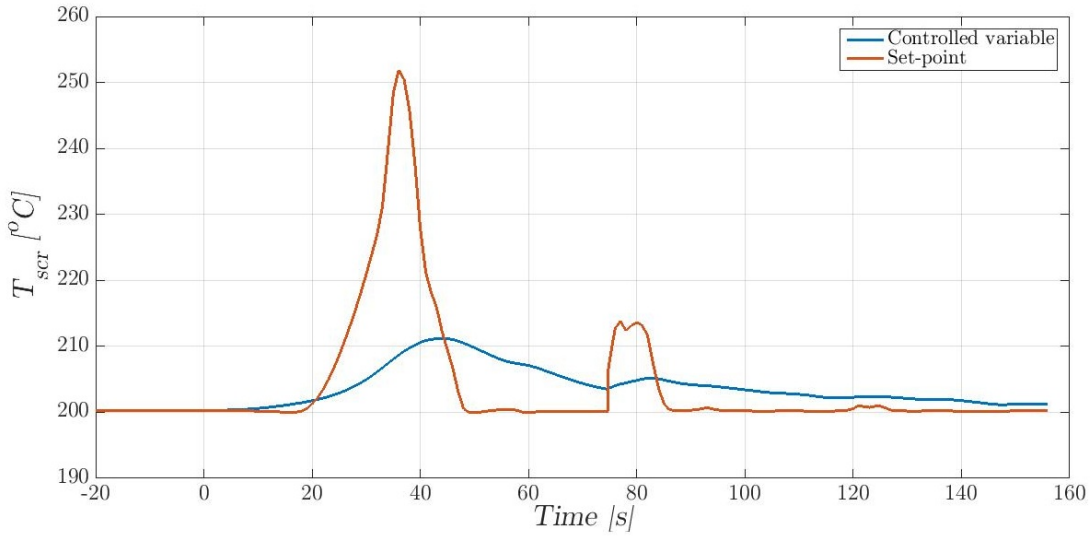

Figure 6.24: Exhaust gases temperature - case B

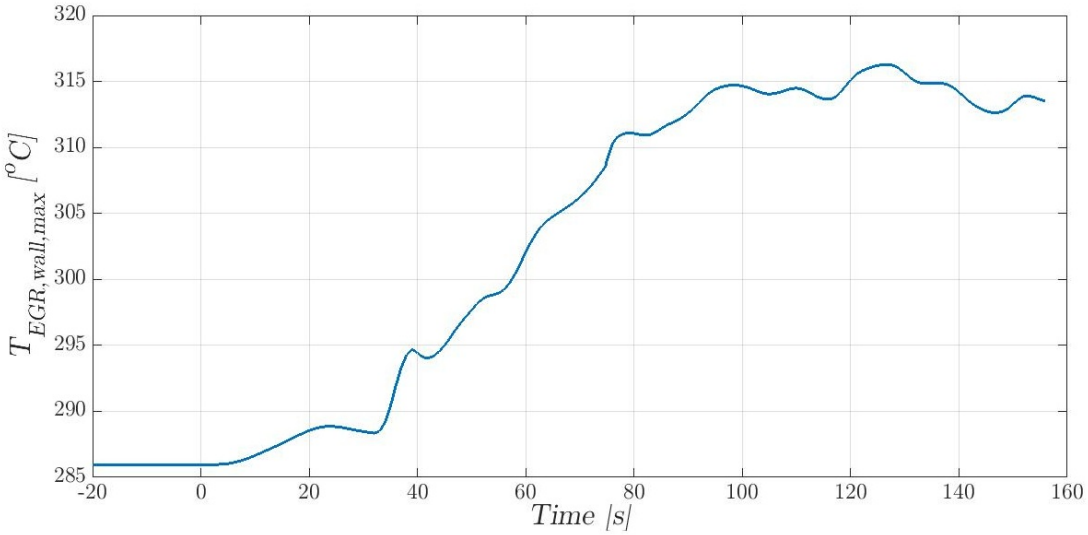

Figure 6.25: Maximum temperature of the working fluid in the EGR evaporator - case B

Conclusion and future developments

The purposes of this work are: i) the design of a WHR unit which exploits, through an ORC system, the thermal energy rejected by a heavy-duty diesel engine, ii) the development of an object-oriented dynamic model of the combined cycle, and iii) the implementation of a first-attempt control system for the WHR unit.

With regard to the system design, the first step has been the analysis of the thermal sources available. A lumped parameter diesel engine model has been chosen from literature, and later extended and tuned, thanks to experimental data provided by DAF Trucks NV. The model results show a good matching with the experimental data, with a mean relative error of 3.9%. Due to the recent developments concerning the ICE efficiency, it is necessary to recover heat from both the EGR circuit and the exhaust gases, in order to achieve performance sufficient to guarantee the system economic feasibility. Other thermal sources such as the turbocharger intercooler and the jacket coolant circuit have not been considered because of their lower temperatures and the higher complexity of the related WHR unit.

The ORC main parameters have been optimized, together with the turbine design, with the in-house "ORCHID_vpe" code, specifically extended to optimize the non-conventional cycle developed in this work. Following this approach it is possible to take into account during the optimization process not only the thermodynamic performance and constraints of the cycle but also the geometrical and mechanical constraints which determine whether the turbine design is feasible or not.

Moreover, a big effort has been made to develop the $MATLAB$ code "Off1D", which evaluates the off-design performance of a small ORC turbine. The need of this tool comes from the high variability of the turbine operating point, depending on the different engine loads. It is worth underlining that such a code can be useful also in other applications where the thermal source of the WHR unit is highly variable as well.

Concerning the dynamic model, the Modelica language represents one of the more advanced tool that allows to simulate the dynamic behaviour of multi-

physical system. Thus, it has been used to code the models of all the components of the combined cycle. Among them, the finite volumes heat exchangers models have been inherited from other libraries, i.e. the *ORC* and *Thermopower* libraries, while all the other components have been coded *ex-novo* and collected within the *ICORC* library, in particular the lumped parameter of the Diesel engine model and the turbomachinery models.

Furthermore, the *ICORC* library contains the models of the topping and bottoming cycle, created by aggregation of the submodels, which can be used to perform further thermodynamic analysis on dynamic simulations of the combined cycle powertrain. The resulting model has been used to test the effectiveness of the control strategy implemented, and represents the basis for the design of an advance control system.

About the control strategy, the optimal set points of the control variables which respect all the constraints have been evaluated for a wide range of operating conditions. In order to more deeply understand the dynamic behaviour of the WHR unit and to tune the control system, a balanced reduced sixth order model has been obtained. This analysis shows the presence of complex conjugated poles and zeros around the desired crossover frequency, but due to the high damping factors they are probably not responsible for the oscillations of the controlled variables shown in Chapter 6.

The main conclusions of the thesis are:

- the most suitable cycle configuration consists of two evaporators in parallel with a regenerator only in the working fluid circuit coupled with the exhaust gases. The best position of the exhaust gases evaporator is upstream the SCR system: in fact, considering the high condensing temperature and the temperature drop over the catalytic reactor, limiting the cooling process to 200 °C is better than starting the heat recovery downstream the SCR system;

- the performance of the WHR unit at the design point is promising. The mechanical power of the ORC system is almost 5% of the engine power at the nominal operating point, which represents, from an economic point of view, the break even point for the application;

- from a dynamic point of view the system control is more challenging, because the control bandwidth is limited by the controlled variable oscillations, which occur with a crossover frequency higher than $0.01\,\mathrm{rad\,s^{-1}}$. Even if the phase margin of the two decoupled open-loop transfer functions is higher than 60°, the real phase margin is lower, probably due to the dynamic interaction between the control loops. Moreover, the heat exchangers inertia decreases the

process gain at frequencies higher than $0.01\,\mathrm{rad\,s^{-1}}$, so that the manipulated variables are highly stressed if the controllers work within that frequency range, possibly causing the actuators saturation. Therefore, since the disturbance is faster than the process, its rejection and the set-point tracking are not satisfactory.

A simple control system with a static decoupler and two PI is then not enough to guarantee acceptable dynamic performance when a realistic disturbance occurs on the WHR unit.

In order to improve the control system, future developments could be the introduction of a dynamic decoupler, in order to avoid the presence of undesirable oscillations, and of a feed-forward compensator. If still the performance does not improve, the implementation of an advanced control system will be necessary, for instance a Model Predictive Control. This solution could lead to better performance, also because it allows to take into consideration all the process constraints and to optimize start-up and shut-down operations. As negative effect, the cost of the control system increases and its reliability decreases.

A statistic analysis on the engine operating loads has to be performed in order to understand if the optimal set-point tracking is the best solution compared with the use of fixed values. In other words, it has to be find out whether or not it is worthy trying to optimize the WHR unit efficiency in off-design conditions, varying the set-point of the controlled variables.

Another solution concerns the process modification. For instance, the heat exchangers mass and volumes could be reduced so that the thermal inertia is lower. This could increase the process gain, so that the controlled variables response is faster, but at the same time also the disturbance gain increases, which is not desirable.

Future works should also investigate the start-up operation, and how to manage the overloads in heat exchangers with the turbine by-pass.

Possible further activities are:

- testing different expander configuration, especially radial turbine;
- adding the model of the truck cooling circuit. This would permit to have the actual values of mass and temperature of the condenser cooling water, which are disturbance variables as well;
- improving the accuracy of the heat exchangers models by solving the numerical problems which rise in the finite volumes models when different heat transfer coefficient for each fluid phase are considered.
- the introduction of the output disturbances;

- the introduction of the control saturations;
- the introduction of the turbine by-pass valve.

Appendix A

Complete engine model

Here the complete extended model of the Internal Combustion Engine is reported. It is based on the equations of [7], extended with the calculation of engine performances, energy balances and turbine outlet temperature. All the equations refer to Fig. 2.1.

The state-space form of the model is:

$$\begin{cases} \dot{x} = f(x,u) \\ x = (p_{im}, p_{em}, y_{O_2im}, y_{O_2em}, \omega_t, \tilde{u}_{egr1}, \tilde{u}_{egr2}, \tilde{u}_{vgt}, \dots \\ \qquad \dots y_{CO_2im}, y_{CO_2em}, y_{N_2im}, y_{N_2em}, y_{H_2Oim}, y_{H_2Oem}, y_{Arim}, y_{Arem}) \\ u = (u_\delta, n_e, u_{egr}, u_{vgt}) \\ y = (T_{out}, \dot{m}_{out}) \end{cases}$$

EQUATIONS:

At a lower level all the engine components are modelled as follows:

INTAKE MANIFOLD

$$\frac{d(p_{im})}{dt} = \frac{R_a\, T_{im}}{V_{im}}\big(W_c + W_{egr} - W_{ei}\big) \tag{A.1}$$

$$x_{egr} = \frac{W_{egr}}{W_{egr} + W_c} \tag{A.2}$$

$$\frac{d(y_{O_2im})}{dt} = \frac{R_a T_{im}}{p_{im} V_{im}}\big[(y_{O_2em} - y_{O_2im})W_{egr} + (y_{O_2c} - y_{O_2im})W_c\big] \tag{A.3}$$

$$\frac{d(y_{CO_2im})}{dt} = \frac{R_a T_{im}}{p_{im} V_{im}} \left[(y_{CO_2em} - y_{CO_2im}) W_{egr} + (y_{CO_2c} - y_{CO_2im}) W_c \right] \quad \text{(A.4)}$$

$$\frac{d(y_{N_2im})}{dt} = \frac{R_a T_{im}}{p_{im} V_{im}} \left[(y_{N_2em} - y_{N_2im}) W_{egr} + (y_{N_2c} - y_{N_2im}) W_c \right] \quad \text{(A.5)}$$

$$\frac{d(y_{H_2Oim})}{dt} = \frac{R_a T_{im}}{p_{im} V_{im}} \left[(y_{H_2Oem} - y_{H_2Oim}) W_{egr} + (y_{H_2Oc} - y_{H_2Oim}) W_c \right] \quad \text{(A.6)}$$

$$\frac{d(y_{Ar,im})}{dt} = \frac{R_a T_{im}}{p_{im} V_{im}} \left[(y_{Ar,em} - y_{Ar,im}) W_{egr} + (y_{Ar,c} - y_{Ar,im}) W_c \right] \quad \text{(A.7)}$$

EXHAUST MANIFOLD

$$\frac{d(p_{em})}{dt} = \frac{R_e \, T_{em}}{V_{em}} \left(W_{eo} - W_{egr} - W_t \right) \quad \text{(A.8)}$$

$$\frac{d(y_{O_2em})}{dt} = \frac{R_e T_{em}}{p_{em} V_{em}} \left[(y_{O_2e} - y_{O_2em}) W_{eo} \right] \quad \text{(A.9)}$$

$$\frac{d(y_{CO_2em})}{dt} = \frac{R_e T_{em}}{p_{em} V_{em}} \left[(y_{CO_2e} - y_{CO_2em}) W_{eo} \right] \quad \text{(A.10)}$$

$$\frac{d(y_{N_2em})}{dt} = \frac{R_e T_{em}}{p_{em} V_{em}} \left[(y_{N_2e} - y_{N_2em}) W_{eo} \right] \quad \text{(A.11)}$$

$$\frac{d(y_{H_2Oem})}{dt} = \frac{R_e T_{em}}{p_{em} V_{em}} \left[(y_{H_2Oe} - y_{H_2Oem}) W_{eo} \right] \quad \text{(A.12)}$$

$$\frac{d(y_{Ar,em})}{dt} = \frac{R_e T_{em}}{p_{em} V_{em}} \left[(y_{Ar,e} - y_{Ar,em}) W_{eo} \right] \quad \text{(A.13)}$$

$$y_{TOT} = \sum_i y_{i,em} = 1 \quad \Rightarrow \quad \text{checking} \tag{A.14}$$

CYLINDERS

$$W_{ei} = \eta_{vol} \frac{p_{im} V_d}{R_a T_{im}} \frac{n_e}{120} \tag{A.15}$$

$$\eta_{vol} = c_{vol1} \sqrt{p_{im}} + c_{vol2} \sqrt{n_e} + c_{vol3} \tag{A.16}$$

$$W_f = \frac{10^{-6}}{120} n_e \, n_{cyl} \, u_\delta \tag{A.17}$$

$$W_{eo} = W_{ei} + W_f \tag{A.18}$$

$$\lambda_O = \frac{W_{ei} \, X_{Oim}}{W_f \, (O/F)_s} \tag{A.19}$$

$$y_{O_2 e} = \frac{W_{ei} \, y_{O_2 im} - W_f \left(\frac{O}{F}\right)_{stec}}{W_{eo}} \tag{A.20}$$

$$T_e = \eta_{sc} \, \Pi_e^{\frac{\gamma_a - 1}{\gamma_a}} \, r_c^{1-\gamma_a} \, x_p^{\frac{1-\gamma_a}{\gamma_a}} \left(q_{in} \left(\frac{1 - x_{cv}}{c_{pa}} + \frac{x_{cv}}{c_{va}} \right) + T_1 \, r_c^{\gamma_a - 1} \right) \tag{A.21}$$

$$\Pi_e = \frac{p_{em}}{p_{im}} \tag{A.22}$$

$$x_p = 1 + \frac{q_{in} \, x_{cv}}{c_{va} \, T_1 \, r_c^{\gamma_a - 1}} \tag{A.23}$$

$$q_{in} = \frac{W_f \, q_{HV}}{W_{ei} + W_f}(1 - x_r) \tag{A.24}$$

$$T_1 = x_r \, T_e + (1 - x_r) \, T_{im} \tag{A.25}$$

$$x_r = \frac{\Pi_e^{\frac{1}{\gamma_a}} \; x_p^{-\frac{1}{\gamma_a}}}{r_c \, x_v} \tag{A.26}$$

$$x_v = 1 + \frac{q_{in}(1 - x_{cv})}{c_{pa}\left[\frac{q_{in} \, x_{cv}}{c_{va}} + T_1 \, r_c^{\gamma_a - 1}\right]} \tag{A.27}$$

$$T_{em} = T_{amb} + (T_e - T_{amb}) \exp\left\{-\frac{h_{tot} \, \pi \, d_{pipe} \, l_{pipe} \, n_{pipe}}{W_{eo} \, c_{pe}}\right\} \tag{A.28}$$

$$M_e = M_{ig} - M_p - M_{fric} \tag{A.29}$$

$$M_p = \frac{V_d}{4\,\pi}\,(p_{em} - p_{im}) \tag{A.30}$$

$$M_{ig} = \frac{u_\delta \, 10^{-6} \, n_{cyl} \, q_{HV} \, \eta_{ig}}{4\,\pi} \tag{A.31}$$

$$M_{fric} = \frac{V_d}{4\,\pi}\,10^5\,(c_{fric1} n_{eratio}^2 + c_{fric2} n_{eratio} + c_{fric3}) \tag{A.32}$$

$$n_{eratio} = \frac{n_e}{1000} \tag{A.33}$$

$$y_{CO_2e} = \frac{W_{ei}\, y_{CO_2im} + W_f \left(\frac{CO_2}{F}\right)_{stec}}{W_{eo}} \tag{A.34}$$

$$y_{N_2e} = \frac{W_{ei}\, y_{N_2im}}{W_{eo}} \tag{A.35}$$

$$y_{H_2Oe} = \frac{W_{ei}\, y_{H_2Oim} + W_f \left(\frac{H_2O}{F}\right)_{stec}}{W_{eo}} \tag{A.36}$$

$$y_{Ar,e} = \frac{W_{ei}\, y_{Ar,im}}{W_{eo}} \tag{A.37}$$

EGR VALVE

$$W_{egr} = \frac{A_{egr} p_{em} \Psi_{egr}}{\sqrt{T_{em} R_e}} \tag{A.38}$$

$$\Psi_{egr} = 1 - \left(\frac{1 - \Pi_{egr}}{1 - \Pi_{egr,opt}} - 1\right)^2 \tag{A.39}$$

$$\Pi_{egr} = \begin{cases} \Pi_{egr,opt} & \text{if} \quad \frac{p_{im}}{p_{em}} < \Pi_{egr,opt} \\ \frac{p_{im}}{p_{em}} & \text{if} \quad \Pi_{egr,opt} \leq \frac{p_{im}}{p_{em}} \leq 1 \\ 1 & \text{if} \quad 1 < \frac{p_{im}}{p_{em}} \Rightarrow \Psi_{egr} = 0 \end{cases} \tag{A.40}$$

$$A_{egr} = A_{egr,max}\, f_{egr}(\tilde{u}_{egr}) \tag{A.41}$$

$$f_{egr}(\tilde{u}_{egr}) = \begin{cases} c_{egr1}\tilde{u}_{egr}^2 + c_{egr2}\tilde{u}_{egr} + c_{egr3} & \text{if} \quad \tilde{u}_{egr} \leq -\frac{c_{egr2}}{2c_{egr1}} \\ c_{egr3} - \frac{c_{egr2}^2}{4c_{egr1}} & \text{if} \quad \tilde{u}_{egr} \geq -\frac{c_{egr2}}{2c_{egr1}} \end{cases} \tag{A.42}$$

$$\tilde{u}_{egr} = K_{egr}\tilde{u}_{egr1} - (K_{egr} - 1)\tilde{u}_{egr2} \tag{A.43}$$

$$\frac{d(\tilde{u}_{egr1})}{dt} = \frac{1}{\tau_{egr1}}\left[u_{egr}(t-\tau_{degr}) - \tilde{u}_{egr1}\right] \tag{A.44}$$

$$\frac{d(\tilde{u}_{egr2})}{dt} = \frac{1}{\tau_{egr2}}\left[u_{egr}(t-\tau_{degr}) - \tilde{u}_{egr2}\right] \tag{A.45}$$

TURBOCHARGER

$$\frac{d(\omega t)}{dt} = \frac{P_t\,\eta_m - P_c}{J_t\,\omega_t} \tag{A.46}$$

$$\eta_{tm} = tm1\left(\frac{1}{\Pi_t}\right)^2 + tm2\left(\frac{1}{\Pi_t}\right) + tm3 \tag{A.47}$$

$$\Pi_t = \frac{p_{es}}{p_{em}} \tag{A.48}$$

$$P_{tm} = \eta_{tm}P_{t,s} = \eta_{tm}W_t c_{pe}T_{em}\left(1 - \Pi_t^{\frac{\gamma_e-1}{\gamma_e}}\right) \tag{A.49}$$

$$\frac{W_t\sqrt{T_{em}R_e}}{p_{em}} = A_{vgt,max}\,f_{\pi_t}(\Pi_t)\,f_{vgt}(\tilde{u}_{vgt}) \tag{A.50}$$

$$f_{\Pi_t} = \sqrt{1-\Pi_t^{k_t}} \Rightarrow \text{Chocking function} \tag{A.51}$$

$$f_{vgt} = c_{f2} + c_{f1}\sqrt{\max\left[0, 1-\left(\frac{\tilde{u}_{vgt}-c_{vgt2}}{c_{vgt1}}\right)^2\right]} \tag{A.52}$$

$$\frac{d(\tilde{u}_{vgt})}{dt} = \frac{1}{\tau_{vgt}}\left[u_{vgt}(t-\tau_{dvgt}) - \tilde{u}_{vgt}\right] \tag{A.53}$$

$$P_c = \frac{P_{c,is}}{\eta_c} = \frac{W_c\, c_{pa}\, T_{amb}}{\eta_c}\left(\Pi_c^{\frac{\gamma_a - 1}{\gamma_a}} - 1\right) \tag{A.54}$$

$$\Pi_c = \frac{p_{im}}{p_{amb}} \tag{A.55}$$

$$\eta_c = \eta_{c,max} - \boldsymbol{x}^T\, \boldsymbol{Q_c}\, \boldsymbol{x} \qquad \text{con} \quad \boldsymbol{Q} = \begin{bmatrix} a_1 & a_3 \\ a_3 & a_2 \end{bmatrix} \tag{A.56}$$

$$\boldsymbol{x} = \begin{pmatrix} W_c - W_{c,opt} \\ \pi_c - \pi_{c,opt} \end{pmatrix} \tag{A.57}$$

$$\pi_c = (\Pi_c - 1)^{c_\pi} \tag{A.58}$$

$$\Psi_c = \frac{2\, c_{pa}\, T_{amb}\left(\Pi_c^{\frac{\gamma_a - 1}{\gamma_a}} - 1\right)}{R_C^2\, \omega_t^2} \tag{A.59}$$

$$\Phi_c = \sqrt{\max\left[0, \frac{1 - c_{\psi_1}(\Psi_c - c_{\psi_2})^2}{c_{\phi_1}}\right]} + c_{\phi_2} \tag{A.60}$$

$$c_{\Psi_1}(\omega_t) = c_{\omega\Psi_1}\omega_t^2 + c_{\omega\Psi_2}\omega_t + c_{\omega\Psi_3} \tag{A.61}$$

$$c_{\phi_1}(\omega_t) = c_{\omega\phi_1}\omega_t^2 + c_{\omega\phi_2}\omega_t + c_{\omega\phi_3} \tag{A.62}$$

$$W_c = \frac{p_{amb}\, \pi\, R_c^3\, \omega_t}{R_a\, T_{amb}}\Phi_c \quad \text{con } R_c = \text{raggio al tip del compressore} \tag{A.63}$$

$$T_{es} = T_{em} \left(\frac{1}{\Pi_t} \right)^{\frac{1}{n}-1} \tag{A.64}$$

$$T_c = T_{amb} + \frac{W_t \; c_{pe}}{W_c \; c_{pa}} \, \eta_{tm} \, T_{em} \left(1 + \Pi_t^{1-\frac{1}{\gamma_e}} \right) \tag{A.65}$$

INTECOOLER

$$T_{out,int} = \text{cost} \qquad \Rightarrow \qquad \text{ideal heat exchanger} \tag{A.66}$$

HEAT BALANCES & PERFORMANCE

At a higher level heat balance and engine performance are evaluated:

$$P_{engine} = M_e \; n_e \; \frac{\pi}{30} \tag{A.67}$$

$$\eta_{engine} = \frac{P_{engine}}{W_f \; q_{HV}} \tag{A.68}$$

$$\dot{Q}_{fuel} = W_f \, q_{HV} \tag{A.69}$$

$$\dot{Q}_{exh} = W_t \, c_{pe} \, (T_{es} - T_{amb}) \tag{A.70}$$

$$\dot{Q}_{egr} = W_{egr} \, c_{pe} \, (T_{em} - T_{out,egr}) \tag{A.71}$$

$$\dot{Q}_{interc} = W_c \, c_{pa} \, (T_c - T_{out,int}) \tag{A.72}$$

$$\dot{Q}_{loss,man} = W_{eo} \, c_{pe} \, (T_e - T_{em}) \tag{A.73}$$

$$\dot{Q}_{loss,turb} = W_t \left(h_{em} - h_{es}\right) - P_{tm} \tag{A.74}$$

$$\dot{Q}_{cool} = \dot{Q}_{fuel} - \dot{Q}_{exh} - \dot{Q}_{egr} - \dot{Q}_{interc} - \dot{Q}_{loss,man} - \dot{Q}_{loss,turb} - P_{engine} \tag{A.75}$$

UNKNOWNS:

The Tab. A.1 reports all the model unknowns:

Actually, the variable Y is a function of the turbine outlet concentrations, and it is declared as:

Tables A.1: Model variables

Thermodynamics	Mass flow	Mechanics	Efficiencies	Powers	Others
p_{im}	W_c	M_e	η_{vol}	P_c	A_{egr}
p_{em}	W_{egr}	M_{ig}	η_{tm}	P_{tm}	Ψ_{egr}
T_{em}	W_{ei}	M_p	η_{engine}	P_{engine}	f_{egr}
$y_{O_2,im}$	W_{eo}	M_{fric}	η_c	$\dot{Q}_{egr}$	$\tilde{u}_{egr}$
$y_{O_2,em}$	W_t	ω_t		$\dot{Q}_{interc}$	$\tilde{u}_{egr1}$
T_e	W_f			$\dot{Q}_{exh}$	$\tilde{u}_{egr2}$
$y_{O_2,e}$	x_{egr}			$\dot{Q}_{fuel}$	f_{Π_t}
x_p				$\dot{Q}_{cool}$	f_{vgt}
q_{in}				$\dot{Q}_{loss,man}$	Ψ_c
T_1				$\dot{Q}_{loss,turb}$	Φ_c
x_r					$\tilde{u}_{vgt}$
x_v					π_c
Π_t					$c_{\Psi 1}$
Π_c					$c_{\Phi 1}$
Π_e					n_{eratio}
Π_{egr}					x
λ_O					
$y_{i,im}$					
$y_{i,em}$					
$y_{i,e}$					
y_{TOT}					
T_{es}					
T_c					

$$Y = \{y_{O_2,em}, y_{CO_2,em}, y_{N_2,em}, y_{H_2O,em}, y_{Ar,em}\}$$

PARAMETERS:

The following two tables give all the model parameters: Tab. A.3 all the geometrical and physic parameters, Tab. A.2 all the experimental closure parameters.

Tables A.2: Model closure parameters

Parameter	Value	UM
c_{vol1}	0.000366536	$\mathrm{Pa}^{-1/2}$
c_{vol2}	0.0000025433	$rpm^{-1/2}$
c_{vol3}	0.809366973	
η_{sc}	1.06994309314312	
x_{cv}	$2.33705844419204e-14$	
η_{ig}	0.476241007720244	
c_{fric1}	0.25834000675772	
c_{fric2}	0	
c_{fric3}	0.428323501332688	
c_{egr1}	-0.00011104237992346	
c_{egr2}	0.0177806122860778	
c_{egr3}	0	
K_{egr}	1.8	
τ_{egr1}	0.05	s
τ_{egr2}	0.13	s
τ_{degr}	0.065	s
$\Pi_{egr,opt}$	0.65000404832614	
t_{m1}	-0.02	
t_{m2}	0.15	
t_{m3}	0.3295	
n	1.26528946498197	
c_{m1}	1.35634406810986	
c_{m2}	2769.20920157669	
c_{m3}	0.0100000987445656	
K_t	2.89019266110711	
c_{f1}	1.94796270043856	
c_{f2}	-0.77631189328675	
c_{vgt1}	126.871935722855	
c_{vgt2}	117.144746882308	

Tables A.2: continues in the next page

Tables A.2: continues from previous page

Parameter	Value	UM
τ_{vgt}	0.025	s
τ_{dvgt}	0.04	s
a_1	3.09189776853185	
a_2	2.14785596204381	
a_3	-2.482320138317	
$\eta_{c,max}$	0.8168034229177559	
$W_{c,opt}$	0.275337574619592	$\mathrm{kg\,s^{-1}}$
$\pi_{c,opt}$	1.04551774682564	
c_π	0.27075947387649	
$c_{\Psi 2}$	0	
$c_{\Phi 2}$	0	
$c_{\omega\Psi 1}$	$1.08820510528987e-8$	$\mathrm{s^2\,rad^{-2}}$
$c_{\omega\Psi 2}$	-0.000173197603596756	$\mathrm{s\,rad^{-1}}$
$c_{\omega\Psi 3}$	1.02861647564086	
$c_{\omega\Phi 1}$	$-1.42977826851097e-8$	$\mathrm{s^2\,rad^{-2}}$
$c_{\omega\Phi 2}$	-0.00154988141455036	$\mathrm{s\,rad^{-1}}$
$c_{\omega\Phi 3}$	29.6461721512908	

Tables A.2: ends from previous page

Tables A.3: Geometrical and physic engine parameters

Parameter	Value	UM
V_{im}	0.022	m^3
V_{em}	0.02	m^3
R_a	287	$J\,kg^{-1}\,K^{-1}$
R_e	286	$J\,kg^{-1}\,K^{-1}$
x_{O_2c}	0.2314	
x_{CO_2c}	0.0005	
x_{H_2Oc}	0	
x_{N_2c}	0.7551	
x_{Arc}	0.013	
n_{cyl}	6	
$(O/F)_s$	3.371498	$kg\,kg^{-1}$
$(CO_2/F)_s$	3.17635573996649	$kg\,kg^{-1}$
$(H_2O/F)_s$	1.19675925773956	$kg\,kg^{-1}$
r_c	17.7	
γ_a	1.402692	
γ_e	1.344621	
c_{pa}	999.7	$J\,kg^{-1}\,K^{-1}$
c_{pe}	1115.9	$J\,kg^{-1}\,K^{-1}$
c_{va}	712.7	$J\,kg^{-1}\,K^{-1}$
c_{ve}	829.9	$J\,kg^{-1}\,K^{-1}$
T_{amb}	307.7	K
p_{amb}	101325	Pa
h_{tot}	127.241616398988	$W\,m^{-2}\,K^{-1}$
d_{pipe}	0.1	m
n_{pipe}	2	
l_{pipe}	1	m
V_d	0.0129	m^3
q_{HV}	42900000	$J\,kg^{-1}$
γ_{cyl}	1.35	
J_t	0.0002	$kg\,m^{-2}$
p_{es}	$p_{amb} + \Delta p$	Pa
$A_{vgt,max}$	0.0004	m^2
$A_{egr,max}$	0.0006	m^2
R_t	0.04	m
R_c	0.04	m

References

[1] Wolfgang Lang, Piero Colonna and Raimund Almbauer, Assessment of waste heat recovery from a heavy-duty truck engine by means of an ORC turbo-generator, *Journal of Engineering for Gas Turbine and Power - ASME* April 2013

[2] N. Espinosa, L. Tilman, V. Lemort, S. Quoilin and B. Lombard, Rankine cycle fo waste heat recovery on commercial trucks: approach, constraint and modelling, *Diesel International Conference Exhibition* May 2010

[3] N. Espinosa, I. Gil-Roman, D.Didiot, V. Lemort, B. Lombard and S. Quoilin, Transient organic Rankine cycle modelling for waste heat recovery on a truck, *24th International Conference on Efficiency, Cost, Optimization, Simulation and Environmental Impact of Energy Systems*, July 2011

[4] Tianyou Wang, Yajun Zhang, Zhijun Peng and Gequn Shu, A review of researches on thermal exhaust heat recovery with Rankine cycle, *Elsevier*, 2010

[5] Charles Sprouse III and Christopher Depcik, Review of organic Rankine cycle for internal combustion engine exhaust waste heat recovery, *Elsevier*, 2012

[6] Yiping Dai, Jiangfeng Wang and Lin Gao Parametric optimization and comparative study of organic Rankine Cycle (ORC) for low grade waste heat recovery, *Elsevier*, 2007

[7] J. Wahlstrom and L. Eriksson, Modelling diesel engines with a variable-geometry turbocharger and exhaust gas recirculation by optimization of model parameters for capturing non-linear system dynamics, *Proceedings of the Institution of Mechanical Engineers*, May 2011

[8] Anna G. Stefanopopoulou, Ilya Kolmanovsky and James S. Freidenberg, Control of variables geometry turbocharged diesel engines for reduced emissions, *IEEE*, July 2000

[9] Ming Zheng, Graham T. Reader and J. Gary Hawley, Diesel engine exhaust gas recirculation - a review on advanced and novel concepts, *Elsevier*, July 2003

[10] Andrew J. Smallbone Amit N. Bhave, Aaron R. Coble, Sebastian Mosbach, Markus Kraft and Robert McDavid, Identifying optimal operating points in terms of engineering constraints and regulated emissions in modern diesel engines, *Cambridge Centre for Computational Chemical Engineering*, January 2011

[11] J. Wahlstrom and L. Eriksson, Non linear EGR and VGT control with integral action for diesel engine, *IFP Energies Nouvelles - Oil & Gas Science and Technology*, 2011

[12] Yue-Yun Wang, Ibrahim Haskara and Oded Yaniv, Model-Based Quantitative Feedback Control of EGR Rate and Boost Pressure for Turbocharged Diesel Engines, *American Control Conference*, 2008

[13] Jonas Olsson and Markus Welander, Optimal control of a diesel engine with VGT and EGR, *Linkoping Universitet* June 2006

[14] Cristian Ciardelli, Isabella Nova, Enrico Tronconi, Daniel Chatterjee, Brigitte Bandl-Konrad, Michel Weibel and Bernd Krutzsch, Reactivity of NO/NO_2–NH_3 SCR system for diesel exhaust aftertreatment: identification of the reaction network as a function of temperature and NO_2 feed content, *Elsevier* 2006

[15] Ezio Alfieri, Emissions-controlled diesel engine, *ETH, Zurich* 2009

[16] J Wahlstrom, Control of EGR and VGT for emission control and pumping work minimization in diesel engines, *Linkoping Universitet*, 2006

[17] H.R.M. Craig, H.J.A. Cox, Performance extimation of axial flow turbines, *Institution of Mechanical Engineers*, 1970

[18] W. Traupel, Thermische Turbomaschinen, *Springer*, 1977

[19] E. Macchi, A. Perdichizzi, Efficiency prediction for axial flow turbines operating with non conventional fluid, *ASME*, 1981

[20] C. Osnaghi, Teoria delle turbomacchine, *Esculapio*, 2013

[21] D. H. Cooke, Modelling of off-design multistage turbine pressures by Stodola's ellipse, *Betchel Power Corporation, Texas*, 1983

[22] Salvatore Vitale, Preliminary design method for small scale centrifugal ORC turbines, *Politecnico di Milano, Milano* 2012

[23] Holger Martin, A theoretical approach to predict the performance of Chevron-type plate heat exchangers, *Elsevier*, 1996

[24] E.H. Wang, H.G. Zhang, B.Y. Fan, M.G. Ouyang, Y. Zhao, Q.H. Mu, Study of working fluid selection of Organic Rankine Cycle (ORC) for engine waste heat recovery, *Elsevier*, 2011

[25] F. Casella, M. Sielemann, L. Savoldelli, Steady-state initialization of object-oriented thermo-fluid models by homotopy methods, *Modelica Association*, 2011

[26] F. Casella, On the formulation of steady-state initialization problems in object-oriented models of closed thermo-hydraulic systems, *Modelica Association*, 2012

[27] R. Franke, F. Casella, M. Otter, M. Sielemann, H. Elmqvist, S. E. Mattsson and H. Olsson, Stream Connectors – an Extension of Modelica for Device-Oriented Modeling of Convective Transport Phenomena, *Proc. 7th International Modelica Conference*, 2009

[28] J. Peralez, P. Tona, O. Lepreux, A. Sciarretta, L. Voise, P. Dufour, M. Nadri, Improving the control performance of an ORC system for waste heat recovery from a heavy-duty diesel engine using a model-based approach, *IEEE Conference on Decision and Control*, 2013

[29] J. Peralez, P. Tona, A. Sciarretta, P. Dufour, M. Nadri, Optimal control of a vehicular ORC via Dynamic Programming with adaptive discretization grid, *International Federation of Automatic Control*, August 2014

[30] F. Casella, T. Mathijssen, P. Colonna and J. van Buijtenen, Dynamic modeling of Organic Rankine Cycle power systems, *Journal of Engineering for Gas Turbine and Power*, 2013

[31] F. Casella and A. Leva, Object-oriented modelling & simulation of power plants with Modelica, *European Control Conference*, 2005

[32] J. M. Pena and T. Sauer, On the multivariate Horner scheme, *Society for Industrial and Applied Mathematics*, 2000

[33] F. Browand, R.McCallen and J. Ross, The Aerodynamics of Heavy Vehicles II: Trucks, Buses and Trains, *ed. Springer*, 2009

[34] G. Ferrari, Motori a combustione interna, *Il capitello*, 2000

[35] S. Skogestad and I. Postlethwaite, MULTIVARIABLE FEEDBACK CONTROL - Analysis and design, *John Wiley and Sons*, 2005

[36] P. Bolzern, R. Scattolini and N. Schiavone, Fondamenti di controlli automatici, *McGraw Hill*, 2008

[37] http://www.vehicular.isy.liu.se/Software/TCDI_EGR_VGT/

[38] http://www.daf.com/~/media/Files/DAF%20Trucks/Trucks/Components/MX-13/PACCAR-MX-13-coach-bus-engine-folder-2013.pdf

[39] http://www.lutzjescoamerica.com/de/products/dosing-pumps/hydraulically-actuated-diaphrag/5700-series/5730-series.html

[40] http://www.asimptote.nl/software/fluidprop

[41] http://www.volvotrucks.com/SiteCollectionDocuments/VTNA_Tree/ILF/Products/Powertrain/i-shift_spec_sheet_ATO3112D.pdf

[42] S. Boni, Sviluppo di una libreria di componenti riconfigurabili per la simulazione di impianti ORC, *Politecnico di Milano, Milano* 2013

[43] F. Schiavo and F. Casella, Object-oriented modelling and simulation of heat exchangers with finite element methods, *Mathematical and Computer Modelling of Dynamical Systems, Taylor & Francis*, 2007

Nomenclature

Latin symbols

c	sound speed - specific heat
f_v	rolling friction factor
h	enthalpy - heat transfer coefficient - blade height
n	rotational speed $[rpm]$
p	pressure
s	entropy - Laplace variable
u	model input
v	absolute velocity
w	relative velocity - mass flow
x	molar fraction - model state
y	mass fraction
z	level
A	area
C_x	air friction factor
D	turbine diameter
E	energy
J	moment of inertia
M	mass - torque - Mach number
$\dot{N}$	molar flow rate
P	power
R	radius
S	surface
T	temperature
V	volume
W	mass flow rate
X	loss coefficient

Greek symbols

α	absolute fluid angle - void fraction
β	relative fluid angle - turbine pressure ratio
ρ	density
η	efficiency
τ	transmission ratio
ω	rotational speed $[rad/s]$ - frequency
σ	Hankel singular value
φ	angular position

Abbreviation

AFR	Air Fuel Ratio
CFD	Computational Fluid Dynamic
DAE	Differential Algebraic Equation
EGR	Exhaust Gas Recirculation
FEM	Finite Element Method
GWP	Global Warming Potential
ICE	Internal Combustion Engine
LTI	Linear Time Invariant
MB	Moving Boundary
$MIMO$	Multi Input Multi Output
ODP	Ozone Depletion Potential
ORC	Organic Rankine Cycle
PID	Proportional Integral Derivative
PHE	Plate Heat Exchanger
RGA	Relative Gain Array
SCR	Selective Catalytic Reduction
TIT	Turbine Inlet Temperature

Subscripts

amb	ambient
c	compressor - crossover
$cond$	condenser
cyl	cylinder
d	displaced
e	engine
egr	exhaust gas recirculation
ei	cylinder inlet
eo	cylinder outlet
em	exhaust manifold
es	exhaust engine's turbocharger
exh	exhaust
$fric$	frictional
f	fuel
ig	indicated
im	inlet manifold
in	inlet
is	isentropic
out	outlet
pa	constant pressure, air
pe	constant pressure, exhaust
$pump$	pump
ref	reference
scr	selective catalytic reduction
sh	super heating
st	stochiometric
t	turbine
va	constant volume, air
ve	constant volume, exhaust
vol	volumetric